8. EFFECTS ON VISIBILITY AND CLIMATE

8.1 INTRODUCTION

Visibility is the yardstick by which the layman measures air quality every day. Air pollutants can change the way he sees the world. The air pollutant that makes the largest contribution to visibility impairment is usually fine particulate matter, more specifically the accumulation mode, ~0.3 to 1.0 μm diameter (see Chapter 3).

The primary objective of the visibility discussion in this chapter is to present the technical basis for understanding the linkage between air pollution, especially particulate matter, and visibility. This linkage can be used to (1) evaluate the visibility effects of different levels for the primary standards for particulate matter concentrations designed to protect public health and (2) evaluate the need for a secondary standard designed to reduce visibility impairment.

The visibility sections of this chapter are complementary to recent reviews of visibility published by the National Research Council (National Research Council, 1993), the National Acid Precipitation Assessment Program (Trijonis et al., 1991), and the U.S. EPA (U.S. Environmental Protection Agency, 1995e). Little of the information in those reviews has been presented again here, with the result that this review does not attempt to present a fully comprehensive overview of the effect of particulate matter on visibility. Instead, the visibility sections of this chapter focus on presenting additional information relevant to the consideration of visibility protection that does not appear in the prior reviews.

8.1.1 Background

In August 1977, Congress amended the Clean Air Act (CAA) to establish as a national goal "the prevention of any future and remedying of any existing impairment of visibility in mandatory Class I Federal areas, which impairment results from manmade air pollution" (Title I Part C Section 169A; 42 U.S.C. 7491). Class I areas include many national parks and wilderness areas, especially in the western portion of the United States. These areas were generally large national parks and federal wilderness areas and included all national parks in existence on August 7, 1977. The visibility protection provisions of section 169A

required the U.S. Environmental Protection Agency (EPA) to establish a regulatory program to assure reasonable progress toward this national goal. In 1980, the EPA established regulatory requirements under section 169A to address Class I protection from visibility impairment that could be reasonably attributed to major stationary air pollution sources. At that time, regulatory action on regional haze (pollution transported long distances from a multitude of sources) was deferred until better scientific tools were developed. The 1977 Amendments also included provisions requiring applicants for new major source permits to assess the potential for their projects to cause adverse impacts on the air quality-related values, including visibility, in nearby Class I areas.

The mandate to protect visibility in national parks and wilderness areas led to the development of the Interagency Monitoring of Protected Visual Environments (IMPROVE), a cooperative visibility monitoring network managed and operated by federal land management agencies, the U.S. EPA, and State air quality organizations (Malm et al., 1994: Sisler et al., 1993). The 1977 CAA amendments also (a) led to major visibility research studies, such as (1) the Visibility Impairment due to Sulfur Transformation and Transport in the Atmosphere (VISTTA) study (Blumenthal et al., 1981); (2) the Subregional Cooperative Electric Utility, and the Department of Defense, National Park Service, and Environmental Protection Agency Study (SCENES) (Mueller et al., 1986); and (b) included the requirement to control sulfur dioxide (SO_2) emissions from the Navajo Generating Station, which is near the Grand Canyon National Park (56 FR 38399, 1991).

The CAA was amended in 1990 by adding section 169B, which authorized the EPA (a) to conduct research on regional visibility impairment and (b) to establish the Grand Canyon Visibility Transport Commission (GCVTC) for the assessment of appropriate actions under section 169A for protecting the Grand Canyon from regional visibility impairment caused by man-made sources. This charge was expanded by the U.S. EPA to include the 15 other Class I parks and wilderness areas on the Colorado Plateau. Work is now being performed to assess the scientific and technical data, studies, and other available information pertaining to adverse impacts on visibility from projected growth in emissions from sources located in the region. The U.S. EPA has also initiated a tracer study to evaluate the effects of emissions from the Mohave Power Project on visibility in the Grand Canyon National Park and other Class I areas in the Colorado Plateau. Because of these events, a major portion of

the funding for visibility research during the last two decades has been directed toward protecting pristine and scenic areas.

Interest in protecting visibility in urban areas has a much longer history and is strong at the present time. Smoke in European cities, especially London, has been a concern for centuries. Many of the modern advances in the understanding of atmospheric fine particles were made during the 1969 Pasadena Smog Experiment (see, for example, Whitby et al., 1972), which was followed by the Aerosol Characterization Experiment (ACHEX) sponsored by the California Air Resources Board (Hidy et al., 1980). The continuing interest in urban visibility is indicated in the list of short-term intensive visibility and aerosol studies summarized by the National Acid Precipitation Assessment Program (NAPAP) report on visibility (Trijonis et al., 1991) and discussed later in this chapter. Many of the studies focused on urban visibility.

Visibility impairment carries significant social and economic costs, which are discussed below.

Particulate matter also affects climate by increasing the absorption of solar radiation within the atmosphere and by increasing the fraction of solar radiation reflected into space (Charlson et al., 1992). The first effect causes heating within the atmosphere, especially where the concentrations of light-absorbing particles are elevated, and the second effect causes a cooling of the Earth. This cooling counteracts the heating caused by the greenhouse effect of gases that absorb infrared radiation.

8.1.2 Definition of Visibility

The National Research Council's Committee on Haze in National Parks and Wilderness Areas said, "Visibility is the degree to which the atmosphere is transparent to visible light." (National Research Council, 1993). Section 169A of the 1977 CAA Amendments (42 U.S.C. 7491) and the 1979 Report to Congress (U.S. Environmental Protection Agency, 1979) define visibility impairment as a reduction in visual range and atmospheric discoloration. Equating visibility to the visual range is consistent with historical visibility measurements at airports, where human observers recorded the greatest distance at which one of a number of pre-selected targets could be perceived.

Visibility may also be defined as the clarity (transparency) and color fidelity of the atmosphere. Transparency can be quantified by the contrast transmittance of the atmosphere. This definition of visibility is consistent with both (1) the historical records based on human observation of the perceptibility of targets, which include both the longest duration and most widespread records now available, and (2) the definition of visibility recommended by the National Research Council (National Research Council, 1993).

Air pollution can also alter the colors of the atmosphere and the perceived colors of objects viewed through the atmosphere. A complete quantification of visibility should include a measure of the color changes caused by the atmosphere. Such measures have been included in plume visibility models (e.g., Latimer et al., 1978), but there is no consensus on the best parameter to quantify color changes caused by air pollution from many sources.

Visibility is an effect of air quality and, unlike the particulate matter concentration, it is not a property of an element of volume in the atmosphere. Visibility can be defined only for a sight path and depends on the illumination of the atmosphere and the direction of view. The factors that control this dependence are described in the succeeding sections of this chapter.

8.1.3 Human Vision

Vision results from the human response to the electromagnetic radiation that enters the eye. Therefore, this presentation of the theory of visibility begins with a brief outline of the relevant properties of human vision.

The eye is most sensitive to green wavelengths, near 550 nm, and can perceive radiation between approximately 400 and 700 nm. The sensitivity of the eye is greatly diminished near the longest and shortest visible wavelengths. When measurements or calculations at only one wavelength are used to characterize visibility, it is customary to select a wavelength between 500 and 550 nm because these wavelengths are in the middle of the visible spectrum and the eye is most sensitive in this range.

The retina of the eye contains two types of receptor cells, rods and cones. The rods, used for nighttime vision, are not capable of perceiving color and are most concentrated in the parts of the retina used for peripheral vision. Rods are most sensitive at a wavelength of 510 nm and are insensitive to wavelengths longer than about 630 nm. The foveal pit, which

subtends an angle of about 1 degree, contains only cones, which are used for daytime color vision. There are no rods in approximately the central 2 degrees of the field of view. As a result, a faint light is best detected at night by looking in a slightly different direction. On the other hand, visual acuity is greatly diminished in peripheral vision. For example, at normal levels of illumination, text which is quite readable becomes unreadable when the direction of view is displaced by a few degrees so that the image of the text no longer falls on the fovea.

Human vision has a dynamic range of about 10^{12} cd/m^2 (candelas per square meter). Radiation becomes perceptible to the completely dark adapted eye at levels of about 10^{-6} cd/m^2. Cones begin to be activated at levels of about 10^{-3} cd/m^2, the rods cease to function at about 125 cd/m^2, and light levels above 10^6 cd/m^2 cause the observer to be uncomfortable and to feel blinded. The visibility regulations are usually interpreted as addressing daytime visibility, which is provided by the cones and is called photopic vision.

Contrast is widely used as a measure of the perceptibility of faint objects because of the following property of human vision. Weber's law, sometimes called Fechner's law or the Weber-Fechner law, states that for a wide range of luminance levels, to be just noticeably brighter, one patch of light must exceed the luminance of another by a constant fraction. Figure 8-1 and Equation 8-1 illustrate the definition of the contrast, C, of an object (target) of radiance, I, viewed against a background of radiance, I_b

$$C = (I - I_b) / I_b \, . \tag{8-1}$$

Figure 8-1 also illustrates the definition of modulation, M, of a sine wave with maximum and minimum radiances, I_{max} and I_{min}, respectively

$$M = (I_{max} - I_{min}) / (I_{max} + I_{min}) \, . \tag{8-2}$$

If the average radiance of the sine wave is indicated by I_b, then Equation 8-2 can be written

$$M = (I_{max} - I_b) / I_b \tag{8-3}$$

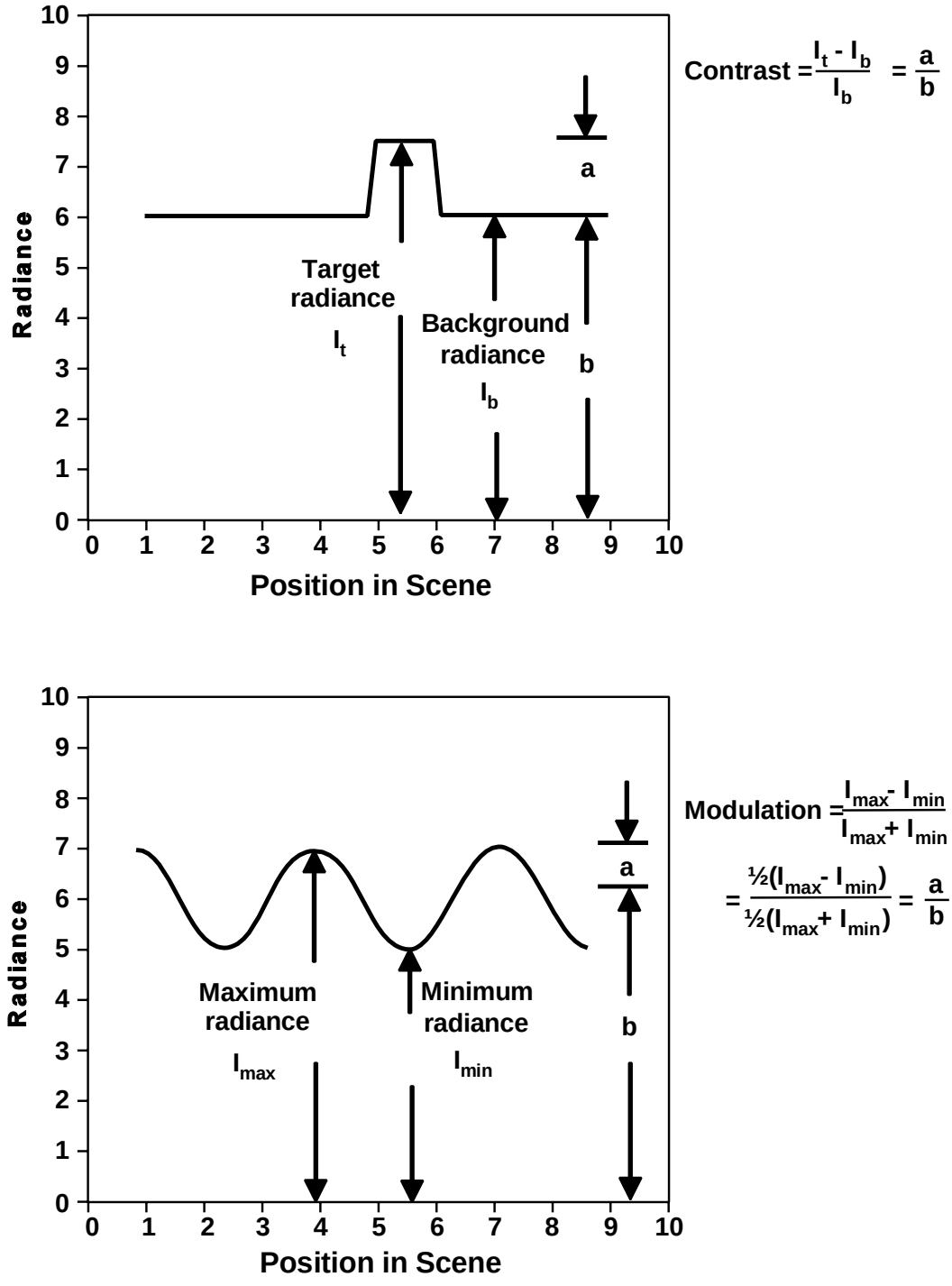

Figure 8-1. Diagrams showing the definitions of contrast and modulation. If the background radiance in the definition of contrast is equated to the average radiance in the definition of modulation, the definitions have the same mathematical form.

Source: Richards (1990).

which is identical in form to Equation 8-1. This transformation allows contrast and modulation to be used interchangeably in visibility calculations. It is shown below that the average radiance or background radiance in Equations 8-1 and 8-3 plays a key role in visibility calculations.

The accommodation of the eye, and its ability to perceive contrasts, changes in response to the general light level. The above definitions of contrast and modulation assume that the eye is accommodated to the background radiance. The effects of the accommodation of the eye can be experienced by first viewing objects in a relatively dark room, then going outside into bright daylight and viewing the same objects through an open window. Radiance differences that were perceptible when the eye was accommodated to those radiances become imperceptible when the eye becomes accommodated to a much greater radiance.

The perception of discoloration in the atmosphere depends on the properties of human color vision. Studies with color matches have shown that color vision is three dimensional. For example, images on color television or computer monitors are made up of red, green, and blue dots. All colors that the screen is capable of displaying can be specified by three numbers that quantify the intensity of the light from each of the three phosphors. For purposes of determining color matches, it is possible to characterize colors by these three numbers, X, Y, and Z, which are called tristimulus values. Colors that have the same tristimulus values will appear to match. In 1931, the Commission Internationale de l'Eclairage (CIE, or International Commission for Illumination) adopted a standard method of calculating these numbers from the spectrum of the light reflected from an object.

The perception of color depends on illumination and setting. For example, when there is a brilliant sunset, a white picket fence will appear to be white, but will be distinctly yellow in a color photograph. A nitrogen dioxide (NO_2) containing plume appears to be yellow against a blue sky even when a photograph or spectral measurement shows that the plume is blue, but less blue than the surrounding sky. The eye correctly perceives that a yellow gas is present in the plume. Spectral measurements have shown that the "Denver brown cloud" is a neutral gray (Waggoner et al., 1983).

These properties of human vision been described and explained by MacAdam (1981). The eye tends to perceive the lightest and brightest object in a scene as white, and to determine the color of other objects by comparison. For example, water clouds are typically

present in the sky above Denver. Spectral measurements show that they are blue compared to the color of sunlight, but the eye perceives them as white. The urban haze is not as blue as the water clouds in the sky, and by comparison, appears yellow or brown.

Because of this property of human vision, plume visibility models calculate the spectral radiance and tristimulus values of a "reference white." This reference is then used in the color calculations in the models.

8.2 FUNDAMENTALS OF ATMOSPHERIC VISIBILITY

This section presents a simple, complete, and reasonably accurate theory of daytime visibility for approximately horizontal sight paths. This theory provides the linkage between the nature and concentration of particulate matter in the atmosphere and visibility.

8.2.1 Geometry of the Atmosphere

The atmosphere is an extremely thin layer on the surface of the Earth, and all of its physical properties have strong vertical gradients. Half the mass of the atmosphere is at altitudes below 5.7 km (18,700 ft) mean sea level. The average of the equatorial and polar radii of the Earth is 6,370 km (3958 mi). Thus, most of the mass of the atmosphere is within a shell having a thickness 0.09% of the radius of the Earth.

The atmosphere is thin enough compared to the radius of the Earth that its curvature can be neglected in most optical calculations. This is not the case for sight paths that are horizontal or nearly so (Malm, 1979). Because of the curvature of the Earth, a sight path that is initially horizontal will have an altitude that increases with distance. Table 8-1 gives the approximate distances for selected increases in height above ground level. Sight paths longer than approximately 100 km (60 mi) are always subject to substantial changes in the properties of the atmosphere over the length of the sight path because of the changes in altitude. The atmosphere rarely has uniform optical properties over distances greater than a few tens of kilometers, even at a constant height above ground. Tabulations of air quality or visibility data that report visual ranges much greater than 100 km are based on assumptions that cannot be valid in the Earth's atmosphere.

TABLE 8-1. APPROXIMATE DISTANCES FOR SELECTED INCREASES IN HEIGHT OF AN INITIALLY HORIZONTAL SIGHT PATH

Height		Distance	
(m)	(ft)	(km)	(mi)
300	1,000	62	39
1,000	3,280	113	70
2,000	6,560	160	99
3,000	9,840	196	122
4,000	13,120	226	140

Optical calculations for the Earth's atmosphere are simplified if it is assumed that the Earth is flat and the atmosphere is horizontally uniform. Except for horizontal, or nearly horizontal, sight paths, it is an excellent approximation to neglect the Earth's curvature. An initially horizontal sight path above a curved Earth can be simulated in the calculations for a flat Earth by a sight path approximately 1.5 degrees above the horizontal sight path (Bergstrom et al., 1981). This angle depends on the vertical profile of the atmospheric haze, and can be calculated from an analytic expression in Latimer et al. (1978).

The variation in the optical properties of the atmosphere in the vertical dimension has received little attention in visibility monitoring and data reporting. Interest in the effects of particulate matter on climate forcing is causing a rapid expansion of the available information on haze aloft (see Section 8.8).

8.2.2 Illumination of the Atmosphere

Illumination of the atmosphere and factors affecting illumination of the sight path will affect visibility and visibility observations. Figure 8-2 shows the spectrum of the direct solar rays at the top of the atmosphere. Much of solar energy is in the visible wavelength range. Figure 8-2 also shows the spectra at the surface of the Earth for increasing amounts of atmospheric attenuation as the sun moves lower in the sky.

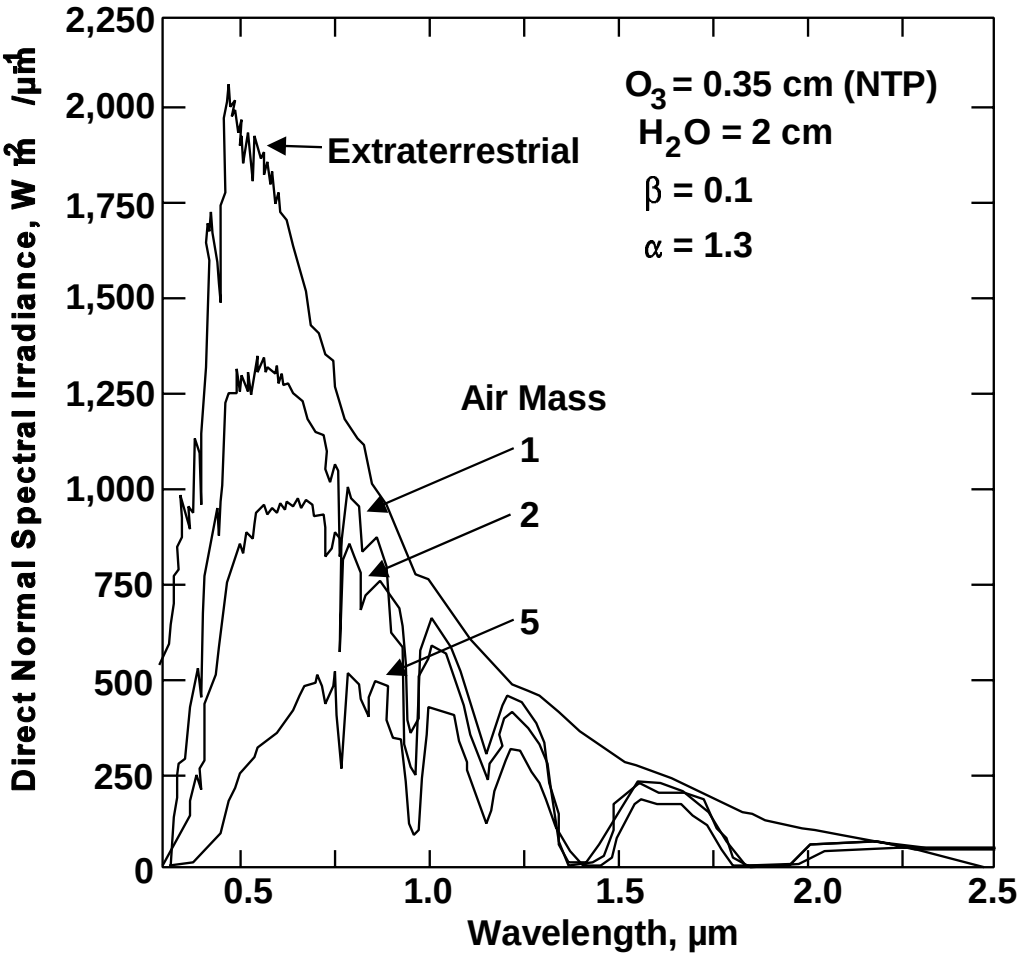

Figure 8-2. Spectrum of direct solar rays at the top of the atmosphere and at the surface of the Earth for various values of the air mass (m). The air mass equals 1 for an overhead sun and increases in proportion to the mass of atmosphere between the observer and the sun as the sun moves lower in the sky. The aerosol optical depth is $m \beta \lambda^{-\alpha}$, where λ is the wavelength in μm.

Source: Duffie and Beckman (1991).

The data in Figure 8-2 show that the atmospheric attenuation is greater at the shorter visible wavelengths than the longer visible wavelengths. This is because light scattering by air molecules depends inversely on the fourth power of the wavelength (as expressed in Equation 8-5). The greater atmospheric light scattering at the shorter wavelengths causes the blue sky in daytime and the familiar red and yellow colors at dawn and sunset. These color changes occur naturally, and are very great. They are much greater than would be caused by typical amounts of NO_2 in haze layers.

On a clear day, 80 to 90% of the visible solar radiation reaches the surface of the Earth without being scattered or absorbed when the sun is high in the sky. At the surface, a variable fraction is reflected upwards, so the atmosphere is illuminated both from above and below. The fraction of the radiation incident on the surface of the Earth that is reflected is known as the surface reflectance or the albedo. Both visibility and visibility observations are affected by clouds in the viewing background or overhead. The effects of clouds are readily apparent and are very great. The illumination of a terrain feature or the atmosphere in a sight path can change by a factor of 10 or more in a few minutes as clouds pass overhead. Very dark terrain can reflect only one tenth as much radiation as snow-covered terrain.

The derivations in the following subsections show that visibility is determined both by the illumination of the sight path and by the air quality in the sight path. The effects of the illumination are great enough and variable enough that it is not appropriate to omit them from quantitative discussions of visibility.

8.2.3 Optical Properties of the Atmosphere

The fate of the solar radiation that enters the Earth's atmosphere is determined by the geometry and optical properties of the atmosphere and the Earth's surface. This section presents definitions of the atmospheric optical properties that affect visibility and also presents data for the optical properties of gases. Data for the optical properties of particles are presented in Section 8.3. All of these optical properties are functions of the wavelength of light.

The atmosphere is a turbid medium, which both scatters and absorbs light. A ray of light passing through the atmosphere is weakened by both of these processes. The distance-rate of energy loss is proportional to the radiance of the ray, and the proportionality constant is the light-extinction coefficient, σ_{ext}, which has units of length^{-1}. The light-extinction coefficient is the sum of the light-scattering coefficient, σ_{scat}, and the light-absorption coefficient, σ_{abs}, which are the proportionality constants for energy loss from the ray caused by scattering and absorption, respectively.

The light-extinction coefficient can be further divided into coefficients for the following components:

σ_{ag}, light absorption by gases,

σ_{sg}, light scattering by gases,

σ_{ap}, light absorption by particles, and

σ_{sp}, light scattering by particles.

Because of their different origins and composition, atmospheric particles are frequently divided into coarse and fine particles (see Chapters 3 and 6). The corresponding division of σ_{sp} is

σ_{sfp}, light scattering by fine particles and

σ_{scp}, light scattering by coarse particles.

These components of the light-extinction coefficient are related as follows:

$$\begin{aligned} \sigma_{ext} &= \sigma_{abs} + \sigma_{scat} \\ \sigma_{ab} &= \sigma_{ag} + \sigma_{ap} \\ \sigma_{scat} &= \sigma_{sg} + \sigma_{sp} \\ \sigma_{sp} &= \sigma_{sfp} + \sigma_{scp} \end{aligned} \qquad (8\text{-}4)$$

Light scattering by gases is also known as Rayleigh scattering, and the coefficient can be calculated from the equation

$$_{sg} = 16.51(p/1013.25\ mb)(273.15\ K/t)\lambda^{-4.07}\ Mm \qquad (8\text{-}5)$$

where p and t are the ambient pressure and temperature and the wavelength, λ, is in micrometers (Edlen, 1953; Penndorf, 1957). Equation 8-5 was obtained by fitting values reported by Bodhaine (1979). At modest elevations and daytime temperatures, the coefficient for light scattering by gases has a value near 10 Mm^{-1} (or 0.01 km^{-1}) at a wavelength of 550 nm. This corresponds to an attenuation of a ray of green light in particle-free air of 1% per kilometer.

Light absorption by gases is predominantly caused by NO_2, and typically accounts for a few percent of the total light extinction in urban atmospheres. It is typically negligible in

remote areas. Nitrogen dioxide absorbs blue light more strongly than other visible wavelengths, and thus contributes to the yellow or brown appearance of urban hazes.

Ozone (O_3) absorbs ultraviolet light strongly and, in the visible range, has a weak absorption at green wavelengths. The absorption in the green wavelength could cause perceptible effects only if the O_3 concentration were much greater than 0.2 ppmv in a long sight path through a very clean atmosphere. These conditions are quite improbable.

The optical properties of particles are complicated enough that all of Section 8.3 is devoted to a summary of current knowledge. The remaining discussions in this section make use of that information as if it were presented here.

The appearance of the atmosphere, especially near the horizon, is affected by the relative importance of light scattering and absorption, which is measured by the single scattering albedo, ω_o,

$$\omega_o = \sigma_{scat}/\sigma_{ext} = \sigma_{scat}/(\sigma_{scat} + \sigma_{abs}) . \qquad (8\text{-}6)$$

When there is no light absorption, $\omega_o = 1$. As light absorption increases, the single scattering albedo becomes smaller, and hazes and the horizon sky become darker. Typical values for ω_o range between 0.8 and 1.0, even in smoke from fires.

When the direction of travel of radiation is changed by light scattering, the redirected radiation is not evenly distributed into all possible angles. The angular distribution of the scattered light is described by the phase function. This function was named by astronomers, and an example of its use is provided by the phases of the moon. The moon scatters light back toward the sun more strongly than in other directions, so the moonlight is strongest when the moon is full. Measuring the light from the moon during the progression from a new moon to a full moon would provide data for the phase function of the moon. The scattering angle is the angle through which radiation is deflected by the scattering process. This angle is near 0 degrees for a new moon and is 180 degrees for a full moon. (The infinitesimal deflection of radiation that passes near the moon is neglected in this discussion.)

The phase function for the scattering of unpolarized light by clear air (Rayleigh scattering) is

$$P(\theta) = (3/4)(1 + \cos^2\theta) \tag{8-7}$$

where θ is the scattering angle. This function is normalized so that the integral from 0 to π radians equals 2.

$$\int_0^{\pi} P(\theta)\sin\theta d\theta = 2 \tag{8-8}$$

This normalization is customarily used for all phase functions, and causes the integral over all scattering angles to equal 4π.

The optical depth, τ, associated with a distance in a turbid medium is equal to the definite integral of the light-extinction coefficient over that distance

$$\tau = \int \sigma_{ext} dx = \overline{\sigma}_{ext} x \tag{8-9}$$

where dx is the element of distance and $\bar{\sigma}_{ext}$ is the average of the light-extinction coefficient over the distance x. The transmittance, T, for a ray of light that passes through a medium of optical depth is

$$T = e^{-\tau}. \tag{8-10}$$

When distances in the atmosphere are specified in terms of the optical depth, the phase function and the single scattering albedo provide all the information about the optical properties of the atmosphere required for visibility calculations. As mentioned above, these quantities must be known as a function of wavelength.

Polarization has not been included. If polarization were included, radiances would be described by the Stokes vector and the phase function would be replaced by a phase matrix. In general, polarization effects are small enough that they can be neglected when considering the effects of air quality on visibility. However, polarization effects are readily apparent, and can be used to infer information about air quality (White, 1975).

Visibility is affected by atmospheric refraction (Minnaert, 1954). Those effects are often important, but are not discussed in any depth here because they are not closely linked to air quality. Atmospheric refraction causes mirages and looming, i.e., causes sight paths to be bent so the apparent positions of objects are displaced from their actual position. The refraction associated with thermal turbulence causes the stars to twinkle at night and distant objects to shimmer in the daytime. In general, an effort is made to eliminate the effects of atmospheric refraction from measurements and analyses to determine the effects of air quality on visibility.

This subsection has listed all the optical properties of the atmosphere that must be known to understand and calculate atmospheric visibility. With the inclusion of the absorption spectrum of NO_2 (Davidson et al., 1988), this section also presents all the required optical data for gases. The necessary optical data for particles are discussed in Section 8.3.

8.2.4 Multiple Scattering

The term, multiple scattering, is used when light is scattered more than once in a turbid medium. Light passing through a turbid medium transmits energy, and this process is known as radiative transfer. (Convective and conductive transfer of energy are also possible.) The equation that governs the light intensities, and hence the radiative transmission of energy in a turbid medium, is known as the equation of radiative transfer. Obtaining solutions of this equation for the Earth's atmosphere requires a knowledge of the optical properties of the atmosphere listed in Section 8.2.3 as a function of position and also a knowledge of the boundary conditions. The boundary conditions at the top of the atmosphere are (1) the atmosphere is illuminated by the solar radiation, and (2) radiation that leaves the top of the atmosphere does not return. The boundary condition at the bottom of the atmosphere is specified by the bidirectional reflectance of the Earth's surface. The reflectance albedo

indicates the fraction of the radiation incident on the Earth's surface that is reflected, and the bidirectional reflectance specifies both this fraction and the angular distribution of the reflected light as a function of the angle of incidence.

The equation of radiative transfer can be written

$$dI/dx = -\sigma_{ext}(I - I_e) \tag{8-11}$$

where dI/dx is the rate of change with distance x of a ray of radiance I and I_e is the source function. All of these quantities (except the distance x) are functions of the wavelength.

Middleton used the name equilibrium radiance for the source function. This name conveys the idea that the radiance of a ray always tends toward the "equilibrium" value as the ray progresses through the atmosphere. Also, if the radiance of a ray is equal to the source function, its value will not change with distance in the atmosphere. These properties are represented in Figure 8-3, which Middleton adapted from Hugon (1930). The rate of approach to the "equilibrium" is determined by the light-extinction coefficient. When the light-extinction coefficient has high values, e.g., in a fog, radiances approach the source function (equilibrium radiance) in short distances.

When the optical depth defined in Equation 8-9 is used in place of distance x in Equation 8-11, the equation of radiative transfer becomes

$$dI/d\tau = I_e - I\ . \tag{8-12}$$

This equation focuses attention on the source function. An intuitive understanding of the properties of radiation in the Earth's atmosphere must be based on an understanding of the source function and the factors that determine its value.

For horizontal sight paths, the horizon sky radiance typically provides a reasonable estimate of the source function. If the surface of the Earth were perfectly flat and the atmosphere and its illumination were perfectly uniform, the sight path into the horizon sky

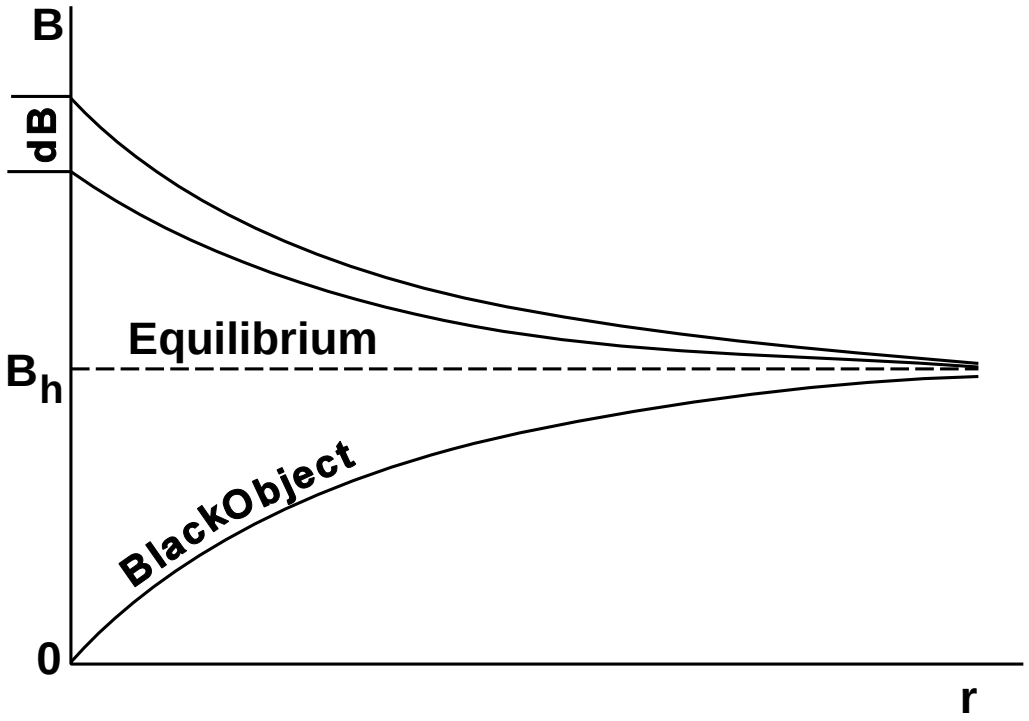

Figure 8-3. The approach of radiances in the atmosphere to the equilibrium radiance or source function.

Source: Middleton (1952).

would be limited in length by the atmospheric extinction. The curves in Figure 8-3 indicate that in this case, the horizon sky radiance would be equal to the source function. In the real world, the horizon sky radiance provides a good estimate of the source function if the light-extinction coefficient is great enough that the curvature of the Earth and nonuniformities of the atmosphere can be neglected for distances with an optical depth approaching a value of 3. This condition can be satisfied in fogs or moderate hazes. In practice, the greatest errors in equating the source function to the horizon sky radiance are due to variations in the optical properties of the atmosphere and its illumination along the sight path toward the horizon and beyond.

Further insight into the properties of the source function can be obtained from the equation of radiative transfer. When the radiance of a ray is equal to the source function, the radiance does not change as the ray is propagated. In this case, the removal of energy

from the ray by light extinction is balanced by scattering of light into the direction of the ray. This balance is expressed by the equation

$$\sigma_{ext} I_e = (\sigma_{scat}/4\pi) \int_{4\pi} I\,(\Omega')\, P\,(\Omega,\Omega')\, d\Omega'. \qquad (8\text{-}13)$$

The left side indicates the removal of energy by extinction per unit distance. The right side indicates the addition of energy by scattering per unit distance. The quantity, $I(\Omega')$, specifies the strength of the illumination of the path of the ray by radiation from the angle Ω'. The quantity $(\sigma_{scat}/4\pi)P(\Omega,\Omega')$ describes the amount of this illumination scattered into the direction of the ray. The phase function for scattering of radiation from the direction Ω' of the illumination into the direction Ω of the ray is $P(\Omega,\Omega')$. Because this function is normalized (see discussion of Equation 8-8), it is necessary to multiply by the light-scattering coefficient, which specifies the strength of the light scattering. The factor of 4π results from the conventions used in the normalization of the phase function. The integration extends over all angles.

Dividing both sides of Equation 8-13 by the light-extinction coefficient and using Equation 8-6 gives

$$I_e = (\omega_o/4\pi) \int_{4\pi} I\,(\Omega')\, P\,(\Omega,\Omega')\, d\Omega' \qquad (8\text{-}14)$$

which is the customary form of the equation for the source function. All the complications of radiative transfer calculations are contained in this equation. The value of the source function at each point in the atmosphere depends on the illumination at that point, which is affected by all the nearby surroundings.

Equation 8-14 can be simplified by making some reasonable, but not strictly valid, assumptions. The purpose of this simplification is to derive a formula that shows the dominant factors that affect the source function for an approximately horizontal sight path. This formula can then be used to develop an intuition for the factors that control visibility in the atmosphere and also to perform simple, approximate visibility calculations.

The first assumption is that the skylight is perfectly diffuse, i.e., that the radiance of the sky is the same in all directions. The second assumption is that the light reflected from the surface of the Earth is also perfectly diffuse. Richards et al. (1983) and Richards (1988) showed that these assumptions permit the integration in Equation 8-14 to be divided into integrations over each of two hemispheres to obtain

$$I_e = (\omega_0 / 4\pi)[2F_+ + 2F_- + F_s P(\Omega, \Omega_s)] \quad (8\text{-}15)$$

where ω_o is the single scattering albedo defined in Equation 8-6, F_+ is the flux of diffuse light reflected upward from the Earth's surface, F_- is the flux of diffuse skylight incident on the Earth's surface, F_s is the direct solar flux on the sight path measured normal to the solar rays, and $P(\Omega,\Omega_s)$ is the phase function for the scattering of radiation from the direction Ω_s of the solar rays into the direction Ω of the line of sight. Near the surface of the Earth, Equation 8-15 can be simplified by the relationship

$$F_+ = \alpha(F_- + F_s \cos\theta) \quad (8\text{-}16)$$

where α is the diffuse reflectance albedo of the Earth's surface and θ is the angle between the sun's rays and the normal to the Earth's surface. It is known that the assumptions used to derive Equations 8-15 and 8-16 are not strictly valid; the radiance reflected from the Earth's surface is not perfectly diffuse (Gordon, 1964), the skylight is also not perfectly diffuse, and these assumptions are worst when the sun is near the horizon.

The use of Equations 8-15 and 8-16 requires data for the flux of diffuse skylight. Figure 8-4 provides the necessary information for a broad range of cases in which the sky is cloud free. The curves in Figure 8-4 were calculated using the data and calculation methods in Richards et al. (1986). The atmosphere is represented by four layers of different composition. The composition and optical properties of the top three layers are kept constant. The curves in Figure 8-4 show the effects of increasing amounts of haze in the

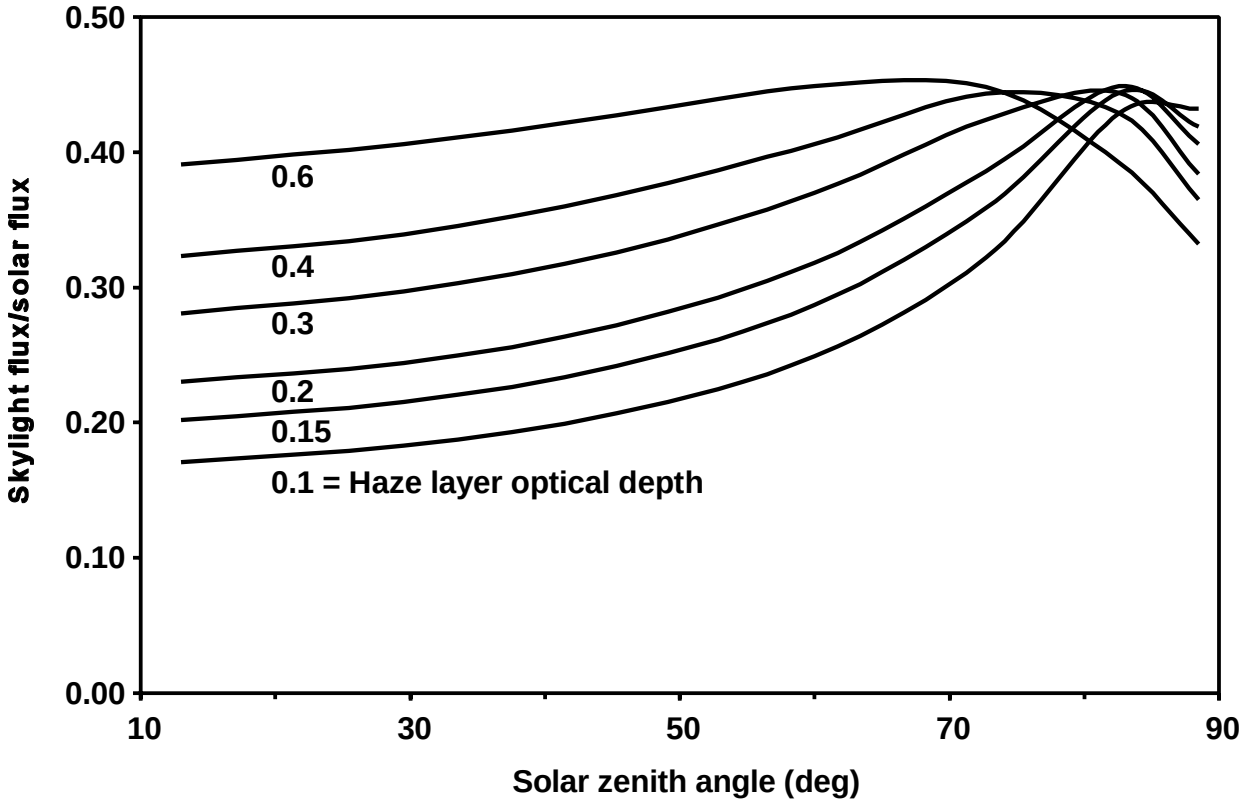

Figure 8-4. Data for the ratio of the total flux of skylight $F_{\downarrow}$ incident of the earth's surface to the solar flux $F_o\cos\theta$ on a horizontal surface at the top of the atmosphere. These data are a function of the solar zenith angle and the optical depth of the haze layer, which is the bottom of four layers used to represent the atmosphere.

Source: Richards et al. (1986).

bottom layer of the atmosphere. The amount of haze is measured by the optical depth, defined in Equation 8-9.

The aerosol in the bottom layer is composed of fine, coarse, and carbon particles with the same physical and optical properties as the bottom haze layer described by Richards et al. (1986). The relative volume concentrations of fine, coarse, and carbon aerosol are 46, 51, and 3%, respectively. The relative contributions to the light-extinction coefficients are 75, 12.5, and 12.5%, respectively. These proportions were kept constant as the total aerosol concentration was changed to vary the optical depth of the haze, τ_h.

The ordinate in Figure 8-4 is the total flux of skylight incident on the Earth's surface divided by the total flux of sunlight incident on a horizontal surface at the top of the

atmosphere, $F_o \cos\theta$. Equation 8-10 can be used to relate the solar flux at the Earth's surface, F_s to the solar flux at the top of the atmosphere

$$F_s = F_o e^{-(\tau_3 + \tau_h / \cos\theta)} \tag{8-17}$$

where τ_3 is the optical depth of the top three layers of the atmosphere used in the calculations (Richards et al., 1986). The optical depth is equal to 0.50, 0.134, and 0.079 at wavelengths of 370, 550, and 650 nm, respectively. These fluxes are for surfaces normal to the solar rays.

Equations 8-15 and 8-16 can be used to evaluate the relative roles of the factors that determine the source function, and hence the horizon sky radiance and path radiance (defined below). The role of the single scattering albedo defined in Equation 8-6 is immediately apparent; light absorption darkens the horizon sky by an amount proportional to the decrease in the single scattering albedo. The relative importance of (1) the direct solar radiation, (2) skylight, and (3) light reflected from the ground can also be evaluated. Table 8-2 presents data showing that light reflected from the ground always makes a significant contribution to the source function, and that sometimes this contribution is dominant. Past reviews of the optics of visibility have not adequately recognized the role of light reflected from the surface of the Earth. Mariners have long known that land over the horizon can be detected by the change in color of the horizon sky (U.S. Naval Oceanographic Office, 1966).

These calculations are simplified in the case of a uniformly overcast sky. In this case, the direct solar flux on the sight path measured normal to the solar rays, F_s, in Equations 8-15 and 8-16 is equal to zero, and these equations can be combined to obtain

$$I_e = (\omega_0 / 2\pi)(1 + \alpha) F_- \tag{8-18}$$

where F_- is the downward flux of diffuse light from the cloud layer. The ratio of the source function to the downward flux depends on the single scattering albedo and the diffuse reflectance albedo.

TABLE 8-2. RELATIVE IMPORTANCE OF LIGHT FROM GROUND, SKY, AND SUN IN CONTRIBUTING TO THE SOURCE FUNCTION AND THE PATH RADIANCE WHEN THE ABSORPTION IS NEGLIGIBLE AND THE NORMALIZED PHASE FUNCTION HAS A VALUE OF 0.4.

Conditions		Ratio of Source Function to Sunlight Flux (%)	Percentage of Source Function or Path Radiance Due to Light from the		
Ground Reflectance α	Ratio of Sky Light to Sunlight $F_{\cdot}/F_s$	100 I_e/F_s	Ground	Sky	Sun
0.10	0.10	6.53	26.83	24.39	48.78
0.15	0.10	7.40	35.48	21.51	43.01
0.20	0.10	8.28	42.31	19.23	38.46
0.40	0.10	11.78	59.46	13.51	27.03
0.80	0.10	18.78	74.58	8.47	16.95
0.10	0.20	8.28	23.08	38.46	38.46
0.15	0.20	9.23	31.03	34.48	34.48
0.20	0.20	10.19	37.50	31.25	31.25
0.40	0.20	14.01	54.55	22.73	22.73
0.80	0.20	21.65	70.59	14.71	14.71

$F_{\cdot}$ = the flux of diffuse light incident on the Earth's surface.
α = diffuse reflectance albedo.
I_e = source function for a ray of radiance.
F_s = the direct solar flux on the sight path measured normal to the solar rays.

Source: Richards (1988).

The equations in this section provide the basis for the radiative transfer calculations required to understand visibility as defined by the clarity (transparency) and color fidelity of the atmosphere (see Section 8.1.2).

The equations apply to a single wavelength; radiative transfer calculations must be performed for a representative series of wavelengths for a complete description of visibility. However, it would be compatible with current practice to perform these calculations only for one wavelength of green light, such as 500 nm or 550 nm, to determine the visibility. When addressing practical problems, it is essential to adequately address the strong temporal and spatial variations in the illumination and the optical properties of the atmosphere.

8.2.5 Transmitted Radiance Versus Path Radiance

The appearance of a distant object is determined by light from two sources. One source is the light reflected from the object itself. This reflected light is attenuated by scattering and absorption as it travels through the atmosphere toward the observer. The portion that reaches the observer is the transmitted radiance, I_t. These processes are illustrated in the top panel in Figure 8-5, where an observer looks at a distant hillside illuminated by direct sunlight, diffuse skylight, and light reflected from the surrounding terrain. The horizontal black bar indicates the light reflected from the hillside into the sight path. The small arrows pointing away from this bar indicate that some light is scattered into other directions. The decrease in the transmitted radiance with distance along the sight path caused by scattering and absorption is indicated by the horizontal bar becoming narrower as the distance increases.

The other source of light seen by the observer is the intervening atmosphere. During the daytime, the sight path is illuminated by the direct rays of the sun, diffuse skylight, light that has been reflected from the surface of the Earth, etc. This is indicated in the bottom panel of Figure 8-5 by the small arrows pointing toward the sight path. Some of this illumination is scattered by the air and particulate matter in the sight path toward the observer. The horizontal bar in the lower panel indicates the path radiance, I_p, which is an accumulation of this light scattered into the sight path. The width of the horizontal bar indicates that the path radiance has a value of zero at the start of the sight path at the hillside and increases with increasing distance along the sight path. Not all of the light scattered into the sight path reaches the observer. Some is absorbed and some is scattered into other directions as indicated by the small arrows pointing away from the sight path. Because the path radiance arises in the atmosphere, it is sometimes referred to as air light. The radiance seen by the observer looking at the hillside is the sum of the transmitted radiance and the path radiance.

The transmitted radiance carries the information about the object; this is the radiance which tells us what the object looks like. The path radiance only carries information about the intervening atmosphere and is often quite featureless. In a dense fog, the transmitted radiance from nearby objects can be seen, but the transmitted radiance from more distant

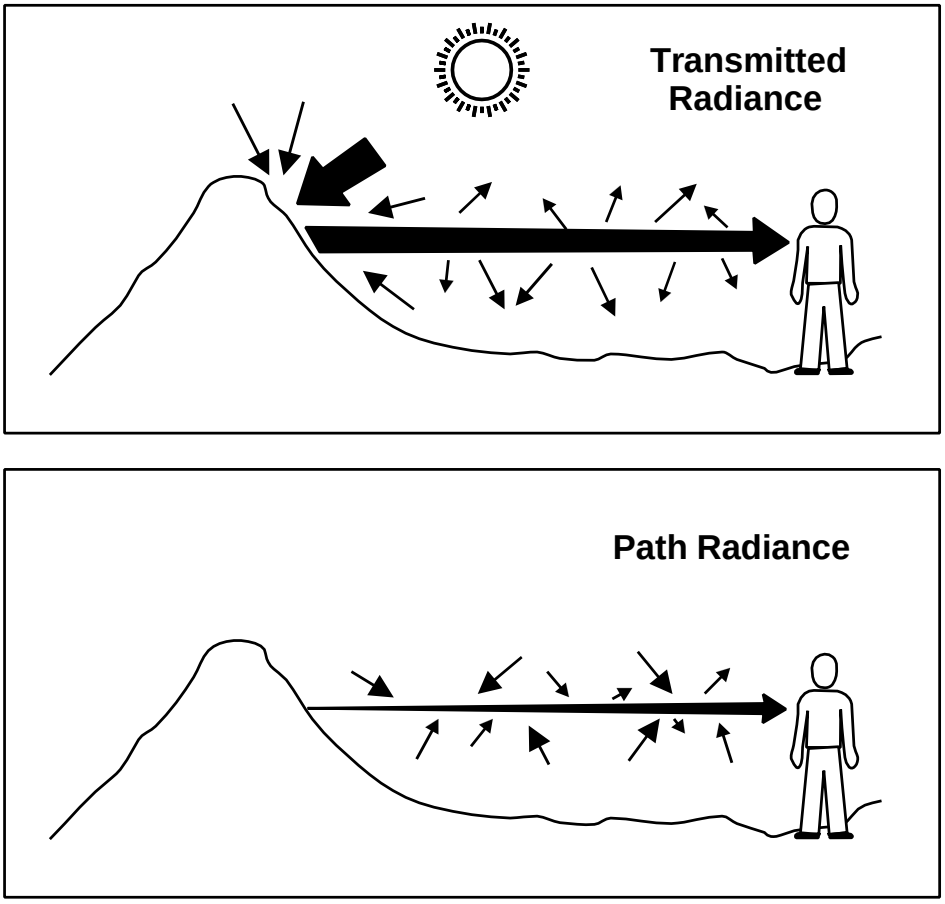

Figure 8-5. (A) Illustration of the transmitted radiance and (B) the path radiance for a sight path toward a hillside.

objects is completely overwhelmed by the path radiance, i.e., the light scattered by the fog. Distant objects are lost in the white (or gray) of the fog.

Visibility is determined by the competition between the transmitted radiance and the path radiance. The effects of this competition can be observed anytime the sun is low in the sky. Distant hillsides viewed toward the sun appear to be silhouettes; all details on their surface are lost in the haze. The reason is that the hillsides are in a shadow and, therefore, are dark. Only a small amount of light is reflected from them, so the transmitted radiance is small and is easily overwhelmed by the path radiance. Hillsides at a similar distance viewed looking away from the sun clearly show the details of trees, gullies, grass patches, etc. A large amount of light is reflected from these hillsides because they are sunlit, so the transmitted radiance is large. These effects can also be observed when portions of a scene

are shadowed by clouds and adjacent portions are sunlit. Cloud shadows on the atmosphere decrease the path radiance and improve the ability to see distant objects, but shadows on the objects themselves decrease the transmitted radiance and make it more difficult to see details in those objects. With practice, a discerning observer can visually evaluate the separate effects of the transmitted radiance and the path radiance on the appearance of a scene.

The remainder of this subsection presents a mathematical description of these effects. The radiance transmitted from an object at a distance x is equal to the initial radiance, I_o, of that object (measured at the object) multiplied by the transmittance, T, of the atmosphere in the sight path (see Equation 8-10).

$$I_t = I_o T = I_o e^{-\tau} \tag{8-19}$$

In general, the value of the light-extinction coefficient will not be uniform over the sight path, and this should be accounted for in the calculation of the optical depth (see Equation 8-9).

The completely general calculation of the path radiance requires solving the equation of radiative transfer for the atmosphere. However, if the illumination and optical properties of the atmosphere were uniform over the sight path, the path radiance could be calculated from the equation

$$I_p = I_e(1 - T) . \tag{8-20}$$

Equations 8-19 and 8-20 are typically used to calculate photographic images that show the effects of haze (see, for example, Equations 1 and 2 in Molenar et al., 1994). With rare exceptions, the calculations used to generate photographic images assume that the atmosphere is uniform.

The apparent radiance, I, is the radiance that enters the eye of an observer or the aperture of a measurement instrument, and is the sum of the transmitted and path radiance.

$$I = I_t + I_p \tag{8-21}$$

The radiances from these two sources must be considered in all visibility calculations. As stated above, it is the competition between the transmitted radiance and the path radiance that determines the visibility.

Because of the role of the path radiance in determining visibility, and because the path radiance is strongly influenced by the illumination of the sight path, daytime visibility is inextricably linked to the illumination of the atmosphere. A knowledge of the atmospheric optical properties alone (e.g., the value of the light-extinction coefficient) is not adequate to predict the visibility. These ideas are quantified in the next section, where contrast and contrast transmittance are used as measures of visibility.

8.2.6 Contrast and Contrast Transmittance as Quantitative Measures of Visibility

It is standard practice in science to define numerical scales that can be used to quantify observations. Because of the properties of human vision described in Section 8.1.3, contrast provides a numerical scale that can be used to quantify visibility. When investigating the ability to perceive faint objects, the use of contrast to quantify visibility is based directly on Weber's law and experiments with perception thresholds (see, for example, Blackwell, 1946). Contrast is defined in Equation 8-1 in Section 8.1.3.

The contrast of a distant object is determined by its initial contrast, C_o, and the contrast transmittance of the atmosphere, C/C_o. The definition of contrast transmittance is analogous to the definition of the transmittance. If C is the apparent contrast, i.e., the observed or measured contrast at the end of the sight path, and C_o is the initial contrast, i.e., the contrast at the start of the sight path, then

$$\text{Contrast transmittance} = C/C_o . \tag{8-22}$$

Modulation is defined in Equation 8-2 in Section 8.1.3. If M is the apparent modulation and M_o the initial modulation, then

$$\text{Modulation transfer} = M/M_0 . \tag{8-23}$$

As indicated by Equation 8-3, modulation and contrast can be used interchangeably. Similarly, contrast transmittance and modulation transfer can be used interchangeably. The more familiar contrast and contrast transmittance are used in this chapter.

The contrast transmittance of the atmosphere in the sight path to a distant object largely determines whether or not that object can be perceived. Thus, the quantitative calculation of contrast transmittance plays a key role in the investigation of the perceptibility of distant objects. At these distances, the contrast transmittance of the atmosphere and the apparent contrast of the object can be used to quantify visibility. If these parameters are used for objects at all distances, then the same numerical scales can be used to quantify the visibility of objects at all distances.

The National Park Service used contrast measurements to quantify visibility for approximately a decade beginning in the late 1970s. This monitoring method is continued in the use of photographs and video images to characterize visibility. Computer-generated photographs are often used to demonstrate the visual effects of haze, and they are generated by calculating the contrast transmittance of the atmosphere and the contrast of objects in the scene.

8.2.7 Contrast Reduction by the Atmosphere

Because of the quantitative relationship between visibility and contrast reduction by the atmosphere, the investigation of the effect of the atmosphere on apparent contrasts has a long history, which has been reviewed by Middleton (1952). An early result was obtained by Haecker (1905), who showed that radiance differences are attenuated by the atmosphere to the same degree as the radiance of a single ray. For example, if two objects at the same distance with initial radiances I_{1o} and I_{2o} are viewed through the same sight path, Equations 8-19 and 8-21 give the result that the difference in the apparent radiances is

$$- I_2 = (I_{1o} e^{-\tau} + I_{1p}) - (I_{2o} e^{-\tau} + I_{2p}) = (I_{1o} - I_{2o}) e^{-\tau} \qquad (8\text{-}24)$$

For the same sight path, the two path radiances have the same value, and therefore have no effect on the radiance difference. Also, the optical depth is the same for both sight paths. This result is valid regardless of the uniformity of the atmosphere and the illumination. If human perception were controlled by radiance differences instead of radiance ratios (as in the formula for contrasts), optical calculations for visibility analyses would have been greatly simplified.

Equation 8-24 applies to any two adjacent objects viewed through sight paths close enough together to have the same optical depths and path radiances. In the following derivation, this equation is applied to a case in which an object with initial radiance, I_o, is viewed against a background with initial radiance, I_{bo}. The definition of contrast in Equation 8-1 and contrast transmittance in Equation 8-22 can be combined to obtain

$$C/C_o = [(I - I_b)/I_b]/[I_o - I_{bo}]/I_{bo}] \; . \qquad (8\text{-}25)$$

Replacing $I - I_b$ by the right-hand side of Equation 8-24 and using Equation 8-19 gives the result

$$C/C_o = I_{bo} e^{-\tau}/I_b = I_{bt}/I_b \; . \qquad (8\text{-}26)$$

In other words, the contrast transmittance of the atmosphere is the transmitted radiance of the background, I_{bt}, divided by the apparent radiance of the background, I_b. The role of the path radiance is made more apparent by writing Equation 8-26 as

$$C/C_o = I_{bt}/(I_{bt} + I_p) \qquad (8\text{-}27)$$

where the apparent radiance of the background is equal to the sum of the background transmitted radiance and the path radiance. Equations 8-26 and 8-27 are completely general and contain no assumptions about the uniformity of the atmosphere or its illumination. They are included in the paper of Duntley et al. (1957), which contains an excellent overview of contrast reduction by the atmosphere.

Exactly the same derivation can be performed using the modulation defined in Equation 8-3 and modulation transfer defined in Equation 8-23 instead of contrast and transmittance. The result is

$$M/M_o = I_b/(I_{bt} + I_p) \tag{8-28}$$

where I_b is now the average radiance of the sine wave instead of the background radiance used in the definition of contrast. Equations 8-27 and 8-28 are identical in form and in interpretation.

Equations 8-19 and 8-21 can be used to show the dependence of contrast transmittance and modulation transfer on the variables T, I_{bo}, and I_e in cases where the atmosphere and the illumination are uniform over the length of the sight path

$$\begin{aligned} C/C_o &= I_{bo}T/[I_{bo}T + I_e(1 - T)] \\ M/M_o &= I_{bo}T/[I_{bo}T + I_e(1 - T)] \end{aligned} \tag{8-29}$$

The dependence of the T on the average light-extinction coefficient for the sight path is given by Equations 8-9 and 8-10.

Koschmieder (1924) derived a simple equation for the contrast of distant objects viewed against the horizon sky. He assumed that the radiance of the background horizon sky at the target initial background radiance is the same as at the apparent background radiance, with the result that Equation 8-26 becomes

$$C/C_o = e^{-\tau} \tag{8-30}$$

This assumption would be valid if the atmosphere and its illumination were uniform, which accounts for the long list of assumptions often associated with discussions of Equation 8-30 (Malm, 1979; U.S. Environmental Protection Agency, 1979). Only the one assumption above is necessary, and that assumption could be valid in a nonuniform atmosphere. If it is further assumed that the target is black, so that $C_o = -1$, Equation 8-30 becomes

$$C = -e^{-\tau} \tag{8-31}$$

but this assumption is not necessary if the value of C_o is measured or can be estimated with sufficient accuracy (see, for example, Malm et al., 1982). The average value of the light-extinction coefficient for the sight path is equal to the optical depth divided by the length of the sight path (see Equation 8-9). Equation 8-31 can be used to estimate the average value of the light-extinction coefficient from only a measurement of the apparent contrast of a dark object against the sky and the distance to the object. However, the assumptions used in the derivation of Equation 8-31 are generally not satisfied, with the result that the values of the light-extinction coefficient obtained from it may not be appropriate when illumination along the sight path is not uniform (White and Macias, 1987).

The nomogram in Figure 8-6A provides an instructive visualization of the factors that determine the visibility. In this figure, the abscissa is a linear measure of the light transmittance or light extinction. This is a change from Figure 8-3, where the abscissa is linear in distance. This change causes the curves for radiances in a uniform atmosphere to be straight lines instead of exponential curves.

The lines at the left side of Figure 8-6A show the radiances measured at the target. The initial radiance of the background (used in the calculation of contrast) measured at the target is I_{bo}. The path radiance is equal to zero. As the distance from the target increases, the initial radiance of the background and the transmittance decreases linearly towards zero. By definition, this line is always straight. With increasing distance, the path radiance (air light) typically increases. If the atmosphere were uniform, Equation 8-20 could be used to

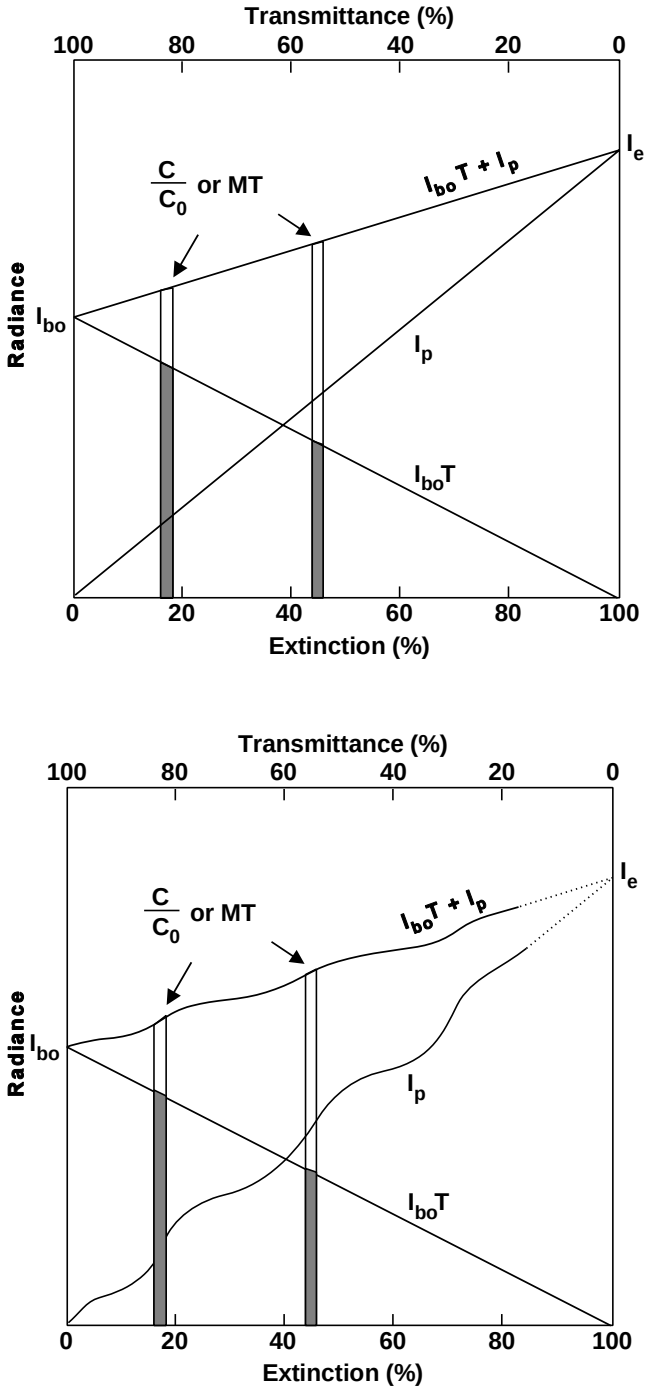

Figure 8-6. (A) Nomogram for the estimation of the contrast transmittance in a uniform region of the atmosphere; (B) Nomogram for the estimation of contrast transmittance in a nonuniform atmosphere. In a nonuniform atmosphere, the curve representing the path radiance will typically not be a straight line.

Source: Richards (1990).

calculate the path radiance, and the values would form a straight line as in Figure 8-6A. When the distance from the target becomes sufficiently great (which is possible in the Earth's atmosphere only for relatively large values of the light-extinction coefficient, the transmitted radiance becomes zero and the path radiance becomes equal to the source function, as at the right edge of the figure. This condition is easily observed in dense fogs.

The apparent radiance is equal to the sum of the transmitted and path radiances, and is shown by the upper line in the figure. The contrast transmittance can be calculated at any place in the figure by drawing a vertical line between the x-axis and the apparent radiance. The contrast transmittance is the fraction of the line due to the transmitted radiance. These fractions are illustrated by the shaded portions of the vertical lines in Figure 8-6A.

This nomogram shows how the relative values of the initial background radiance used to calculate contrast and the source function interact with the transmittance of the sight path to determine the contrast transmittance of a sight path, i.e., the visibility. When the initial background radiance is small compared to source function, the transmitted radiance rather quickly becomes a small part of the apparent radiance, and the visibility in that sight path is rapidly degraded by increasing light extinction. However, if the initial background radiance is much larger than source function, as is the case for snowcapped mountains, the transmitted radiance is not so quickly dominated by the apparent radiance as the light extinction in the sight path increases. Sometimes, snowcapped peaks at a distance appear to float in the sky because the transmitted radiance from the dark mountainsides below the snow line is completely dominated by the path radiance, making the dark mountainsides invisible.

The initial and apparent background radiances may be assigned to different parts of the scene in different calculations. If the contrast of an object against the horizon sky is to be calculated, the background is the horizon sky. When the horizon sky radiance is approximately equal to the source function, initial background radiance is approximately equal to the source function. However, if the contrast of a feature on a hillside, such as a tree or a rock, is to be calculated, then the background is the hillside. In this case, it is necessary to determine the ratio of the initial radiance of the hillside to the source function. In cases where the horizon sky radiance is approximately equal to the source function, this ratio is equal to the initial contrast used in contrast teleradiometry. Data for these initial contrasts have been tabulated for a range of types of ground cover and illumination (Malm et al.,

1982). These data provide an acceptable basis for estimating values of the background initial radiance/source function when measurements are not available.

The nomogram for a nonuniform atmosphere is shown in Figure 8-6B. Because the source function varies along the sight path, the path radiance does not vary linearly with the light extinction. This is indicated by the curve in Figure 8-6B. Regardless of the form of the curve for the path radiance, the apparent radiance is the sum of the transmitted and path radiances and the contrast transmittance is the transmitted radiance divided by the apparent radiance. Therefore, the calculations represented in the nomogram remain exactly valid for any curve representing the dependence of the path radiance on the fraction of the initial radiance removed by light extinction along the sight path. If the curve for the path radiance is properly calculated, the relations shown by the nomogram in Figure 8-6B are exact and contain no approximations.

8.2.8 Relation Between Contrast Transmittance and Light Extinction

The light-extinction coefficient determines the transmittance of a sight path (see Equations 8-9 and 8-10). The nomogram in Figure 8-6A shows that the transmittance provides a reasonable estimate of the contrast transmittance only when the initial radiance of the background is approximately equal to the source function (or equilibrium radiance). The only situation where this approximation is reliable enough to be useful is for a target viewed against the horizon sky when it is hazy enough that the horizon sky radiance is approximately equal to the source function. The southern and eastern United States have many days that are hazy enough to satisfy this criterion, so the use of the light-extinction coefficient as a measure of visibility frequently gives a satisfactory indication of the perceptibility of targets against the sky in those locations. However, the light-extinction coefficient may not provide a satisfactory indication of the perceptibility of features viewed against other backgrounds (e.g., trees on a hillside), because the radiances of other backgrounds will not, in general, be approximately equal to the source function.

Data for both the transmittance and modulation transfer of a sight path were measured during the Southern California Air Quality Study (SCAQS) (Richards, 1989) and are shown in Figure 8-7. Modulation and modulation transfer were used to present these data because the white and black pattern of the target were more like the sine wave pattern in Figure 8-1

than the pattern in that figure used to define contrast. It is shown in Equation 8-28 that the modulation transfer is mathematically equivalent to the contrast transmittance. It is apparent that the data for modulation transfer in Figure 8-7 are poorly correlated with the sight path transmittance. In particular, when the sight path transmittance was 50%, the modulation transfer varied from 5 to 70%. When the modulation transfer was 5%, the target was barely perceptible. A modulation transfer of 70% corresponds to the visibility for a 30-km (19-mi) sight path through particle-free air under conditions where the Koschmieder equation is valid. Thus, at the same value of the light-extinction coefficient, the visibility ranged from excellent to nearly obscured. However, the inability of the light-extinction coefficient to represent the perceived visibility of any specific scene does not affect its ability to characterize the visual effects on a sensitive scene caused by the combination of air pollutants and relative humidity. The data points in Figure 8-7 are scattered in the vertical direction, and do not tend to cluster along a simple relationship between modulation transfer and transmittance.

The lack of correlation between modulation transfer and light extinction in Figure 8-7 shows that the light-extinction coefficient does not, in the general case, provide a reliable quantitative measure of the visibility and specifically not under conditions of varying illumination. When using airport visibility data to estimate values for the light-extinction coefficient, it is common practice to select only midday data. This practice minimizes variations in the illumination of the atmosphere, and would reduce the variability of the data in plots such as Figure 8-7.

On the other hand, the light-extinction coefficient is an optical property of each point in the atmosphere and is closely linked to air quality. It also plays a key role in radiative transfer calculations. However, although the light-extinction coefficient is a key input to visibility calculations, it does not, by itself, provide a reliable quantitative measure of the degree to which the atmosphere is transparent to visible light under varying illuminations.

8.3 OPTICAL PROPERTIES OF PARTICLES

The 1978 report on the technical basis for visibility protection in Class I areas that was prepared for the Council on Economic Quality stated, "From a scientific and technical point of view, the optical effects of particles are also the best understood and most easily measured

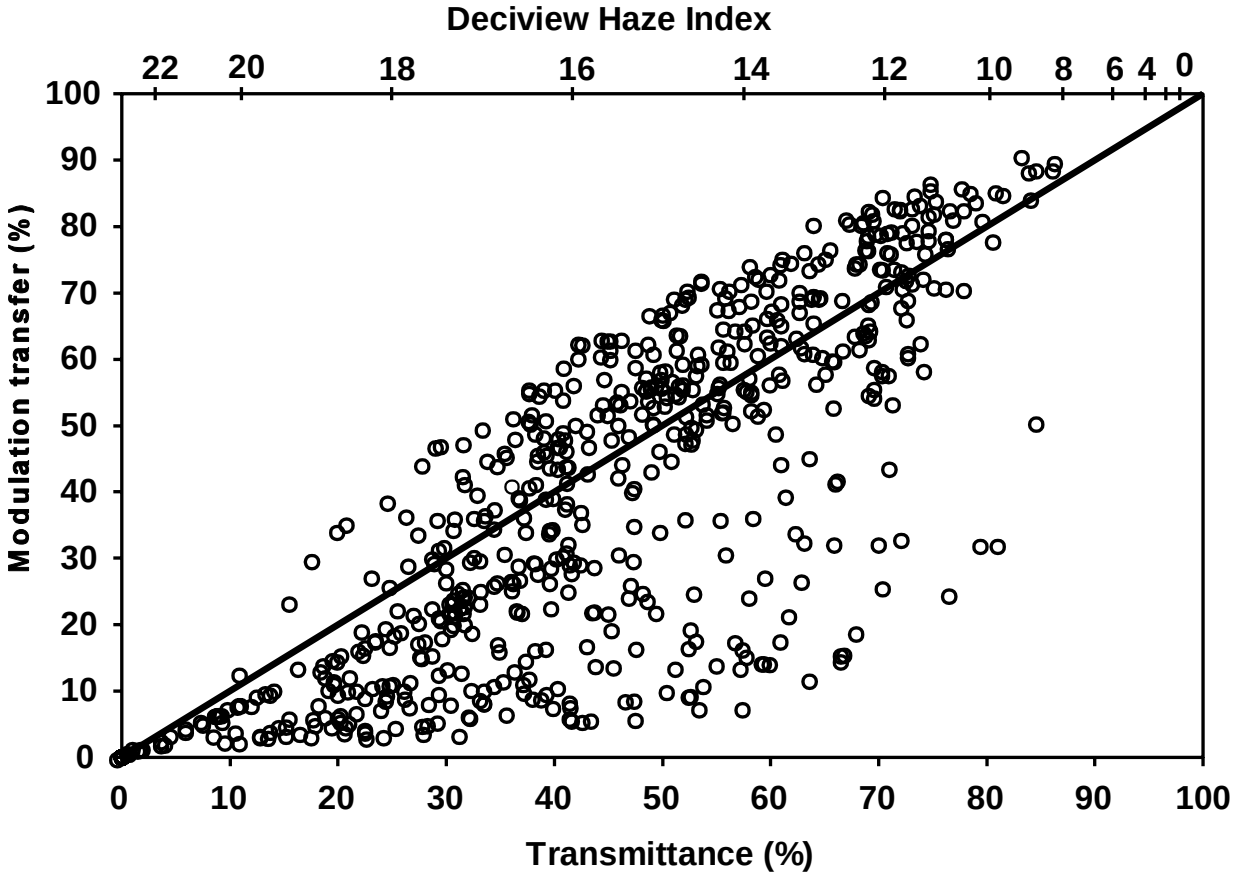

Figure 8-7. Hour-average values of the modulation transfer and transmittance measured in a 2.20-km sight path during the 1987 summer intensive of the Southern California Air Quality Study. These data show that the modulation transfer (and contrast transmittance) are poorly correlated with the light-extinction coefficient. At 50% transmittance (σ_{ext} = 315 Mm^{-1}), the visibility ranged from excellent to nearly obscured. The scale at the top shows the value of the deciview haze index, an index of haze that is scaled to correspond to properties of human vision.

Source: Richards (1989).

effects of air pollution." (Charlson et al., 1978). There was much truth in that statement, but since then, significant advances have been made in the understanding of the physical, chemical, and optical properties of fine particulate matter. At the present time, this is an active area of research and an area where significant future advances can be expected.

8.3.1 Optical Properties of Spheres

Fine particles, which are typically the dominant cause of visibility impairment, are small enough in comparison with the wavelength of visible light that their optical properties are nearly the same as those of homogeneous spheres of the same volume and average index of refraction. This approximation is good enough that by far the greatest uncertainty in using light-scattering equations for homogeneous spheres to calculate the optical properties of fine particles is due to uncertainties in their size distribution. Uncertainties in the index of refraction, due to lack of knowledge of the detailed particle composition, is the next greatest source of uncertainty in these calculations.

These assertions are supported by an example from the pigment industry. Titanium dioxide (TiO_2), the universally used white pigment, has a size distribution similar to atmospheric fine particles. Titanium dioxide particles are crystalline, and therefore have angular shapes. Titanium dioxide is birefringent, i.e., has different indices of refraction for different directions in the crystal. The size distribution of TiO_2 samples can be estimated by measuring the size of 1000 particles in an electron micrograph. Alternatively, it can be estimated by measuring the light-extinction coefficient as a function of wavelength for a dilute suspension and comparing the result with theoretical curves calculated assuming the particles were homogeneous spheres. It was found that one light-extinction spectrum gave a better estimate of the size distribution determined from repeated counts of 1000 particles than did one count of 1000 particles (Richards, 1973). A knowledge of the size distribution is key to calculating the optical properties of fine particles.

The equations for calculating the optical properties of homogeneous spheres in the size range of atmospheric particles are known as the Mie equations (Mie, 1908), but Lorenz, Debye, and others made substantial contributions to this theory (Kerker, 1969). The only inputs to these calculations are the particle-size parameter $\alpha = \pi D/\lambda$, where D is the particle diameter and λ is the wavelength of light, and the ratio of the index of refraction of the particle to the index of refraction of the medium surrounding the particle. For collections of particles, it is assumed that there is no phase coherence in the scattering by neighboring particles, so that the intensity of the light scattered by an ensemble of particles is the sum of the intensities scattered by the individual particles. Therefore, the optical properties of atmospheric particles are calculated by representing the aerosol particle-size distribution by a

histogram, performing Mie calculations for each particle-size bin in the histogram, weighting the results by the amount of aerosol in each bin, and calculating the sum.

The output of the Mie calculations includes efficiency factors for extinction, scattering, and absorption, Q_{ext}, Q_{scat}, and Q_{abs}, respectively. These factors give the fraction of the incident radiation falling on a circle with the same diameter as the particle that is either scattered or absorbed, only scattered, or only absorbed, respectively. Figure 8-8A shows the scattering efficiency factor for a sphere with an index of refraction of 1.5 as a function of the size parameter, α. Many fine aerosol particles have an index of refraction near this value. Because of diffraction, all particles with an index of refraction of 1.5 and a size parameter larger than about 1.6 scatter more radiation than falls on the geometrical cross section of the particle. The scattering efficiency factor tends toward a value of 2.0 for large particles.

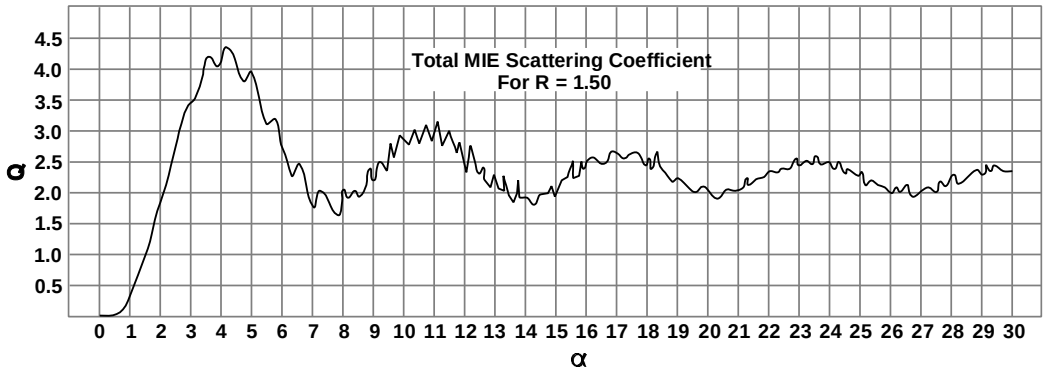

Figure 8-8a. Light-scattering efficiency factor for a homogeneous sphere with an index of refraction of 1.50 as a function of the size parameter $\alpha = \pi D/\lambda$.

Source: Penndorf (1958).

The major oscillations and ripples in the curve in Figure 8-8A are typical. The data in Figure 8-8B show that when the size parameter is scaled by the index of refraction minus 1, scattering efficiency factors for a range of indices of refraction fall in a narrow range of efficiency factors. The index of refraction range extends from water (n = 1.33) to a reasonable value for dry fine particulate matter (n = 1.5). For example, Hering and McMurry (1991) found that calibration of an optical particle counter with oleic acid, with an

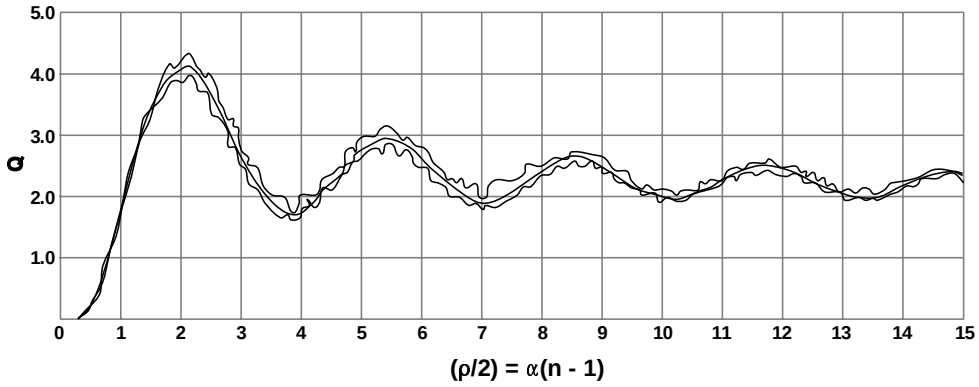

Figure 8-8b. Maximum and minimum values for light-scattering efficiency factors for homogeneous spheres with indices of refraction between 1.33 and 1.50 as a function of the normalized size parameter.

Source: Penndorf (1958).

index of refraction of 1.46, gave better results than did calibration with polystyrene latex spheres, with an index refraction of 1.59, for monodisperse samples of Los Angeles aerosol obtained from a differential mobility analyzer. Thus, within the range of indices of refraction that most commonly occur in atmospheric fine particles, the results of Mie calculations can be scaled to account for the effect of the index of refraction.

Figure 8-9 shows the same data as in Figure 8-8b, except that the scattering efficiency factor Q was multiplied by the cross section of the sphere to obtain the scattering cross section and divided by the volume of the sphere to obtain the volume-specific light-scattering efficiency factor, E_v, in units of μm^{-1}. A wavelength of 550 nm was assumed in these calculations. Multiplying the values of the light-scattering efficiency factor by the aerosol volume concentration (in units of $\mu m^3/cm^3$) gives the value of light-scattering coefficient, σ_{sp}, (in units of Mm^{-1}) for these particles. Thus, the curves in Figure 8-9 gives the light-scattering coefficient for a unit concentration of aerosol if all particles have the same diameter and index of refraction.

Dividing the curves in Figure 8-9 by the density of the particulate material (in units of g/cm^3) gives the mass-specific light-scattering efficiency, E_m (in units of m^2/g). Multiplying the values of the mass-specific light-scattering efficiency by the aerosol mass concentration (in units of $\mu g/m^3$) gives the value of the light-scattering coefficient (in units of Mm^{-1}) for these particles. Thus, the mass-specific light-scattering efficiency for water, which has an

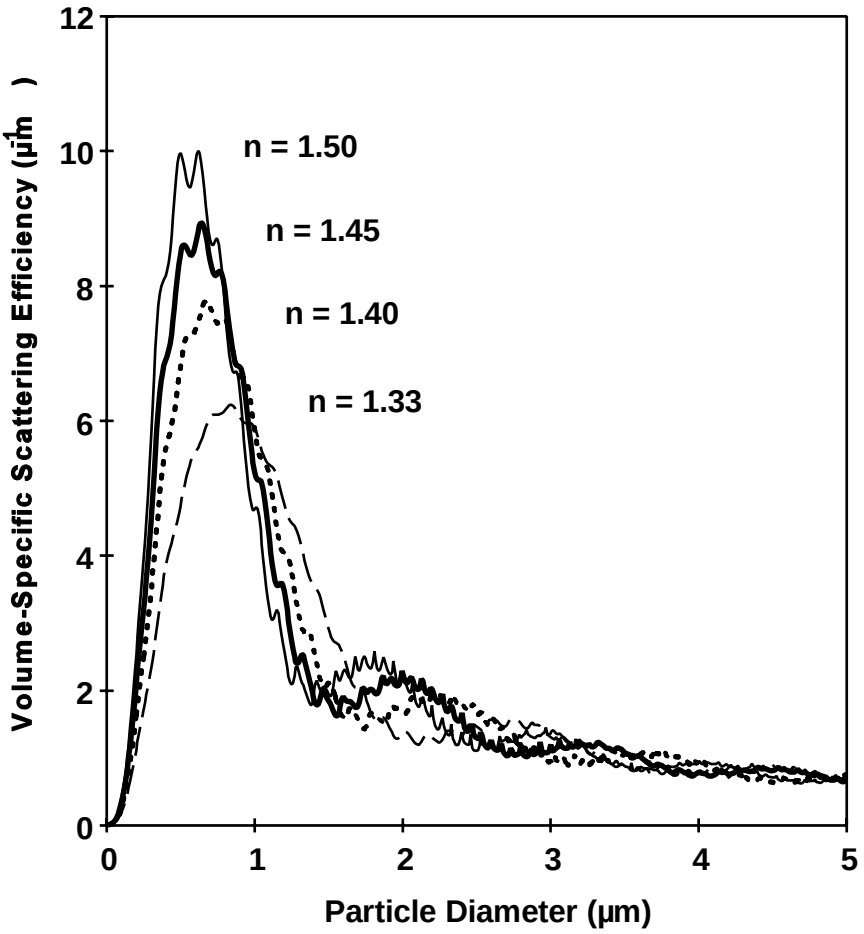

Figure 8-9. Volume-specific light-scattering efficiency as a function of particle diameter D_p. The calculations were performed for the indicated indices of refraction and a wavelength of 550 nm. For large particle diameters the scattering efficiencies tend toward a value of $3/D_p$. Mass-specific light-scattering efficiencies (in units of m^2/g) can be obtained by dividing the values of the curves by the particle density (in units of g/cm^3).

index of refraction of 1.33 and a density of 1.0, is shown by the curve for n = 1.33 in Figure 8-9. Ammonia salts have a density near 1.75 g/cm^3 and an index of refraction near 1.5, so the mass-specific light-scattering efficiency for these compounds can be obtained by dividing the curve for n = 1.5 in Figure 8-9 by 1.75 g/cm^3. The maximum value for mass-specific light-scattering efficiency for both water and ammonia salts is close to 6 m^2/g.

The particle diameter at the maximum light-scattering efficiency for green light with a wavelength of 550 nm is approximately given by the relationship

$$D = 0.28/(n-1)\ \mu m \qquad (8\text{-}32)$$

although the exact value depends on the ripples in the curve. This formula gives a diameter of 0.85 μm for an index of refraction of 1.33 and a diameter of 0.56 μm for an index of refraction of 1.5. Most fine aerosol particles are smaller, so it is generally true that processes which tend to increase the size of fine particles tend to increase their scattering efficiency. The absorption of water at high humidity is an example of such a process.

The Mie equations can also be used to calculate the efficiency factors for light absorption by particles. The results of these calculations contain significant uncertainties because (1) the imaginary component of the refractive index of the particles is usually not accurately known, and (2) light-absorbing particles are frequently chained agglomerates that do not have a spherical shape. In some aerosol particles, light absorption is caused by elemental carbon particles coated with chemical species that absorb light much less strongly (see, for example, Husar et al., 1976). For these reasons, the theoretical calculation of the strength of light absorption by atmospheric particles is significantly less reliable than the calculation of light scattering.

Computer codes are available for calculating the light scattering and light absorption by particles composed of a spherical core and a concentric shell (Toon and Ackerman, 1981; Appendix B of Bohren and Huffman, 1983; Kerker and Aden, 1991). These codes are used to determine the optical properties of particles with a solid core and a liquid shell, which can be formed by the absorption of water at high humidities by particles that contain insoluble species. A core-and-shell particle can also be formed by condensation and coagulation of materials of one refractive index on pre-existing particles that have a different refractive index.

The data for the volume-specific light-scattering efficiency for particles of one size in Figure 8-9 can be made more useful by averaging the values for log-normal size distributions. Results from such calculations are presented in Figure 8-10. As before, the calculations are performed for a wavelength of 550 nm. A value of 2.0 was used for the sigma of the log-normal size distributions, and the scattering efficiency was calculated as a function of the geometric mean diameter, D_{gv}. For water, the index of refraction is 1.33 and

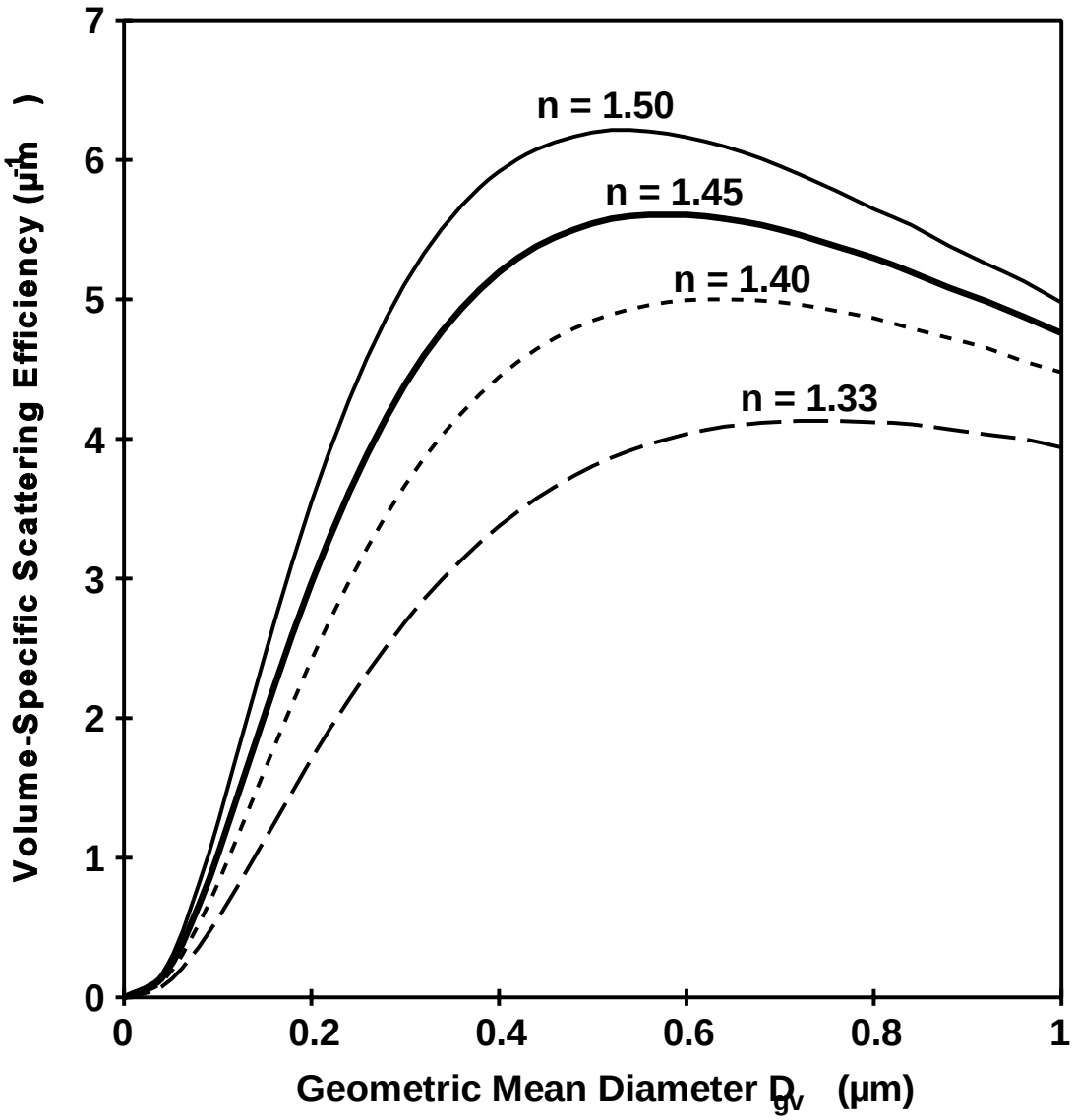

Figure 8-10. Volume-specific light-scattering efficiency as a function of geometric mean particle diameter D_{gv} for log-normal size distributions. The calculations were performed for the indicated indices of refraction, a wavelength of 550 nm, and size distributions with a sigma of 2.0. Mass-specific light-scattering efficiencies (in units of m^2/g) can be obtained by dividing the values of the curves by the particle density (in units of g/cm^3).

the maximum volume-specific scattering efficiency of 4.1 μm^{-1} occurs at a geometric mean diameter of 0.74 μm. For the index of refraction of 1.5, the maximum volume-specific scattering efficiency of 6.2 μm^{-1} occurs at a geometric mean diameter of 0.53 μm. If these particles had a density of 1.75, then the maximum mass-specific scattering efficiency would be 3.5 m^2/g. The curves in Figure 8-10 show that the scattering efficiency increases rapidly

with increasing particle size in the 0.2- to 0.4-µm-diameter range. The accumulation-mode aerosol is typically in this size range. Therefore, the uptake of water by aerosol particles can cause significant increases in the light-scattering coefficient.

Computer codes to calculate the optical properties of log-normal size distributions of homogeneous spheres can be obtained from the U.S. Environmental Protection Agency Support Center for Regulatory Air Models (SCRAM) by calling 919-541-5742 and downloading the files for the PLUVUE II plume visibility model. The FORTRAN source code is in the file RNPLUVU2.ZIP, code compiled for Intel 386- or 486-compatible computers is in the file RUNPLUVU.ZIP, and the manual is in PLVU2MAN.ZIP. These codes are available at no charge, and the program MIETBL.EXE calculates the normalized phase function and the efficiencies for light scattering, absorption, and extinction. These codes will run on any personal computer with enough speed, memory, and hard drive space to run Microsoft Windows®. If the parameters of the log-normal size distribution and the index of refraction can be satisfactorily estimated, these codes will generate all the information on the optical properties of particles required for the calculations described in Section 8.2.

Coarse particles in the atmosphere are large enough that the effects caused by their non-spherical shape can be detected (see, for example, Holland and Gagne, 1970; Wiscombe and Mugnai, 1988). However, in most actual cases, the dominant uncertainty in using the Mie equations to calculate the optical properties of coarse particles in the atmosphere is due to uncertainties in their size distribution. Therefore, obtaining data for particle-size distributions is more important than determining the shape of coarse particles in the atmosphere.

8.3.2 Optical Properties of Fine and Coarse Particles

Field measurements of the optical properties of fine and coarse particles have produced results compatible with the theoretical results described above. The mass-specific light-scattering efficiency is usually used to report these results. The mass-specific light-scattering efficiency (in units of m^2/g) multiplied by the particle concentration, c, (in units of $\mu g/m^3$) is equal to the light-scattering coefficient for particles (in units of Mm^{-1}). For these units, no

conversion factor is required. As discussed above, the value of the mass-specific light-scattering efficiency is different for different particle-size fractions.

White et al. (1994) determined the value of E_{fp}, the scattering efficiency for particles smaller than 2.5-µm diameter, at two sites in the desert southwest and obtained values of 2.4 and 2.5 m^2/g. These experiments were unique in that both the light scattering and particulate-mass concentration measurements were made with a 2.5-µm-diameter cutpoint. The relative humidity was generally low, so these values are appropriate for dry particles.

In the same experiments, White et al. (1994) also determined the value of E_{cp}, the scattering efficiency for coarse particles, and obtained values that ranged from 0.34 to 0.45 m^2/g. Earlier, White and Macias (1990) obtained an estimate of 0.4 m^2/g. Watson et al. (1991) also obtained a value of 0.4 m^2/g. One of the first determinations of the scattering efficiency for coarse particles was by Trijonis and Pitchford (1987), who obtained the value of 0.6 m^2/g. In all cases, these authors estimated that the integrating nephelometer responds to approximately half the light scattered by coarse particles (White et al., 1994), so the scattering efficiency for coarse particles observed by the nephelometer would be approximately 0.2 m^2/g. This is mentioned here to provide assurance that the values of the scattering efficiency for coarse particles near 0.4 m^2/g are not biased by the failure of nephelometers to detect light scattered at angles near 0 and 180 degrees.

A review article by Waggoner et al. (1981) indicates that at moderate or low humidities, the mass-specific light-scattering efficiency, measured by a nephelometer without a size-selective inlet, was equal to 3.1 ± 0.2 m^2/g using the fine-particle mass concentration. A good correlation was obtained even though the nephelometer measurements included both coarse and fine particles because of the small scattering efficiency of coarse particles. The nephelometer response to all particles reported by White et al. (1994) was 2.8 and 3.1 m^2/g times the fine-particle mass concentration at their two sites.

As a general rule, the above values of mass-specific light-scattering efficiencies can be used at moderate to low humidities. The effect of water uptake by particles at high humidities is discussed in Section 8.3.3.

Widely varying mass-specific scattering efficiencies can be observed near sources, in plumes, and in cases where particle formation occurred in clouds and fog. Particles formed in power station plumes in clean areas can be quite small. For example, during the Navajo

Generating Station Visibility Study (NGSVS), a pulse of SO_2 and sulfate from the station was observed at Hopi Point, 100 km from the source. Mie calculations based on the measured size distribution of the sulfate formed in the plume indicated a light-scattering efficiency for ammonium sulfate of 1.2 m^2/g, and this result agreed with the value determined from the integrating nephelometer readings and the sulfate concentrations determined by filter sampling (Richards et al., 1991). Closer to the source, the sulfate formed in the plume was in still smaller particles with an even smaller light-scattering efficiency (Richards et al., 1981).

Larger light-scattering efficiencies for fine particles have been observed when significant numbers of the particles are in the 0.5- to 1.0-μm size range. The measurements of John et al. (1990) provide an example of data for particles in this size range. Secondary particles in this size range are the result of heterogeneous gas-to-particle conversion in fogs or clouds (Meng and Seinfeld, 1994). However, heterogeneous particle formation in fogs or clouds does not always produce large particles. Events in which large amounts of sulfate were rapidly formed in clouds were observed in the NGSVS, and these typically produced sulfate with a smaller mean diameter than the background aerosol (Richards et al., 1991).

Because of the strong dependence of both the light-scattering efficiency and settling velocity of coarse particles on particle size, it would be expected that the light-scattering efficiency of coarse particles in an air parcel would vary with time. In cases where coarse particles are not being added to the air parcel, the light-scattering efficiency of the coarse particles would increase with time.

The great majority of light absorption by particles is caused by elemental carbon (Rosen et al., 1978, Japar et al., 1986). Determinations of the mass-specific light-absorption efficiency of elemental carbon gives values in the range of 9 to 10 m^2/g (Japar et al., 1984; Adams et al., 1989). A value of 9 m^2/g has been used in recent studies of urban haze with satisfactory results (Watson et al., 1988, 1991).

8.3.3 Effect of Relative Humidity on Particle Size

Water in the atmosphere exists in both the particle and vapor phases. Great reductions in visibility occur when water condenses to form fog or clouds. Water is also present in all

ambient particles, even on relatively clear days. The increase in the amount of water in the particle phase that occurs at high relative humidity (RH) has a significant effect on visibility.

The effect of water has been understood for many decades, and was one of the key areas of investigation in the Aerosol Characterization Experiment (ACHEX) in California in the 1970s (Hidy et al., 1980). Figure 8-11 shows a summary of Humidogram data measured in several parts of the United States. These data were obtained by comparing the integrating nephelometer signal from an ambient aerosol sample conditioned to 30-% RH with the signal from the same aerosol conditioned to a higher RH (Covert et al., 1980). The increase in light scattering with increasing RH is due to two factors: (1) the absorption of water by the aerosol particles increases the volume of the particle phase, and (2) the absorption of water increases the size of the aerosol particles, which increases the light-scattering efficiency of most particles.

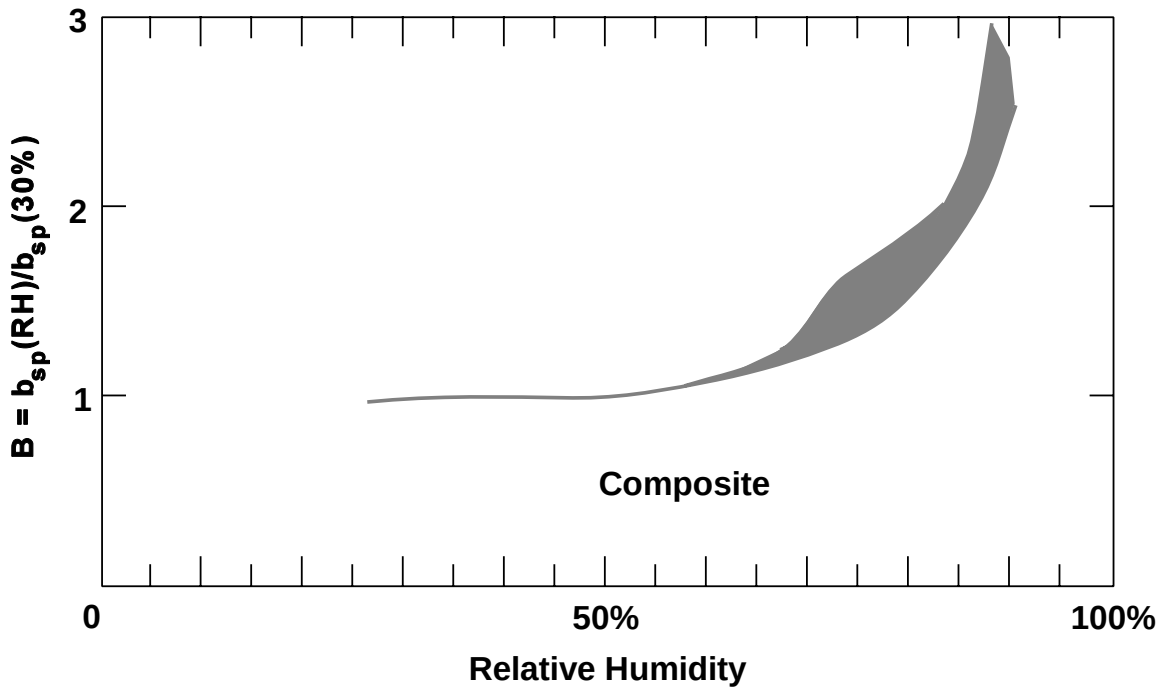

Figure 8-11. Humidogram showing the dependence of the light-scattering coefficient of ambient aerosol on the relative humidity. The shaded area shows the range of values obtained in various areas of the United States. The vertically hatched area shows data for strongly deliquescent sulfate aerosol observed at Tyson, MO and marine aerosol at Point Reyes, CA.

Source: Covert et al. (1980).

Ammonium salts are an aerosol component that contribute to the absorption of water at high RH. Figure 8-12 shows the relative diameter of a pure ammonium sulfate particle as a function of RH. At humidities above the deliquescence point of 80%, the particle is a liquid solution, the higher the RH, the more dilute the solution and the larger the particle. When the RH is below 80%, the particle is a dry ammonium sulfate crystal at equilibrium. If the RH of the air surrounding liquid ammonium sulfate decreases through the deliquescence RH, it is necessary for a crystal to nucleate for the conversion from liquid to solid to occur. For pure solutions, this can require either tens of minutes to hours or the reduction of the RH far below the deliquescence point. Thus in ambient air deliquescence particles frequently exist in a non-equilibrium state, containing water even though the RH is below the deliquescence point.

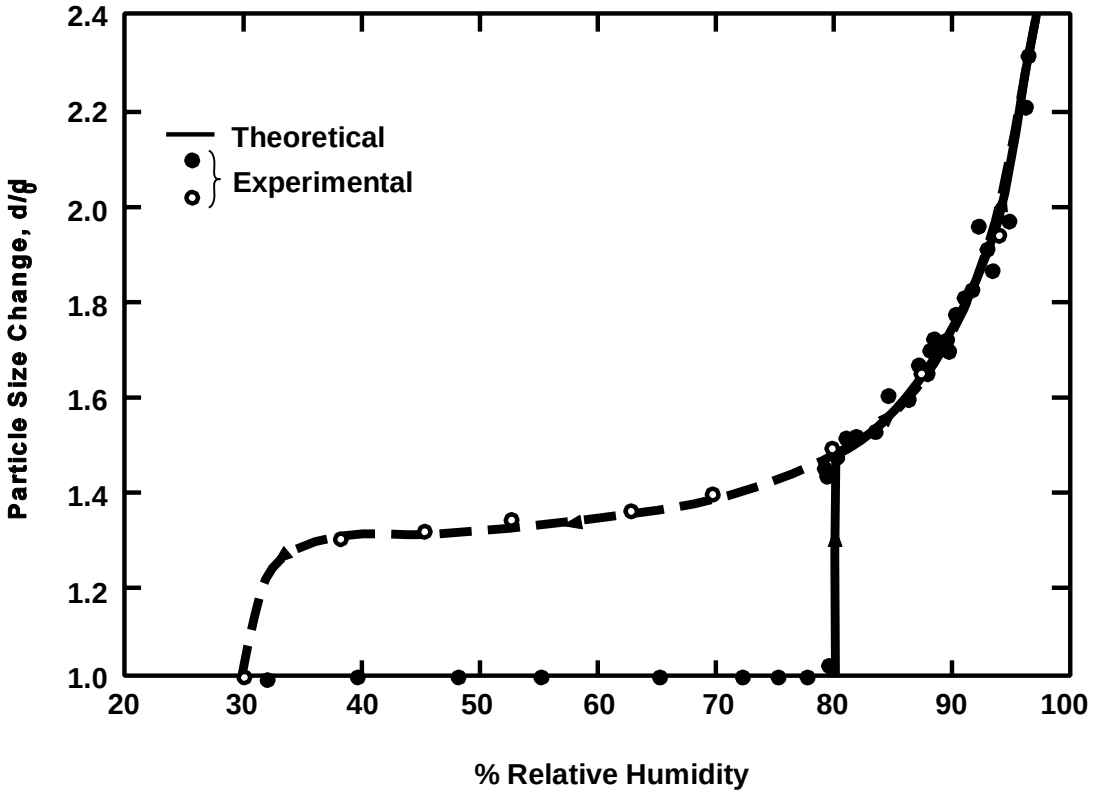

Figure 8-12. Relative size growth is shown as a function of relative humidity for an ammonium sulfate particle at 25° C. The dotted line indicates the size of the liquid particles when the RH decreases below the deliquescence point without nucleation of the solid phase.

Source: Tang et al. (1981).

Ambient particles are always a mixture of chemical compounds. Different salts have different deliquescence points, and some aerosol components, such as sulfuric acid and perhaps some organic compounds, have water absorption properties represented by a smooth curve. Therefore, a typical sample of ambient aerosol shows a smooth dependence of light scattering on RH, as shown in Figure 8-11. Figure 8-13 shows data from experiments that can detect the change in size of individual particles in response to a change in RH. These data show that the ambient particles in the Los Angeles Basin tended to fall either in a more hygroscopic class, presumably containing inorganic salts and acids, and a less hygroscopic class, which may be predominantly composed of primary organic species (McMurry and Stolzenburg, 1989). The particles in the desert Southwest tended to grow more with increasing RH, suggesting that ammonium salts are present in most fine particles (Zhang et al., 1993, 1994) and that the organic compounds in the particles are more oxidized (Saxena et al., 1995).

The RH of the atmosphere is nonuniform in both space and time, so the ambient aerosol is continually subjected to cycles of RH. Radiational cooling increases the RH at night near the surface of the Earth, and this tends to increase the haze in the early morning. Also, atmospheric convection frequently cycles the aerosol particles through clouds during the day. Rood et al. (1989) have shown that hysteresis like that shown in Figure 8-12 exists in the atmosphere, so it is reasonable to believe that the ambient particles are commonly on the upper curve, which represents the properties of the particles that have recently been exposed to high values of RH.

Data for the dependence of the particle size of the ambient aerosol on RH have also been obtained by cascade impactor measurements in urban and rural environments, and are in reasonable agreement with the Humidogram in Figure 8-11. Good examples of this type of measurement appear in a report by Watson et al. (1991) and papers by Zhang et al. (1993, 1994). A more detailed discussion of the effects of RH on the size distribution of ambient particles is given in Chapter 3.

8.3.4 Extinction Efficiencies and Budgets

The attribution of visibility impairment to emission sources can proceed through a series of steps in which the following are determined in sequence: (1) emissions,

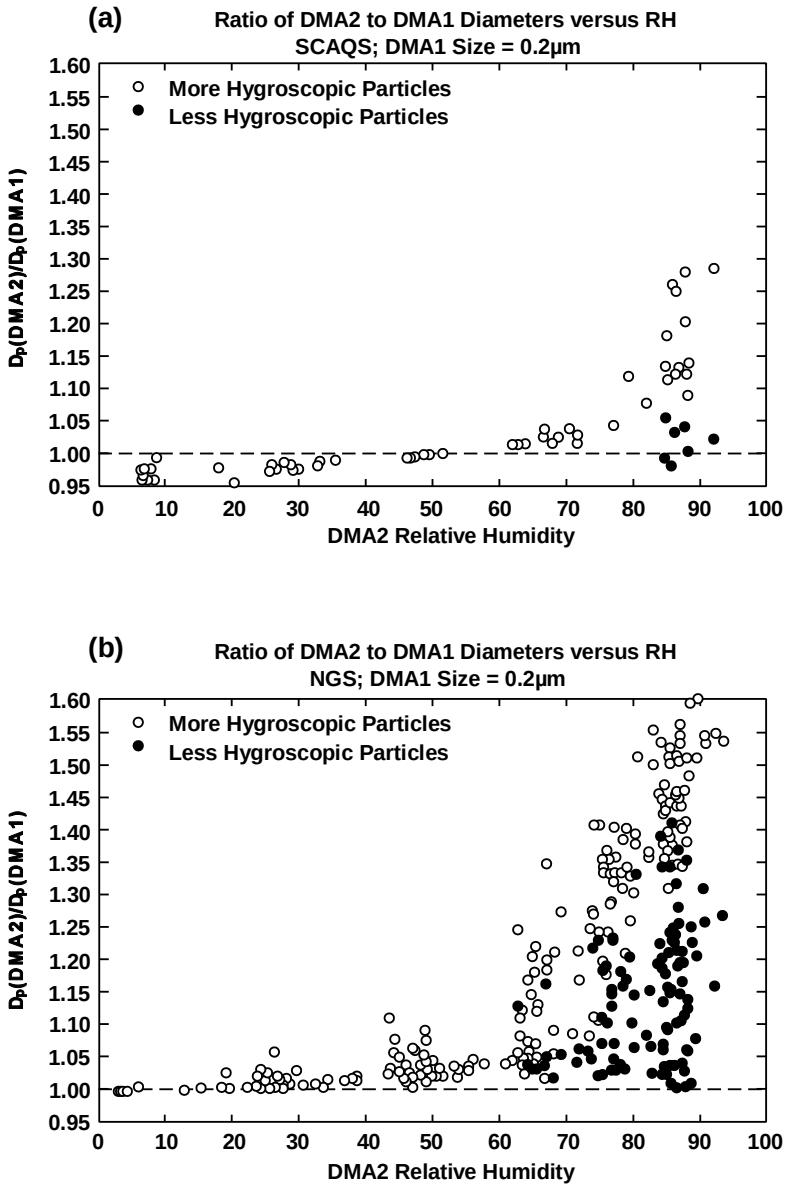

Figure 8-13. Summary of all relative humidity-dependent particle growth factors for 0.2 μm diameter particles measured (a) in Claremont, CA during the SCAQS and (b) at Hopi Point in the Grand Canyon National Park during the Navajo Generating Station Visibility Study.

Source: McMurry and Stolzenburg (1989); Zhang et al. (1993).

(2) composition of the atmosphere, (3) optical properties of the atmosphere, (4) optical properties of sight paths, and (5) visibility. In principle, the effects of selected emissions can be determined by performing the above analysis steps with and without those emissions.

This section addresses the calculation of the optical properties of the atmosphere from a knowledge of its composition. This is an essential step in the source attribution of visibility impairment. This calculation is also useful in understanding current visibility conditions. Portions of this calculation proceed through simple addition. Section 8.2.3 showed how the optical properties of the atmosphere can be represented as the sum of the components of light extinction. It also indicated that the light-scattering coefficient for particles can be represented as the sum of the scattering by coarse and fine particles. Operationally, the separate contributions of coarse and fine particles to the light-scattering coefficient can be determined by using instruments with size-selective inlets.

It would be convenient if the light-scattering coefficient for fine and coarse particles, σ_{sfp} and σ_{scp}, could each be represented as the sum of the light scattering by the chemical constituents of those particles. Then the components of light extinction could be calculated from

$$\sigma_{sfp} = \Sigma E_j c_j \qquad (8\text{-}33)$$

where E_j is the light-scattering efficiency of fine-particle species j whose concentration is c_j and the sum includes all species. Unfortunately, there is no theoretical basis for such a representation, because the light-scattering efficiency depends strongly on the particle size, and changing the atmospheric concentration of one chemical species can change the size distribution of the other particulate species (White, 1986; Sloane, 1986; Sloane and White, 1986).

Simple additive calculations can be justified theoretically only in the hypothetical case of an externally mixed aerosol, in which each particle contains only one chemical species. In this case, the contribution of each chemical species to light extinction can be determined by summing the contributions of the particles of each species. The calculation in Equation 8-33 can be performed on either a particle volume or particle mass basis. The mass basis is customarily used because aerosol mass concentrations are more easily monitored, so most ambient data are for particulate mass concentrations.

In practice, useful approximations exist that allow the estimation of light extinction by ambient particles from the aerosol composition. White (1986) showed that it made little

difference in the calculated optical properties of an aerosol mixture to assume either that the chemical species are externally mixed, as described above, or internally mixed. In an internally mixed aerosol, all particles in a stated particle-size cut have the same composition, i.e., they each have the same proportions of all chemical species. This finding has been confirmed by other authors, including Lowenthal et al. (1995). Lowenthal et al. (1995) showed that for an internally mixed aerosol, it made little difference whether each particle was assumed to be homogeneous, or assumed to be composed of a core of insoluble species and a shell of species that form a solution at high humidities. Thus, useful estimates of the aerosol optical properties can be constructed by assigning extinction efficiencies to chemical species, multiplying the ambient concentrations by the efficiencies, and summing the results.

Two key inputs to this estimation are (1) estimates of the size of the (dry) particles and (2) estimates of the water uptake associated with each chemical species with increasing RH. If it is known that the chemical species were mostly formed in homogeneous (i.e., dry) photochemical reactions, then it can be assumed that most particles are in a size mode with a diameter in the 0.2- to 0.3-μm size range (see, for example, Meng and Seinfeld, 1994; John et al., 1990). However, in locations where particle formation is active, the particle-size distribution can be shifted toward smaller particle sizes. If it is known that most particles were formed heterogeneously (i.e., in liquid particles), then the particle size is less certain. John et al. (1990) observed that the droplet mode particles formed in the Los Angeles Basin typically had a mean size near 0.7 μm. Sulfur particle-size distributions measured in the NGSVS show that droplet mode particles formed in a relatively clean environment could have a mean size near 0.2-μm diameter (Richards et al., 1991). Small particles are formed when only a small amount of particulate matter is formed in each cloud drop. The effects of water uptake on light extinction are discussed in Section 8.3.3.

When designing control strategies to improve visibility, it is necessary to estimate the change in light extinction that would result from a change in the atmospheric composition. It would be convenient if Equation 8-34 could be used for this calculation.

$$\Delta\sigma_{sfp} = \Sigma E_j \Delta C_j \qquad (8\text{-}34)$$

However, as illustrated by the hypothetical curves in Figure 8-14, the light-scattering efficiency of fine particle species j is typically not a linear function of the species concentration. Therefore, the value of the light-scattering efficiency for fine particles to be used in Equation 8-33 to calculate the contribution of species j to light scattering when its concentration has the value indicated by point a, (shown by the slope of the dashed line through the origin), is typically different from the value of the light-scattering efficiency of fine particle species j to be used in Equation 8-34 to calculate the change in the contribution to light scattering when the concentration is reduced from point a to point b (shown by the slope of the dotted line that passes through points a and b).

The literature contains data for extinction efficiencies defined both ways, so the reader should maintain an awareness of this distinction. Lowenthal et al. (1995) have published an analysis of the sensitivity of light-extinction efficiencies to the methods and assumptions used in their calculation and have presented values calculated using different assumptions.

Light-extinction budgets have the objective of estimating the fraction of the total light extinction contributed by each chemical species. Because the chemical species in particles do not scatter light independently, light-extinction budgets are somewhat arbitrary. Budgets can be calculated from estimated extinction efficiencies and measured species concentrations using Equation 8-33, but the values obtained depend on the assumptions used. Many tabulations of light-extinction efficiencies and budgets have been published. Some of the more recent data and reviews are in the National Acid Precipitation Assessment Program report (Trijonis et al., 1991), a separate publication of some of those data (White, 1990), a summary of IMPROVE data (Malm et al., 1994), and a review of light-extinction calculation methods and the results from their application to data from recent field studies (Lowenthal et al., 1995).

8.4 INDICATORS OF VISIBILITY AND AIR QUALITY

8.4.1 Introduction

Air quality standards to protect human health designate an indicator, which is the atmospheric constituent (such as O_3) whose concentration is regulated. The standards also specify a concentration level and a form. The form specifies such variables as the averaging

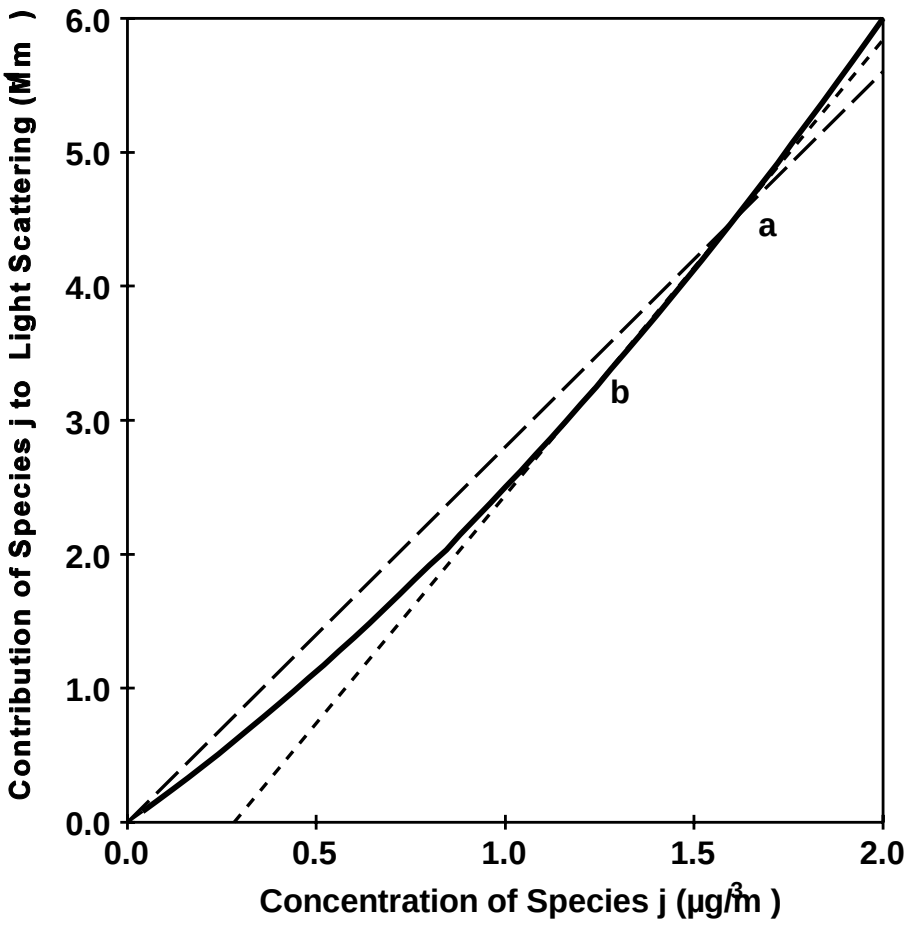

Figure 8-14. Hypothetical curves showing the effect of nonlinearities on the mass-specific light-scattering efficiency. The bold curve shows the contribution of species j to the light-scattering coefficient as a function of the concentration of species j. The slope of the dashed curve gives the mass-specific light-scattering efficiency to be used in Equation 8-33 for the species concentration at point a. The slope of the dotted curve gives the efficiency to be used in Equation 8-34 when the species concentration changes from point a to point b.

time and the number of times the average concentration may exceed the concentration level of the standard in a specified length of time. Indicators are selected on the basis of their linkage to the human health of populations, and the levels are set based on data for the health of classes of sensitive individuals.

A similar approach is also useful when considering visibility standards; some property of the atmosphere related to visibility must be selected as an indicator. Factors which may be considered in making this selection include (1) the linkage between the indicator and

visibility, (2) the cost and feasibility of monitoring the indicator to determine compliance with the standard as well as progress toward achieving the standard, (3) the nature and severity of the interferences inherent in the available monitoring methods, (4) the relationship between the visibility indicator and indicators for other air quality standards, and (5) the usefulness of monitoring data in analyses which have the purpose of determining the optimum control measures to achieve the standard.

Even though contrast and contrast transmittance provide numerical scales that can be used to quantify visibility, they are not suitable indicators of visibility for regulation of visibility protection based on air quality. Visibility is strongly affected by the illumination of the sight path, which is largely determined by natural processes that are not subject to regulation. Visibility is also affected by meteorological conditions, such as very high humidity, precipitation, and fog, which are also not subject to regulation. Furthermore, the derivations presented above show that complex calculations are required to relate contrast and contrast transmittance to air quality.

A secondary standard to protect visibility has the objective of setting an air quality standard that ensures visibility protection. Therefore, it is appropriate to select an indicator more closely linked to air quality than to visibility. In this case, the indicator would not be closely linked to the visibility along a specific sight path at a specific time. Instead, the indicator would be linked to the distribution of visibilities observed as a function of the value of the indicator. The level of the standard could be set to protect sensitive views under specified illumination conditions. This relationship between the indicator and visibility is similar to that for standards set to protect human health.

The following sections discuss parameters that could be used as indicators for regulation of visibility protection based on air quality.

8.4.2 Visual Range from Human Observation

The use of visual range from human observation as an indicator of visibility is listed here for historical reasons. The National Weather Service is discontinuing the observations at airports, so the number of locations at which observations are being made is now declining rapidly. In 1989, the California Air Resources Board changed the standard for visibility

reducing particles, replacing the observation of visual range with an instrumental measurement (VanCuren, 1989a,b).

There is a long history of recording the most distant target that can be perceived, or alternatively, whether or not a distant target can be perceived. For example, Husar et al. (1981) cited data from visibility observations at the Blue Hill Observatory in Massachusetts that extended from the 1880s to the 1950s. During recent decades, visibility at all major airports throughout the United States has been recorded hourly during the daytime by human observation. These data have been used to determine visibility trends in the United States as well as the spatial distribution of current visibility conditions (see, for example, Trijonis et al., 1991; Husar and Wilson, 1993). No other visibility measurement provides an historical record for the United States of comparable usefulness.

The advantages of human observations of visibility are: (1) they provide a direct measure of the visibility as defined in Section 8.1.2, (2) no special equipment is required, and (3) manpower requirements are minimal if an observer is already present for other reasons. The disadvantages are: (1) the results depend on the observer and the available visibility targets, and (2) in general, the data are poorly related to air quality. However, the linkage to air quality can be improved by using only midday observations not influenced by meteorological effects such as fog, precipitation, or very high humidities.

Middleton (1952) reports data from experiments in which photometric measurements were made in parallel with routine visibility observations. There was a wide range in the measured contrasts of the targets selected by the observers to indicate the visual range. These data document only one source of uncertainty in human observations.

8.4.3 Light-Extinction Coefficient

The light-extinction coefficient is the parameter most frequently used by the air quality community to characterize visibility because it is closely linked to air quality. The advantages of using the light-extinction coefficient are that it is: (1) an intensive property of the atmosphere (i.e., a property of an element of volume of the atmosphere), (2) closely linked to air quality, (3) can be directly measured by a commercially available instrument, and (4) is a key input for the radiative transfer calculations needed to calculate the visibility.

The light-extinction coefficient can be directly measured by a transmissometer (Molenar et al., 1990, 1992) or it can be estimated by measuring the components of light extinction listed in Equation 8-4 (dry scattering and absorption, or ambient scattering and absorption) and calculating the sum (see, for example, Malm et al., 1994; Richards, 1995). There are several key disadvantages of using the transmissometer to monitor the light extinction coefficient. These disadvantages include: (1) transmissometer measurements respond to meteorological effects such as fog and precipitation, and (2) the commercially available transmissometer is difficult to calibrate and maintain. For example, the optical windows need to be cleaned frequently. It is a further disadvantage of transmissometer measurements that the measurement error is large compared to the effects of air pollution when the atmosphere is very clear.

The effects of meteorological conditions on light extinction can be very great; they frequently completely obscure the sight path. In applications such as airport runway control, where visibility is the prime concern, it is appropriate to include these effects in the monitoring data. However, when the effect of air quality on visibility is the prime concern, it is important to remove meteorological effects from the monitoring data. This is recognized by the IMPROVE protocols for processing transmissometer data. Measurements made at relative humidities above 90% are flagged because they may be affected by meteorological effects such as fog, clouds, or precipitation (Blandford, 1994). It is standard practice to exclude these data from statistical summaries (Mercer, 1994). However, it is nearly impossible to remove these effects to a satisfactory degree because it is nearly impossible to distinguish between snow flurries or rain showers on the one hand or puffs of haze on the other. Subjective judgement enters into the flagging of transmissometer data. Furthermore, particle formation is often enhanced at high humidity, so failing to collect visibility-related air quality data at high humidities is a significant omission (Richards, 1994).

The value of the light-extinction coefficient calculated from the sum of its components listed in Equation 8-4 could be used in place of transmissometer measurements as an indicator of visibility. In this case, it is an option to exclude the contribution of gases to the light-extinction coefficient and to include only the contribution of particles. Light scattering by gases can be omitted because it is nearly constant and cannot be regulated. Light absorption by gases can be omitted because it is primarily due to NO_2, whose concentrations

are (1) already subject to regulation, and (2) typically too small outside urban areas to have a significant effect on visibility. If such calculations use the ambient scattering, the light-extinction coefficient, as is the case with transmissometer measurements, will be strongly dependent upon the relative humidity and so will not be a good indicator of air quality. If the air sample is dried the light-extinction coefficient will be a better indicator of air quality but a poorer indicator of visibility.

In 1989, the California Air Resources Board adopted a standard for visibility reducing particles that is calculated from the sum of the light-scattering coefficient for particles and the light-absorption coefficient for particles. Light scattering by particles is measured by a heated, enclosed integrating nephelometer (see Section 8.4.5) and light absorption by particles is measured with a tape sampler (VanCuren, 1989a,b).

8.4.4 Parameters Calculated From the Light-Extinction Coefficient

8.4.4.1 Visual Range

The visual range can be calculated from a measurement of the light-extinction coefficient at a point by assuming (1) that the atmosphere and the illumination over the sight path is uniform and (2) the threshold contrast is 2%. Then, for a black target, the left side of Equation 8-31 has the value -0.02 and Equation 8-9 can be used to obtain

$$\text{Visual Range} = 3.91/\sigma_{ext} \tag{8-35}$$

which is known as the Koschmieder equation. This equation is useful when the value of the light-extinction coefficient is large enough that the visual range is small enough for the assumptions to be valid. The assumptions are quite questionable for visual ranges larger than 10 to 20 km, and invalid for visual ranges greater than about 100 km (see Section 8.2.1).

In addition, the use of visual range calculated from a point measurement of the light-extinction coefficient is useful as an indicator of visibility related to air quality. It does, however, have the same disadvantages as associated with the use of transmissometer measurements of light-extinction coefficients listed in Section 8.4.3.

8.4.4.2 Deciview Haze Index

The deciview haze index, dv, was proposed by Pitchford and Malm (1994) to provide an indicator of haze that is scaled to correspond to the properties of human vision. It is calculated from the light-extinction coefficient for green light by the equation

$$dv = 10 \log_{10}(\sigma_{ext}/10\ Mm^{-1}) \quad (8\text{-}36)$$

This index has a value of zero, approximately 10 Mm^{-1} at sea level, where the light-extinction coefficient has the value for particle-free air (see Equation 8-5) and increases by one unit for each 10% increase in the value of the light-extinction coefficient. The logarithmic scaling is similar to that of the decibel scale, which is also related to human perception.

As described in Section 8.2.8 and the above sections, the light-extinction coefficient is closely linked to air quality. Therefore, the deciview haze index is similarly a measure of haze, and is closely related to air quality. The scale at the top of Figure 8-7 indicates that for a given sight path, the deciview haze index is linked to the visibility only in the range of light-extinction values that correspond to sight path transmittances between roughly 20 and 80%. Outside this range, changes in the deciview haze index have a greatly decreased effect on visibility. For example, increases in the deciview haze index will not change the appearance of features that are already completely obscured by haze.

The deciview haze index is well suited for presenting data for spatial and temporal trends of haze. It is not influenced by the many factors unrelated to air quality that affect visibility, and it is scaled to approximately linearize the relationship between human perception and the haze index. However, its use as an indicator of visibility has the disadvantages associated with the use of transmissometer measurements of light-extinction coefficients listed in Section 8.4.3.

8.4.5 Light-Scattering Coefficient Due to Particles

There are several advantages to using the light-scattering coefficient for particles as an indicator of visibility effects. They include: (1) it is the component of the light-extinction

coefficient primarily responsible for visibility impairment; (2) it is closely linked to fine particle concentrations; (3) a number of monitoring methods and commercial instruments are available; (4) the cost of implementing the monitoring methods and maintaining measurement instruments is competitive with those for other indicators; (5) accurate instrument calibration methods are available; (6) interferences can be reduced to an acceptable level and are as well understood as for any other indicator; (7) it is typically measured continuously; and (8) commercial instruments are available that are either designed to include or designed to exclude meteorological effects.

There is a linkage between the light-scattering coefficient for particles and visibility because the dominant cause of visibility impairment is light scattering by particles. The components of the light-extinction coefficient other than the coefficient for light scattering by particles are the coefficient for light scattering by gases, which is nearly constant, and the coefficient for light absorption by gases and particles. Light absorption does not contribute to the path radiance, and under some circumstances, decreases it significantly. Therefore, under some lighting conditions, light absorption does not degrade visibility as effectively as does light scattering. In extreme cases, the addition of absorption to the sight path has no effect on visibility (e.g., sun glasses), or can even increase the apparent contrast of bright objects viewed against the horizon sky by darkening the background sky and thereby increasing the initial contrast (Dessens, 1944; Middleton, 1952). On the other hand, increasing the light-scattering coefficient for particles always decreases the transmitted radiance and increases the path radiance, so it always impairs visibility, which depends on the competition between the transmitted radiance and path radiance. However, athough the light-absorption coefficient is not significant to visibility impairment for every scene as is the light-scattering coefficient, the light-absorption component of the light-extinction coefficient is important in overall visibility impairment.

The available monitoring instruments include: (1) the enclosed integrating nephelometer (Ahlquist and Charlson, 1967), (2) the open integrating nephelometer (Molenar et al., 1992), and (3) forward scatter visibility monitors (see, for example, National Oceanic and Atmospheric Administration, 1992). The enclosed nephelometer can be fitted with a size-selective inlet, which excludes the large particles that cause meteorological interferences and provides control over the particle-size fraction that is sampled (White et al., 1994; Richards,

1994). Enclosed nephelometers that use an incandescent lamp heat the sample a few degrees, but this heating can be less than 1°C in nephelometers that use a flashlamp. Sample heating reduces the RH of the sample air, which causes absorbed water to evaporate from particles in the sample chamber.

The California Air Resources Board Method V for monitoring ambient concentrations of visibility-reducing particles uses an enclosed nephelometer that is deliberately heated to minimize the effects of high humidities on the monitoring data (VanCuren, 1989a, 1989b). This drying of the aerosol particles is similar to the drying which occurs when filter samples are conditioned to a standard humidity before being weighed in the laboratory.

Open nephelometers were designed to reduce the heating of the sample to a fraction of a degree, and to admit a broad range of particle sizes (Molenar et al., 1992). Therefore, open nephelometers respond to meteorological effects such as fog and snow. The standard IMPROVE protocol flags open nephelometer data influenced by meteorological effects and excludes them from some the statistical presentations of the data (Cismoski, 1994). The difficulties associated with this data flagging are the same as those for flagging light-extinction coefficient data listed in Section 8.4.3.

Forward scatter meters have been selected by the National Weather Service to replace human observers for visibility measurements at airports (National Oceanic and Atmospheric Administration, 1992). The sample volume is in the open air, so the instrument responds to meteorological effects as well as air quality effects. This instrument is significant because it is in use at approximately 600 locations as of the end of 1995, and additional installations are planned. Data from this instrument have the potential to provide a database for the evaluation of spatial and temporal trends in the light-scattering coefficient for particles that is more useful than the historical records of visual range at airports. However, this will require a change in the way data are archived by the National Weather Service because current practice is to report all visibilities greater than 10 mi in one bin.

The cost of most instruments to measure the light-scattering coefficient for particles is in the range of typical monitoring instruments. They operate for long periods of time unattended, but do require routine lamp replacement and occasional cleaning.

Integrating nephelometers can be accurately calibrated with gases of varying scattering coefficients (see, for example, Bodhaine, 1979; Ruby and Waggoner, 1981). These

calibrations are applicable to the measurement of light scattering by fine particles. Because integrating nephelometers are blind to light scattered near 0 and 180 degrees, their response to particles in the 2.5- to 15-μm-diameter range is roughly half the correct value (White et al., 1994). This property of nephelometers, known as the truncation error, has been quantified (Ensor and Waggoner, 1970; Heintzenberg and Quenzel, 1973; Heintzenberg, 1978; Hasan and Lewis, 1983; White et al., 1994).

The measurement of the light-scattering coefficient has the potential to be an indicator for health effects as well as visibility effects. Enclosed nephelometer readings are highly correlated with the mass of fine particles collected on a filter (see, for example, Waggoner et al., 1981). The correlation between nephelometer readings and the mass concentration of fine particles is improved by using the same size selective inlet on both the nephelometer and filter sampler (White et al., 1994). Filter samples are typically equilibrated to a standard RH before being weighed. The correlation between nephelometer readings and mass concentrations measured by filter can be improved minimizing the occurrence of high RH in the nephelometer scattering chamber. This can be accomplished by heating the sample air a few degrees, as in the California Air Resources Board Method V (VanCuren, 1989a,b) or by passing the air sample through a dryer that removes water. Heating the air sample has the potential to volatilize particulate species other than water.

8.4.6 Contrast of Terrain Features

Data for the contrast of terrain features provides a direct measure of the visibility. In current practice, the contrasts of features in a scene are most commonly monitored photographically and determined by film densitometry (Johnson et al., 1985).

Because of the close relationship to visibility, contrast measurements were used by the National Park Service when instrumental visibility monitoring in Class I areas began in the late 1970s (Malm, 1979). A teleradiometer was used to measure the contrast of a distant terrain feature against the horizon sky.

When contrasts and background radiances are measured at both ends of the sight path, Equations 8-26 and 8-9 can be used to accurately determine the average light-extinction coefficient of the atmosphere in the sight path. These measurements are rarely made. It is more common to assume that the background radiances are equal at each end of the sight

path (Malm, 1979) to estimate the initial contrast (Malm et al., 1982) and to calculate the average light-extinction coefficient from Equations 8-30 and 8-9. Values of the light-extinction coefficient calculated by this method have been found to be unreliable (White and Macias, 1987). For this reason, the National Park Service has discontinued making instrumental contrast measurements in favor of the direct measurement of the light-extinction coefficient or the light-extinction coefficient due to particles.

The contrast monitoring data provide a direct measure of the visibility, which is affected by many factors other than the air quality (see Section 8.2.9). Sections 8.2.5 through 8.2.8 provide the methods for calculating contrasts and contrast transmittances from air quality data. It is expected that improvements in these calculation methods will lead to, increasing emphasis on the contrasts of terrain features and contrast transmittances for specific sight paths as measures of visibility. The calculation methods presented in this chapter can be used to calculate contrasts of terrain features when the air quality and land-use data are available and the skies are either reasonably free of clouds or are uniformly overcast.

8.4.7 Particulate Matter Concentrations

The fine-particle concentration could be used as an indicator of visibility because (1) the data cited below show that the coefficient for light-scattering by particles is closely linked to the mass concentration of fine particles, and (2) the coefficient for light-scattering by particles is the component of light extinction primarily responsible for visibility impairment. This alternative would be attractive if fine particle concentrations were monitored to determine compliance with a primary air quality standard because no additional monitoring would be required to determine compliance with a visibility standard. The calculation methods presented in Sections 8.2 and 8.3 could be used to relate the visibility (as measured by contrast and contrast transmittance) to the fine-particle concentration for purposes of evaluating various options for the level and form of a fine-particle standard designed to protect visibility.

A number of studies report data for the relationship between the coefficient for light-scattering by particles (as measured by an integrating nephelometer) and the fine-particle concentration. Most of these studies report correlation coefficients of 0.9 or greater. Early

results were reported by Waggoner and Weiss (1980), who measured correlation coefficients greater than 0.95 at Mesa Verde, CO, and at industrial, residential, and rural sites in the Pacific Northwest. The nephelometer measurements were made using an enclosed nephelometer without a size selective inlet and with some sample heating caused by the lamp. Dichotomous samplers with a 3 μm cutpoint were used to collect fine particles on teflon or Nuclepore substrates. No special precautions were taken in the filter sampling to prevent the evaporation or collection of semi-volatile species. The mass-specific light-scattering efficiencies determined from regression analysis of the data from each of the five sites ranged from 2.9 to 3.2 m^2/g. These data were also reported by Waggoner et al. (1981).

The results of Koenig et al. (1993) are of interest because pulmonary function changes in children were associated with integrating nephelometer readings in Seattle, WA. The studies were conducted during two winter heating seasons in areas affected by wood smoke. The year following these studies, $PM_{2.5}$ samples collected at pre-set time intervals over 1-week periods from January 17 to December 12, 1991, were compared with integrating nephelometer measurements averaged over the sample collection times. Regression analysis gave a mass-specific light-scattering efficiency of 4.9 m^2/g, which is larger than typically observed, and a regression coefficient of 0.97.

The results of White et al. (1994) are of interest because size-selective inlets with cutpoints of 2.5 and 15 μm were used on both the integrating nephelometer and the filter sampler. As in the previous studies, the nephelometer sample chamber was heated by the lamp. The samples were collected in a desert climate in northern Arizona. As described in Section 8.3.2, the mass-specific light-scattering efficiency of particles that pass the 2.5 μm cutpoint at two sites was 2.8 and 3.1 m^2/g and the correlation coefficients were 0.86 and 0.84.

Integrating nephelometer readings are not as well correlated with total suspended particulate concentrations (Waggoner et al., 1981) or with particle concentrations measured with a 15 μm cutpoint (White et al., 1994). The reasons are (1) fine particles have mass-specific light-scattering efficiencies 5 to 10 times greater than the efficiencies of coarse particles, (2) the integrating nephelometer responds to roughly half the light scattered by coarse particles (White et al., 1994), and (3) the relative amounts of coarse and fine particles in the atmosphere are typically quite variable. Therefore, the coefficient for light-scattering

by particles is much less closely linked to the PM_{10} concentration than to the fine-particle concentration, making PM_{10} less satisfactory as an indicator of visibility than the fine-particle concentration.

8.4.8 Measures of Discoloration

The 1977 Clean Air Act Amendments define visibility impairment as a reduction in the visual range or atmospheric discoloration. Color calculations have been included in plume visibility models (see, for example, Latimer et al., 1978), and quantitative color measurements have been made for urban hazes (e.g., Waggoner et al., 1983). Less emphasis has been placed on the color of regional hazes. A brief review of methods for specifying the colors of hazes appears in the National Acid Precipitation Assessment Program report on visibility (Trijonis et al., 1991).

For plume visibility analyses, the most commonly used parameter is the color difference $\Delta E(L^*a^*b^*)$ between the apparent spectral radiances for a sight path with and without the plume. The equations for calculating this parameter are presented in an EPA workbook (U.S. Environmental Protection Agency, 1988). It is the intent of these equations to linearize the human perception of color differences, so color differences with equal values of $\Delta E(L^*a^*b^*)$ are equally perceptible. It was also an intent of these equations to assign a $\Delta E(L^*a^*b^*)$ value of unity to color differences that were just perceptible when presented as two, side-by-side, uniform areas of color that each subtended angles of a few degrees or more. For plume visibility analyses, the threshold for the perception of color differences is greater than for color patches separated by a sharp edge because of the diffuse edges of the plume. It also depends on the apparent angle subtended by the plume, i.e., the apparent width of the plume (U.S. Environmental Protection Agency, 1988).

The apparent color of an urban or regional haze depends on the element of the scene used by the human visual system as a reference white (MacAdam, 1981). Water clouds in the sky typically have spectra that are strong in the blue. If such water clouds are used as the reference white for color perception, hazes that have a more neutral spectrum (Waggoner et al., 1983) can appear yellowish or brown by comparison. Thus, an analysis of haze colors requires an analysis of both the spectral radiance of the haze and the spectral radiance of the elements of the scene used by the observer as the reference white (MacAdam, 1981).

8.5 VISIBILITY IMPAIRMENT

8.5.1 National Patterns and Trends

National patterns and historical visibility trends are summarized in the National Acid Precipitation Assessment Program report by Trijonis et al. (1991). They were also reviewed in the National Research Council report prepared by the Committee on Haze in National Parks and Wilderness Areas (National Research Council, 1993). Data for spatial and temporal patterns of haze measured by the IMPROVE (Interagency Monitoring of Protected Visual Environments) protocol in Class I areas, mostly in the western United States, have been summarized by Sisler et al. (1993) and Malm et al. (1994).

Patterns and trends in visibility are closely linked to patterns and trends in particulate matter concentrations, which are reviewed in Chapter 6 of this document. Because of the close linkage to data appearing elsewhere in this document and the availability of good, current reviews in publications of the federal government, the data for visibility patterns and trends are not summarized again here.

8.5.2 Visibility Monitoring

Visibility observations have long been made as part of weather observations. Since the advent of aviation, visibility observations have routinely been made at airports. The 1977 Amendments to the Clean Air Act generated a need for visibility and air quality monitoring to determine the visibility conditions in Class I areas and a need to monitor progress toward the national goal of eliminating man-made air pollution in Class I areas.

A recent report summarizes current visibility monitoring activities (U.S Environmental Protection Agency, 1995e). The following sections give additional information which supplements the information in the U.S Environmental Protection Agency report.

8.5.2.1 Point Versus Sight Path Measurements

The monitoring methods used in visibility studies can be divided into point measurements, which measure properties of the atmosphere at the sampler inlets, and path measurements, which determine the optical properties of a sight path through the atmosphere. This distinction is blurred only in mobile or airborne sampling, where the sampler inlets can be moved through a sight path.

Visibility, by definition, is linked to sight paths and can be quantified only after a sight path is specified. Sight path measurements, such as human observations of the visual range, the instrumental measurement of the contrast of distant terrain features, or contrasts measured from photographs provide a direct measure of the visibility.

Most air quality measurements measure the air quality at the sampler inlets. This is typically true of trace gas monitors, aerosol filter samplers, and optical monitors such as the integrating nephelometer. Some remote sensing instruments measure air quality parameters, such as trace gas concentrations or light extinction, for a sight path. However, the sight paths for these instruments are typically short enough that the measurements are more appropriately classified as point measurements rather than sight path measurements.

The Optec Transmissometer is an example of a remote sensing instrument that typically produces data that can be classified as a point measurement. To conserve electric power in remote locations, the IMPROVE protocol for the transmissometer calls for collecting data for 10 min each hour. For typical wind velocities, the spatial and temporal averaging resulting from a 10-min measurement each hour for a sight path a few kilometers in length is comparable to the hour-average data continuously measured at a sampler inlet. An exception to this classification occurs when the transmissometer sight path is strongly slanted, with the result that different layers in a stable atmosphere may be sampled. An example is the transmissometer with one end of the sight path at Hopi Point on the rim of the Grand Canyon and the other end of the sight path at Indian Gardens within the Canyon.

When air quality measurements made at a point satisfactorily represent the conditions in the surrounding region, the methods in Section 8.2 can be used to calculate the visibility from the air quality data. Uncertainties in the representativeness of the air quality data should be evaluated when estimating the uncertainties in the visibility calculations.

8.5.2.2 Instrumental Monitoring Networks

According to present plans, the largest instrumental visibility monitoring network in the United States will be operated by the National Oceanic and Atmospheric Administration and cooperating agencies to measure airport visibility. The primary purpose of this network is to provide real-time data for runway visibility to aid in controlling airport operations. The visibility measurements are one component of the Automated Surface Observing System

(ASOS) and are made by the Belfort Visibility Sensor (National Oceanic and Atmospheric Administration, 1992). This instrument uses a flash lamp to illuminate a volume of open air and a sensor to measure the scattering of visible light at angles near 40 degrees. The signals from the visibility sensor have been calibrated by comparison with transmissometer measurements during episodes of haze, fog, rain, snow, etc., and a calibration curve is used to convert the sensor readings to units of light extinction and visual range. Between 400 and 600 installations are now operating.

The IMPROVE is the largest network that includes both visibility and air quality measurements. Most sites are operated by the National Park Service, but sites are also operated by the U.S. Forest Service and other agencies. Data are being collected using the IMPROVE protocols at more than 40 sites, most of which are in or near federal Class I areas (Malm et al., 1994; Sisler et al., 1993; U.S. Environmental Protection Agency, 1995e).

The Clean Air Status and Trends Network (CASTNET), which is no longer in operation, included the CASTNET Visibility Network, which had nine sites, primarily in the eastern United States (U.S. Environmental Protection Agency, 1995e). The California Air Resources Board operates integrating nephelometers (to measure light scattering by visibility-reducing particles) at approximately 16 sites and tape samplers (to measure light absorption by particles) at nearly 40 sites (VanCuren, 1989a,b). Data from many of these sites are used when forecasting agricultural burn days. Other monitoring activities are listed in a recent U.S. Environmental Protection Agency report (U.S. Environmental Protection Agency, 1995e) and in Tables 8-3 and 8-4 adapted from the National Acid Precipitation Assessment Program report (Trijonis et al., 1991).

8.5.3 Recent Observations

This section briefly summarizes results presented in selected papers published since the U.S. Environmental Protection Agency review was prepared (U.S. Environmental Protection Agency, 1995e).

Vasconcelos et al. (1994) examined data from Subregional Cooperative Electric Utility, Department of Defense, National Park Service, and EPA Study (SCENES) conducted from 1984 to 1989 in the area surrounding the Grand Canyon. Aerosol concentrations showed

TABLE 8-3. LONG-TERM VISIBILITY AND AEROSOL DATA BASES

Study/Data Base	Air Sheds	Period	Type of Data	Purpose of Study	Comments	References [a]
		National and Regional Networks				
Analyses of National Weather Service (NWS) Airport Visibility Data	Rural and urban airports all over the nation.	1918 to present	Human estimates of prevailing visibility mainly in support of aircraft operations	To assess visibility trends; Assessment of the role of meterology on visibility impairment.	Quality varies from site to site; natural causes of visibility impairment (rain, snow, fog) included in data.	Trijonis (1979, 1982a,b); Sloane (1982 a,b, 1983); Patterson et al. (1980); Husar and Patterson (1984)
Interagency Monitoring of Protected Visual Environments (IMPROVE)	Twenty remote locations nationwide, though primarily in the West.	1987 to present	Aerosol and visibility; PM and fine particle mass. Fine particle elements, ions, organic and light absorbing carbon. σ_{ext}, σ_{ap} , and σ_{sp} and photography.	To establish baseline values and identify existing impairment in visibility protected federal Class I areas.	Employs "state-of-art" methods for long term routine monitoring. Operated jointly by U.S. EPA four federal land managers.	Joseph et al. (1987) Sisler et al. (1993) Malm et al. (1994)
Eastern Fine Particle Visibility Network	Five eastern rural locations.	1988-89 five sites; after 1989 two sites	Aerosol and visibility; fine particle elements organic and soot carbon. σ_{ext}, σ_{ap}, and σ_{ag}, and photography.	A research monitoring program to provide information needed to quality support development of a secondary fine particle standard.	An U.S. EPA operated network. Sites are collocated with other air monitoring programs.	Handler (1989)
National Park Service Network (NPS)	About 37 remote locations nationwide, though primarily in the west.	1987 to present Seventeen sites started in 1987.	Aerosol & visibility; 17 sites operated with IMPROVE measurements. Other have some subset of the IMPROVE measurements.	To document visibility and aerosol levels and to identify sources of visibility impairment measurements in NPS.	Represents the longest period of record for visibility and aerosol monitoring at remote locations.	Joseph et al. (1987)
SCENES	Eleven rural and remote southwestern locations.	1984-1989	Aerosol and visibility; PM and fine particle mass, elements, organic and light carbon at most sites. σ_{ext} or σ_{sp} and σ_{sg}, and photography at most sites.	To document levels and causes of visibility impairment in northern Arizona and southern Utah.	This cooperative research program included several intensive and special studies. An ambitious quality assurance protocol identified many monitoring method difficulties which new techniques ultimately solved.	McDade and Tombach (1987)
Western Regional Air Quality Study (WRAQS)	Eleven nonurban locations in the western U.S.	1981-1982	Aerosol and visibility; PM and fine particle mass, elements, ion.	To document bacground levels of visibility and related aerosols, organic and elemental carbon. σ_{sg} and σ_{sp}, observed visual range and photography.	Represents the highest times resolution for routinely collected filter samples (two four-hour samples each day).	Macias et al. (1987)

TABLE 8-3 (cont'd). LONG-TERM VISIBILITY AND AEROSOL DATA BASES

Study/Data Base	Air Sheds	Period	Type of Data	Purpose of Study	Comments	References [a]
National Air Surveillance Network (NASH)	Urban & rural areas of U.S.	1975 to present	Aerosol only; TSP ions, and some elements.	Air quality monitoring.	No size-fractioned data; collected only once every six days; artifact on filter possible.	Shah et al. (1986) Mueller and Hidy (1983)
Inhalable Particle Network (IP Network)	Urban and rural areas of U.S. Evans (84) Rodes and Evans (85)	June 1979 to present	Aerosol only; fine and coarse aerosol mass, PM_{15} mass, elements, and ions (every fourth sample).	Characterize inhalable particles.	Discrepancy exists between PM_{15} and IP mass (sum of fine and coarse). Screening of the data required to remove invalid data points (~25%).	Pace et al. (1981) Watson et al. (1981)
Sulfate Regional Experiment (SURE)	Nonurban areas of eastern U.S. (9 Class I sites and 45 Class II sites)	1977-1978	Aerosol only; TSP, fine and coarse aerosol mass, ions and elements.	Sulfate characterization pollutant source characterization	Class I sites operated for 18 months continuously; Class II sites operated for one month every season for a total of six.	Mueller and Hidy (1983)
Eastern Regional Air Quality Studies (ERAQS)	Nine nonurban areas in northeastern U.S. SURE Class I sites.	1978-1979	Aerosol and visibility; TSP, fine and coarse aerosol mass, ions, elements, σ_{sg} and σ_{sp}, σ_{ext}, and photography.	To characterize visibility (at two sites only) and air quality in the northeastern U.S. region.	The only long-term instrumental visibility data set generated in the eastern U.S. Visibility monitored only at 2 sites; intercomparison of visibility measurement methods made.	Mueller and Watson (1982) Tombach and Allard (1983)
Ohio River Valley Study	Three rural sites in Ohio River Valley.	May 1980-August 1981	Aerosol only; fine and coarse aerosol mass and elements.	Characterization of fine and coarse aerosols in the region.	Portion of aerosol composition was not accounted for due to limitations in XRF analysis used. A long-term daily monitoring of aerosol in rural areas of the Ohio River Valley.	Shaw and Paur (1983)
Harvard School of Public Health's Six Cities Study	Portage, WI; Topeka, KS; Kingston, TN; Watertown, MA; St. Louis, MO; Steubenville, OH	Spring 1979	Aerosol and visibility; fine and coarse aerosol mass, elements, $SO_4^{=}$, σ_{sg} and σ_{sp}.	Mass and elemental characterization of aerosol and their temporal variations to assess health effects of air pollution.	Portion of aerosol composition was not accounted for due to limitations in XRF analysis used.	Spengler and Thurston (1983)

TABLE 8-3 (cont'd). LONG-TERM VISIBILITY AND AEROSOL DATA BASES

Study/Data Base	Air Sheds	Period	Type of Data	Purpose of Study	Comments	References [a]
RESOLVE	Seven remote sites in the California Mojave Desert	1983-1985	Aerosol and visibility; PM_{10} and fine particle mass, elements, organic and elemental carbon, σ_{ext}, σ_{sp} and σ_{sg}, σ_{ap} and σ_{ag}, and photography.	To document levels and identify causes of visibility impairment in the R-2508 military air space.	DOD sponsored study to provide information needed to limit future additional degradation of military testing by visibility impairment.	Blumenthal et al. (1987)
Single Air Shed Studies						
Great Smoky Mountain National Park Visibility and Air Quality Study (TVA)	Great Smoky Mountain National Park	1980-1983	Aerosol and visibility; fine and coarse aerosol mass and elements; σ_{sp} and σ_{sg} and σ_{ext}; photography.	Characterize visibility and aerosol.	Because of instrument problems, teleradiometer data were lost. Total particulate matter mass only estimated in some cases. PIXE analysis could not provide some major elemental data.	Valente and Reisinger (1983) Reisinger and Valente (1984, 1985)
Regional Air Pollution Study (RAPS)	100 km region around St. Louis, MO	1974-1977	Aerosol only; fine and coarse mass, $SO_4^=$, elements.	Develop and evaluate regional air quality models.	Comparison of Hi-Vol and dichotomous samplers.	Jaklevic et al. (1981) Altshuller (1982, 1985)
Portland Aerosol Characterization Study (PACS)	Two rural and four urban areas in Portland, OR	July 1977-April 1978	Visibility and aerosol; fine and coarse mass, TSP, ions, elements, σ_{sp} and σ_{sg}.	Aerosol characterization source apportionment.	Significant role of carbonaceous aerosols recorded.	Copper and Watson (1979) Shah et al. (1984)

[a]Visibility data include light scattering and light extinction measurements using integrating nephelometer, teleradiometers, cameras, and human observers.

Adapted from: Trijonis et al. (1991).

TABLE 8-4. SHORT-TERM INTENSIVE VISIBILITY AND AEROSOL STUDIES

Study/Data Base	Air Sheds	Period	Type of Data	Purpose of Study	Comments	References
			Rural Studies			
Allegheny Mountain Studies	Rural Allegheny Mountain site	24 July-11 Aug 1977 and Aug 1993	Visibility and aerosol; TSP, fine and coarse aerosol mass, ions, elements, σ_{sp} and σ_{sg}.	Characterization of visibility and $SO_4^=$ in the region.	Filter artifact investigated; no size fractionated data in 1977.	Pierson et al. (1980a,b)
Shenandoah Valley Studies	Rural Shenandoah Valley	15 July - 15 Aug 1980	Visibility and aerosol; fine and coarse aerosol mass, ions, elements, σ_{ext}, human estimates of visibility.	To characterize visibility and aerosol in the rural eastern U.S.	Since three different groups performed the study, intercomparability of data possible.	Stevens et al. (1984) Weiss et al. (1982) Ferman et al. (1981) Wolff et al. (1983)
Great Smoky Mountain Study (EPA)	Great Smoky Mountain National Park	20-26 Sept 1978	Aerosol and gaseous pollutants; fine and coarse aerosol mass and elements.	Characterize aerosol in a rural area.	Comparison of day and night aerosol data made.	Stevens et al. (1980)
Research Triangle Park Visibility Study	Rural Research Triangle Park, NC	8 June - 3 Aug 1979	Visibility and aerosol; fine and coarse aerosol mass, elements, σ_{ext}, and σ_{sp} and σ_{sg}.	Characterize visibility and aerosol in the region.	Comparison of different visibility measurement methods studies.	Dzubay and Clubb (1981)
Louisiana Gulf Coast Study	Gulf Coast	8 Aug - 7 Sept 1979	Visibility and aerosol; fine and coarse aerosol mass, ions, elements, σ_{sp} and σ_{sg}.	Investigation of sources of O_3 and haze.	Calibration errors of MRI 1550 integrating nephelometer applied to data.	Wolff et al. (1982)
Atlantic Coastal Study	Lewes, DE	1-31 Aug 82, 25 Jan - 28 Feb 1983	Visibility and aerosol; fine and coarse aerosol mass and chemistry, σ_{sp} and σ_{sg}.	Air quality and sources of haze.		Wolff et al. (1985a)
Pacific Northwest Regional Aerosol Mass Apportionment (PANORAMAS)	Twenty-six rural and remote locations in Washington, Oregon, and Idaho	May - Nov 1984	Visibility and aerosol; fine particle mass, elements, and ions. σ_{ext}, σ_{ap}, σ_{ag}, and photography.	To document the levels and sources of summer visibility impairment in the Northwest.	This cooperative monitoring program identified smoke as a major contributor to visibility impairment.	Core et al. (1987)

TABLE 8-4 (cont'd). SHORT-TERM INTENSIVE VISIBILITY AND AEROSOL STUDIES

Study/Data Base	Air Sheds	Period	Type of Data	Purpose of Study	Comments	References [a]
			Rural Studies			
California Aerosol Characterization Study (ACHEX)	Fourteen southern California cities	July- Nov 72, July - Oct 73	Aerosol and visibility TSP, fine and coarse aerosol mass, ions, elements, σ_{sg} and σ_{sp}.	Characterization of urban aerosols in California.	The most complete classic aerosol experiment. New methods sampling and analysis tested.	Hidy et al. (1975) Hidy et al. (1980) Charlson et al. (1972)
Denver Winter Haze Study I	Denver, CO	Nov - Dec 78	Visibility and aerosol; fine and coarse aerosol mass, ions, elements, σ_{sg} and σ_{sp}, and σ_{ext}.	Investigation of sources of Denver haze.	Role of local sources and the significant role of carbon in the air documented.	Countess et al. (1980, 1981) Wolff et al. (1981) Groblicki et al. (1981) Heisler et al. (1980a,b)
Denver Winter Haze Study II	Denver, CO	Jan 1982	Visibility and aerosol; fine and coarse aerosol mass, ions, elements, σ_{sp} and σ_{sg}.	Investigation of sources of Denver haze.	Role of local sources and the significant role of carbon in the air documented.	Lewis and Stevens (1983) Hasan and Dzubay (1987)
Metro Denver Brown Cloud Study	Denver, CO	Nov 1987 - Jan 1988	Visibility and aerosol; fine particle elements ions, organic and light absorbing carbon, σ_{ext}, σ_{sp} and σ_{sg}, σ_{ap} and σ_{ag}, and photography.	Investigate the sources of Denver haze.	Comprehensive spatial and temporal measurements included fuel switching to see effects of source modulation.	Watson et al. (1988)
Detroit Visibility Study	Urban Detroit, MI	15-21 July 1981	Aerosol and visibility; fine and coarse aerosol, ions, elements, σ_{sp} and σ_{sg}.	Identification of chemical components of TSP.	Data from a major industrial and urban areas.	Wolff et al. (1982, 1985b) Sloane and Wolff (1984, 1985)
Houston Visibility Study	Houston, TX	11-19 Sept 1980	Visibility and aerosol; fine and coarse aerosol, ions, elements, σ_{sp} and σ_{sg}, and σ_{ext}.	Characterization of visibility and aerosol.	Comparison of day and night aerosols and different visibility measurement devices made.	Dzubay et al. (1982)
CARB Los Angeles Basin Study	Los Angeles Basin	Aug 1992	Visibility and aerosol; fine and coarse aerosol mass, ions, and σ_{sp} and σ_{sg}.	Characterize visibility and aerosol in the basin.	Significant roles of NO_3^- and organics shown; the importance of filter artifacts reported.	Appel et al. (1983)

TABLE 8-4 (cont'd). SHORT-TERM INTENSIVE VISIBILITY AND AEROSOL STUDIES

Study/Data Base	Air Sheds	Period	Type of Data	Purpose of Study	Comments	References
Northern New Jersey Air Pollution Study	Newark, NJ Elizabeth, NJ Camden, NJ Ringwood, NJ	Winter 1982-1983	Aerosol only.	Inhalation toxicology studies.	Urban contributions of carbonaceous particles to air pollution episodes.	Lioy et al. (1983, 1985)
Willamette Valley Field and Slash Burning Study	Willamette Valley, OR	Summer 1978	Aerosol; fine and coarse mass, TSP, elements (carbon), ions	Assessment of field and slash burning on air quality.	Significant role of carbonaceous particles in fine aerosol demonstrated.	Lyons and Tombach (1979)
San Joaquin Valley Aerosol Study	San Joaquin Valley, CA	Nov-Dec 78, Jul and Sept. 79	Aerosol only; fine and coarse mass, ions.	Characterize ambient aerosols termittent data sets.		Heisler and Baskett (1981)
Southern California Air Quality Study (SCAQS)	Los Angeles Basin	June-Sepemter and December 1987	Meteorological air quality data to address O_3 and aerosol formation.	Characterization of air quality, including aerosol and visibility in the basin.	Comprehensive data base for O_3 and aerosol analyses.	Lawson (1990) Air and Waste Management (1993)

[a]Visibility data include light scattering and light extinction measurements using integrating nephelometer, teleradiometers, cameras, and human observers.

Adapted from: Trijonis et al. (1991).

substantial seasonal variation but little systematic diurnal variation. Aerosol composition, but not total concentration, depended strongly on ambient relative humidity, with crustal materials augmented at low humidities and sulfates augmented at high humidities. Total fine-particle concentrations showed the expected strong correlation with light scattering, but the aerosol composition was essentially the same on clear days and hazy days.

Saxena et al. (1995) analyzed data for particle growth as a function of RH and particle composition to evaluate the effect of organic compounds on water uptake. They analyzed the data from which the examples in Figure 8-13 were taken. They compared the observed water content with the water content expected to be associated with the inorganic fraction, and found that the aggregate hygroscopic properties of inorganic particles were altered substantially when organic compounds are also present. The alterations can be positive or negative. For the nonurban location near the Grand Canyon, organics enhance water absorption by inorganics. In the RH range of 80 to 88%, organics account for 25 to 40% of the total water uptake, on average. For the urban location in the Los Angeles Basin, the net effect of organics is to diminish water absorption of the inorganics by 25 to 35% in the RH range of 83 to 95%.

8.6 VISIBILITY MODELING

Three types of models are discussed in this section: plume models; regional haze models; and models for photographic representation of haze. Plume visibility models and regional haze models are source models which simulate the transport, dispersion, and transformation of chemical species in the atmosphere. Plume models use the resulting air quality data to calculate the values of parameters related to human perception, such as contrast and color difference. Regional haze models currently calculate aerosol species concentrations and the light-extinction coefficient. Models for the photographic representation of haze use air quality data as an input, and perform the optical calculations required to create images that represent the visual effects of the air quality.

8.6.1 Plume Visibility Models

As part of the 1977 amendments of the Clean Air Act (Section 169A to Part C) of Title I), the U.S. Environmental Protection Agency sponsored the development of the plume visibility model (PLUVUE) to be used during the preparation of a permit application to determine whether or not a proposed new facility would cause visibility impairment in a class I area (Latimer et al., 1978; Johnson et al., 1980; White et al., 1985). Plume visibility models estimate the value of optical parameters related to human perception, such as contrast and color differences. The calculated values for these parameters are then compared with perception thresholds to determine whether or not the plume would be perceptible in each simulated case (U.S. Environmental Protection Agency, 1988; Latimer, 1988).

Other plume visibility models have been developed by the Los Alamos National Laboratory (Williams et al., 1980, 1981), Environmental Research and Technology, Inc. (Drivas et al., 1981), and the University of Washington (Eltgroth and Hobbs, 1979). Additional citations for these models and a comparison of results from PLUVUE and the other models with experimental data have been reported by White et al. (1985). The PLUVUE model (PLUVUE I) has been refined, now known as PLUVUE II (Seigneur et al., 1983; Seigneur et al., 1984) and has been evaluated (White et al., 1986).

To minimize the cost of visibility analyses in cases where a full plume visibility analysis is not necessary, the U.S. Environmental Protection Agency sponsored the development of a visibility screening model, VISCREEN (U.S. Environmental Protection Agency, 1988). When used for Level-1 analyses, default values are used for most input data to evaluate the visibility effects of a worst case scenario. If necessary, a Level-2 analysis is performed with more realistic values for the input data. If these screening analyses indicate a potential for visible effects, a full Level-3 analysis must be performed with a plume visibility model.

It is anticipated that an improved version of the PLUVUE II plume visibility model will be available on the U.S. Environmental Protection Agency's Support Center for Regulatory Air Models bulletin board in 1995.

8.6.2 Regional Haze Models

The primary sources of anthropogenically induced, regional visibility degradation (also referred to as regional haze) measured as light extinction, are fine particles in the atmosphere. In the eastern United States, these anthropogenic particles are composed primarily of sulfate compounds, organic compounds, and to a much lesser extent nitrate compounds. These are important constituents in other areas of the United States as well; their relative importance, however, changes. For example, in some areas of the Pacific Northwest, organic aerosols are as, or more, important than sulfate aerosols. In some parts of Southern California, nitrate aerosols are the dominant species.

Sulfate aerosols are mostly formed from SO_2 emissions, which are predominantly due to fuel combustion. The sources of organic aerosols can be both natural and anthropogenic. Organic aerosols may be primary, emitted directly from a source, or secondary products of chemical reactions which occur in the atmosphere during transport and dispersion downwind from the source. The processes which lead to their formation are not altogether well understood.

For the purposes of calculating regional visibility degradation due to specific sources of air pollution, the primary focus has been on the contribution to light extinction of fine particles of sulfate and nitrate compounds. Once these particles are formed, their size can change, and thus their light scattering efficiency, due to changes in the RH of the atmosphere. In order to account for the contribution for light extinction of either sulfate or nitrate compounds, the mass of these constituents and the RH of the atmosphere in which these particles reside must be known. The calculations of the extinction due to primary fine particles are assumed to be non-hygroscopic.

Depending on the modeling situation, regional haze assessment can involve one to several sources, or it can involve a multitude of sources spanning several states. The first situation (involving isolated source impacts) most often arises within the context of assessing air quality impacts on Class I wilderness areas, which often involve transport of 50 km or more. The second situation (involving nationwide or regional impact assessments) most often arises within the context of assessing the impacts of new or existing air quality regulations. The modeling requirements for regional-scale multiple-source haze models are nearly identical to the modeling requirements for simulations of regional-scale multiple-source fine

particle impacts. Hence, the Eulerian-based grid models currently under development to support fine particle impact assessments will be relied upon to provide a means for assessing large-scale multiple-source haze impacts. Middleton (1996) described the findings of such a modeling effort; the Denver Air Quality Modeling Study (DAQMS). The Denver Air Quality Model was designed to apportion sources of visibility degradation and to evaluate the benefits of future emission controls in the Denver Metropolitan area. The results of the study demonstrated an association between visibility and air quality issues in the Colorado Front Range area. As this latter modeling is still under development, the following discussion summarizes recent efforts to improve the Lagrangian-based modeling products available for characterizing isolated source impacts involving long-range transport and dispersion.

A requirement of the CAA concerns air pollution impacts of proposed new sources on federal Class I areas and prevention of significant deterioration. The Class I areas (e.g., national parks, national wilderness areas, and other areas of special national value) are the responsibility of Federal Land Managers. The responsibility for prevention of significant deterioration is shared with U.S. Environmental Protection Agency and the States. However, the air quality assessment for proposed new sources often involves the simulation of air transport and dispersion over large distances (greater than 50 km). This creates a problem since Lagrangian-based simulation methods capable of reliably handling the complex transport and dispersive process unique to such long-range transport assessments have not been developed as yet to a point where guidance can be offered on how to apply these methods routinely (see section 7.6.2 of the Guideline on Air Quality Modeling, 40 CFR Appendix W to Part 51).

To address the joint responsibilities of various governmental agencies involved, a memorandum of understanding was established in November 1991 which formed a working group, known as the Interagency Workgroup for Air Quality Modeling. The purpose of the working group was to foster cooperation among the U.S. Environmental Protection Agency, the U.S. Forest Service, the Fish and Wildlife Service, the National Park Service, and selected State representatives. The goal was to foster development of applied mathematical modeling techniques needed by Federal Land Managers, and others, to make informed

decisions regarding the protection of federal Class I areas, especially within the context of assessing individual source impacts.

A two phased approach was devised (U.S. Environmental Protection Agency, 1992), given (1) the immediate need for guidance on modeling techniques for impact assessments involving regional scale (greater than 50 km) transport, (2) the complexity of applicable modeling systems and data bases, and (3) the spatial scales and potential numbers of sources for consideration. The first phase involved a review of available modeling techniques and construction of an interim recommendation for use by concerned technical and regulatory communities until such time that more permanent guidance could be offered. The second phase involved development, testing and application of state-of-the-art meteorological processors and dispersion modeling systems, to establish a basis for enhancement and perhaps replacement of the Phase I interim recommendations..

Following a series of model comparison and sensitivity analyses, a technical review was completed of meteorological data processing and dispersion modeling systems (U.S. Environmental Protection Agency, 1993b). This served as the basis for the Phase I interim recommendations. These findings facilitated use of the MESOPUFF II system (U.S. Environmental Protection Agency, 1994) within established national guidance provided in the Guideline on Air Quality Modeling. For the purposes of assessing regional haze impacts, the light extinction is estimated using 3- to 24-h concentration averages for the sulfate and nitrate compounds. The use of longer-period concentration averages to compute a light extinction coefficient (inverse of visual range) provides a pragmatic surrogate for assessing visibility degradation and avoids the overwhelming complications introduced when one attempts to invoke a line of sight visibility assessment for an actual vista.

The interim recommendations were applied in simulating pollutant impacts on the Shenandoah National Park to provide further technical information on the strengths and weaknesses of the available modeling systems (U.S. Environmental Protection Agency, 1995a). These results demonstrated that sources beyond 100 km might be expected to contribute and should not be arbitrarily excluded from assessments. They also demonstrated that such assessments are currently best accomplished on a case-by-case basis using expert judgement.

The technical work associated with phase II involves: (1) testing and assessment of possible benefits to be achieved through the use of state-of-the-art mesoscale meteorological (MM) processors employing four dimensional data assimilation (FDDA); (2) development of a state-of-the-art Lagrangian puff modeling system; and (3) testing of the developed modeling methods. Following completion of these technical efforts, an update to the Guideline on Air Quality Modeling can be proposed describing the modeling methods to be routinely accepted for characterization of long-range transport and dispersion from isolated sources.

The first step was addressed by initiating an analysis, in which MM-FDDA meteorological model was used to develop an hourly characterization of meteorological conditions (on a 80-km resolution) for an entire one-year period for the contiguous United States, northern Mexico and southern Canada. It was shown that MM-FDDA meteorological models could be applied operationally. Use of sophisticated meteorological processors provides a means for realistic characterization of long-range transport trajectories.

The second step involved enhancement of an advanced modeling system, entitled CALPUFF, capable of processing mesoscale meteorological data and capable of addressing dispersive processes of a regional nature. The modeling system was evaluated demonstrating the benefits of MM-FDDA meteorological data in characterizing long-range pollutant trajectories. Simulated trajectories were successfully compared to results from a field study involving transport to 1000 km downwind (U.S. Environmental Protection Agency, 1995b). The CALPUFF system was incorporated into a user-friendly windows-based environment with an on-line electronic user's guide (U.S. Environmental Protection Agency 1995c,d).

Previous evaluation results of puff dispersion models for transport distances of 30 to 100 km (Carhart et al., 1989), have illustrated the difficulty in characterizing the transport trajectory, but have seen a bias on the order of 30% on average towards overestimating the magnitude of the maximum surface concentration values. One of the findings of the trajectory comparisons (U.S. Environmental Protection Agency, 1995b), was that Lagrangian puff dispersion modeling involving transport of 200 km or more will underestimate the horizontal extent of the dispersion, thereby overestimate surface concentration values if delayed shear enhancement of dispersion (Moran and Pielke, 1994) is not addressed. In anticipation that CALPUFF will likely find widespread use in a variety of situations, a puff splitting algorithm was added to CALPUFF.

However, there remains a need to determine how best to invoke this algorithm for improved characterization of surface concentration values.

The third step towards providing enhanced guidance on methods for characterizing long-range dispersion for individual sources has been initiated by placing the CALMET/CALPUFF modeling system on the Support Center for Regulatory Models electronic bulletin board system for testing. Currently, this stage of the process must primarily rely on volunteer efforts from the public at large. It is hoped these efforts will prove successful in resolving the remaining technical issues, and that an update to the modeling guidance can be drafted for comment and review late in 1997.

8.6.3 Photographic Representations of Haze

Photographs are frequently used to illustrate visibility conditions. However, it is difficult to take a series of photographs of an actual scene under known, uniform conditions to illustrate the effects of various intensities of haze. Therefore, computer-generated photographs have been used for this purpose. Examples of this use of photographs appear at the back of the National Acidic Precipitation Assessment Program report on visibility (Trijonis et al., 1991). The current status of photographic representations of haze has been described by Molenar et al. (1994) and Eldering et al. (1993).

A photograph is taken on a very clean, cloud-free day and scanned to generate an initial image. The most laborious step is the creation of a distance map, which assigns a distance to each element in the scene. The estimated value of the light-extinction coefficient when the photograph was taken is used to calculate the initial radiances for each element in the scene. The horizon sky radiance can be used to estimate the source function in the calculations for the clean day.

The equations to generate images showing the effects of haze must calculate the value of the source function appropriate for the haze represented. Larson et al. (1988) have shown that the common practice of using the horizon sky radiance in the clean photograph as an estimate of the source function produces distorted results. Radiative transfer calculations can be used to derive the source function from the haze composition (Molenar et al., 1994; Eldering et al., 1993). Equations 8-19 and 8-20 are used to calculate the radiances presented in the photographic images.

The use of photographic models for representation of haze requires many approximations. The softening of shadows caused by the diffuse lighting when it is hazy is neglected, and it is usually assumed that the haze is uniformly distributed throughout the scene. Photographs also have the limitation that they are expensive to produce, so are typically used to illustrate only a few conditions. Often, the selected conditions are idealized, so the full range of conditions that occur in a scene are not represented.

8.7 ECONOMIC VALUATION OF EFFECTS OF PARTICULATE MATTER ON VISIBILITY

The effects of particulate matter on visibility were described in previous sections of this chapter and are hazes and reductions in visual range in all of the United States. This section discusses the available economic evidence concerning the value of preventing or reducing these types of effects on visibility. The following brief summary of economic estimation methods and available results is derived from the document, Air Quality Criteria for Oxides of Nitrogen (U.S. Environmental Protection Agency, 1993a). A comprehensive study on the economic impact of visibility impairment on national parks and wilderness areas and the cost of controls is currently being conducted by the Grand Canyon Visibility Transport Commission.

8.7.1 Basic Concepts of Economic Valuation

Studies on the economic impact of visibility degradation have mainly focused on consumer activities, specifically on the individuals response to the aesthetic aspects. Studies on the effects of visibility degradation on commercial activities are limited. However, airport operations may be affected by visibility degradation, but available evidence suggests that the economic magnitude of the effects of haze on commercial operations probably is very small. Based on a 1985 report by the U.S. Enviromental Protection Agency the percentage of the visibility impairment incidents sufficient to affect air traffic activity might be attributable, at least in part, to manmade air pollutants (possibly 2% to 12% in summer in the eastern United States).

That people notice changes in visibility conditions and that visibility conditions affect the well-being of individuals has been verified in scenic and visual air quality rating studies (Middleton et al., 1983; Latimer et al., 1981; Daniel and Hill, 1987), through the observation that individuals spend less time at scenic vistas on days with lower visibility (MacFarland et al., 1983), and through use of attitudinal surveys (Ross et al., 1987).

8.7.2 Economic Valuation Methods for Visibility

Two main economic valuation methods have been used to estimate dollar values for changes in visibility conditions in various settings: (1) the contingent valuation method (CVM), and (2) the hedonic property value method. Both methods have important limitations, and uncertainties surround the accuracy of available results for visibility. Ongoing research continues to address important methodological issues, but at this time some fundamental questions remain unresolved (Chestnut and Rowe, 1990a; Mitchell and Carson, 1989; Fischhoff and Furby, 1988; Cummings et al., 1986). See Fischhoff and Fauby (1988), Kahneman and Knetsch (1992), Rowe and Chestnut (1982), Mitchell and Carson (1989), and Cummings et al. (1986) for details on these methods and its usefulness in economic valuations.

The CVM involves the use of surveys to elicit values that respondents place on changes in visibility conditions. The most common variation of the CVM relies on questions that directly ask respondents to estimate their maximum willingness to pay (WTP) to obtain or prevent various changes in visibility conditions based on photographs and verbal descriptions, and some hypothetical payment mechanism, such as a general price increase or a utility bill increase.

Among the fundamental issues concerning the adequacy of CVM for estimating visibility values are (1) the ability of researchers to present visibility conditions in a manner relevant to respondents and to design instruments that can elicit unbiased values; and (2) the ability of respondents to formulate and report values with acceptable accuracy. Another important issue in CVM visibility research concerns the ability of respondents to isolate values related to visibility aesthetics from other potential benefits of air pollution control such as protection of human health.

The hedonic property value method uses relationships between property values and air quality conditions to infer values for differences in air quality. The approach is used to determine the implicit, or "hedonic," price for air quality in a residential housing market, based on the theoretical expectation that differences in property values that are associated with differences in air quality will reveal how much households are willing to pay for different levels of air quality in the areas where they live. This approach uses real market data that reflect what people actually pay to obtain improvements in air quality in association with the purchase of their homes. Hedonic property value studies provide estimates of total value for all perceived impacts resulting from air pollution at the residence, including health, visibility, soiling, and damage to materials and vegetation. The most important limitation is the difficulty in isolating values for visibility from other effects of air pollution at the residence.

8.7.3 Studies of Economic Valuation of Visibility

Economic studies have estimated values for two types of visibility effects potentially related to particulate matter and NO_x: (1) use and non-use values for preventing the types of plumes caused by power plant emissions, visible from recreation areas in the southwestern United States; and (2) use values of local residents for reducing or preventing increases in urban hazes in several different locations.

8.7.3.1 Economic Valuation Studies for Air Pollution Plumes

Three CVM studies have estimated on-site use values for preventing an air pollution plume visible from recreation areas in the southwestern United States (Table 8-5). One of these studies (Schulze et al., 1983) also estimated total preservation (use and non-use) values held by visitors and non-visitors for preventing a plume at the Grand Canyon. The plumes in all three studies were illustrated with actual or simulated photographs showing a dark, thin plume across the sky above scenic landscape features, but specific measures such as contrast and thickness of the plume were not reported. The estimated on-site use values for the prevention or elimination of the plume ranged from about $3 to $6 (1989 dollars) per day per visitor-party at the park. A potential problem common to all of these studies is the use of daily entrance fees as a payment vehicle.

TABLE 8-5. ECONOMIC VALUATION STUDIES FOR AIR POLLUTION PLUMES

Study	Location of Plume	Study Subjects	Year of Interviews	Type of Value	Valuation Method[a]	Payment Vehicle	Mean Results ($ 1989)
Schulze et al. (1983)	Grand Canyon National Park	Urban residents who have visited or plan to visit Grand Canyon	1980	Daily use value at park per household	Contingent valuation, direct WTP question	Daily park entrance fee	$6.17 per day at park per household
		Urban residents in Denver, Los Angeles, Chicago, Albuquerque; visitors and non-visitors	1980	Monthly preservation value per household	Contingent valuation, direct WTP question	Monthly utility bill increase	$5.31 per month per household
MacFarland et al. (1983)	Grand Canyon National Park	Park visitors	1980	Daily use value at park per visitor-party (household)	Contingent valuation, direct WTP question	Daily park entrance fee	$2.84 per day at park per visitor-party (household)
Brookshire et al. (1976)	Glen Canyon National Recreation Area (Lake Powell)	Nearby residents and lake visitors	1974	Daily use value at recreation area per visitor-party (household)	Contingent valuation, direct WTP question	Daily entrance fee	Visitors: $3.32 per day additional to prevent visible plume Residents: $2.21 per day additional to prevent visible plume

[a]WTP = Willingness to pay.

The Schulze et al. (1983) study suggest that on-site preservation values for preventing a plume at the Grand Canyon every day, based on 1.3 million visitor-parties of about three people per party, would be about $8 million. Based on their results, the implied preservation value for preventing a visible plume most days (the exact frequency was not specified) at the Grand Canyon would be about $5.7 billion each year when applied to the total U.S. population. However, Chestnut and Rowe (1990b) reported that the Schulze et al. (1983) preservation value estimates for haze at national parks in the Southwest are probably overstated by a factor of two or three and the same probably applies to the preservation value estimates for plumes.

8.7.3.2 Economic Valuation Studies for Urban Haze

Six economic studies concerning urban haze caused by air pollution are summarized in Table 8-6. The implicit values obtained for a 10% change in visual range are reported in Table 8-6 to allow a comparison of results across the studies. Values for a 10% change are shown to illustrate the range of results across the different studies. These estimates are based on a model developed for comparison purposes that assumes economic values are proportional to the percentage change in visual range. Values for a 20% change, for example, would be about twice as large as those shown for a 10% change, given the underlying comparison model. Each of these studies relied on a reasonably representative sample of residents in the study area, such that a range of socioeconomic characteristics and of neighborhood pollution levels was included in each sample.

The first five studies in Table 8-6 all focused on changes in urban hazes with fairly uniform features that can be described as changes in visual range. The sixth study (Irwin et al., 1990) focused on visual air quality in Denver, where a distinct edge to the haze is often noticeable, making visual range a less useful descriptive measure because it would vary depending on the viewpoint of the individual and whether the target was in or above the haze layer. The studies conducted in Denver and in the California cities are likely to have a higher NO_x component than in the eastern cities.

Both of the CVM studies in California asked respondents to consider health and visual effects but used different techniques to have respondents partition the total values. They found that, on average, respondents attributed about one-third to one-half of their total values

TABLE 8-6. ECONOMIC VALUATION STUDIES ON URBAN HAZE

Study	Location	Year	Valuation Method	Payment Vehicle	Presentation/Definition of Change in Visibility	Implied Mean Annual WTP[a] for a 10% Change in Visual Range ($ 1989)
PART I. UNIFORM URBAN HAZE						
Western Cities						
Loehman et al. (1981)	San Francisco	1980	Contingent valuation, direct WTP question	Monthly utility bill increases	Change in frequency distribution illustrated with local photos for 3 levels of air quality	$106 per household
Brookshire et al. (1982)	Los Angeles	1978	Contingent valuation, direct WTP question	Monthly utility bill increases	Change in average visibility illustrated with local photos for 3 levels of air quality	$10 per household
Trijonis et al. (1984)	San Francisco	1978-79	Hedonic property value		Light extinction based on airport visibility data	$208-231 per household
	Los Angeles	1978-79	Hedonic property value		Light extinction based on airport visibility data	$112-226 per household
Eastern Cities						
Tolley et al. (1986)	Chicago; Atlanta; Boston; Mobile; Washington, D.C.; Miami; Cincinnati	1982	Contingent valuation, direct WTP question	Monthly payment for visibility improvement program	Change in average visibility illustrated with Chicago photos for levels of air quality	$8-51 per household

[a]

TABLE 8-6 (cont'd). ECONOMIC VALUATION STUDIES ON URBAN HAZE

Study	Location	Year	Valuation Method	Payment Vehicle	Presentation/Definition of Change in Visibility	Implied Mean Annual WTP[a] for a 10% Change in Visual Range ($ 1989)
PART I (cont'd). UNIFORM URBAN HAZE						
Rae (1984)	Cincinnati	1982	Contingent valuation, direct WTP question	Monthly payment for visibility improvement program	Change in average visibility illustrated with Chicago photos for 3 levels of air quality	$48 per household
PART II. URBAN HAZE WITH BORDER						
Irwin et al. (1990)	Denver	1989	Contingent valuation, direct WTP question	General higher prices each year	1-step change in 7-point air quality scale, illustrated with photos	Preliminary results indicate mean annual WTP of about $100 per household for a 1-step change in the 7-point scale, with about one-third of the value attributed to visibility alone

[a]WTP = Willingness to pay.

to aesthetic visual effects. In spite of many similarities in the approaches used, the CVM results for San Francisco are notably higher than for Los Angeles when adjusted to a comparable percentage change in visual range. One potentially important difference in the presentations was that Loehman et al. (1981) defined the change in visibility as a change in a frequency distribution rather than simply a change in average conditions. This type of presentation is more realistic but more complex; and it is unclear how it may affect responses relative to presentation of a change in the average. It is possible that the distribution presentation might elicit higher WTP responses because it may focus respondents' attention on the reduction in the number of relatively bad days (and on the increase in the number of relatively good days), whereas the associated change in the average may not appear as significant. The implied change in average conditions in the Loehman et al. (1981) San Francisco study was considerably smaller than that presented in the Brookshire et al. (1982) Los Angeles study, which may have also resulted in a higher value when adjusted to a comparable size change in average visual range because of diminishing marginal utility (i.e., the first incremental improvement is expected to be worth more than the second).

The California studies in Los Angeles and San Francisco provide some interesting comparisons because two different estimation techniques were applied for the same locations. Property value results for changes in air quality for both cities were found to be higher than comparable values (for changes in total air quality) obtained in the CVM studies. This is as expected given the theoretical underpinnings of each estimation method, although Graves et al. (1988) have reported that subsequent analysis of the property value data revealed that the estimates are more variable than the original results suggest. These property value results are not reported here because they are for changes in air pollution indices that are not tied to visual air quality.

The property value study results reported in Table 8-6 from Trijonis et al. (1984) were estimated using light extinction as the measure of air quality. However, as discussed in the previous section on the hedonic property value method, these estimates are still likely to include perceived benefits to human health for reductions in air pollution as well as values for visual aesthetics. Consistent with this expectation, the results for a 10% change in light extinction are higher than the CVM results for visual range changes for the same cities. Respondents in several CVM studies have reported that, on average, they would attribute to

visibility aesthetics about one-fourth to one-half of their total WTP for improvements in air quality. This would imply that the Trijonis et al. (1984) results may reflect $25 to $100 for a change in visibility alone.

The results for the uniform urban haze studies in cities in the eastern United States fall between the respective CVM results for the California cities. The changes in visual range presented in these studies were similar to those presented in the Los Angeles study. In all of the eastern studies respondents were simply asked to consider only the visual effects when answering the WTP questions. This approach is now considered to be inadequate (Irwin et al., 1990; Carson et al., 1990).

McClelland et al. (1991) conducted a mail survey in 1990 in Chicago and Atlanta. Residents were asked what they would be willing to pay to have an improvement in air quality, which amounted to about a 14% improvement in annual average visual range. Respondents were then asked to say what percentage of their response was attributable to concern about health effects, soiling, visibility, or other air quality effects. Respondents, on average, attributed about 20% of their total WTP to visibility. The authors conducted two analyses and adjustments on the responses. One was to estimate and eliminate the potential selection bias resulting from non-response to the WTP questions (including what has been called protest responses). The other was to account for the potential skewed distribution of errors caused by the skewed distribution of responses (the long tail at the high end). Both of these adjustments caused the mean value to decrease. The annual average household WTP for the designated visibility improvement was $39 before the adjustments and $18 after the adjustments. This adjusted mean value implies about $13 per household for a 10% improvement in visual range. This is at the low end of the range of estimates shown in Table 8-6. If peer-review of this research effort confirms the appropriateness of the study design and analysis, the results suggest that greater confidence should be placed in the lower end of the range of results shown in Table 8-6 because this study represents an improvement in approach over the other eastern-cities studies.

Irwin et al. (1990) have reported preliminary results for the Denver study (Part II, Table 8-6). Comparison of these preliminary results with results from other studies is difficult because the photographs used to illustrate different levels of air quality were not tied to visual range levels. Instead, they were rated on a seven-point air quality scale by the

respondents, who were then asked their maximum WTP for a one-step improvement in the scale. This study reports some important methodological findings. One of these is confirmation that simply asking respondents to think only about visibility results in higher WTP responses for visibility changes than when respondents are asked to give WTP for the change in air quality and then to say what portion of that total they would attribute to visibility only. The latter approach produced a mean WTP estimate for a one-step change in visibility that was about one-half the size of the mean WTP estimate given when respondents were simply asked to think only about visibility. This may result from the effect of budget constraints on marginal values (the respondent has less to spend on visibility when he also is buying health); however, the authors express the concern that some, but not all, of the value for health may be included in the response when respondents are told to think only about visibility. They recommend that respondents be asked to give total values for changes in urban air quality and then be asked to say what portion is for visibility.

8.8 CLIMATIC EFFECTS

8.8.1 Introduction

Aerosols of submicron size in the atmosphere can affect the Earth's climate directly through the absorption of radiation and indirectly by modifying the optical properties and lifetime of clouds (perturbation of the radiative field). Perturbation of the radiation field generally is expressed as a *radiative forcing*, which is the change in average net radiation at the top of the troposphere because of a change in solar (shortwave) or terrestrial (longwave) radiation (Houghton et al., 1990). Note that it is the net effect at the top of the troposphere (i.e., the tropopause) that forces climate, and not the change at the surface, because the surface and troposphere are intimately coupled through atmospheric energy exchange processes such as dry and moist convection (Ramanathan et al., 1987). The radiative forcing due to aerosols is negative (i.e., aerosols have a cooling effect through the enhanced reflection of solar energy). This is in contrast to radiatively active trace ("greenhouse") gases associated with industrial and agricultural activities, which produce a positive longwave radiative forcing (i.e., "greenhouse" gases cause a warming of the earth-troposphere system). A large fraction of atmospheric particulate matter is of anthropogenic origin, the chief

sources being the emission of sulfur-containing aerosols by industry and the large-scale burning of biomass.

8.8.2 Radiative Forcing

There is now little doubt that long-lived, optically thick, aerosol layers may have modified the Earth's climate in the past. Geologic evidence suggests that there have been episodic injections of massive amounts of material into the Earth's atmosphere as a result of the impact of large asteroids or comets. The diminution of solar radiation reaching the surface has been suggested as the most likely cause of mass extinctions of species at the Cretaceous-Tertiary boundary (Alvarez et al., 1980) and also in the Late Devonian (Claeys et al., 1992). The possibility of a similar climatic catastrophe following a nuclear war has also been raised (Turco et al., 1983, 1990). However, these are examples of massive injections of particulate matter that result in extremely large radiative forcings. Current interest is focused on much more modest injections of materials that form thin aerosol layers in the troposphere. Although the radiative effects are smaller and have been generally ignored in climate model simulations (Hansen and Lacis, 1990), recent studies have estimated that they are not negligible and that their radiative forcing may be comparable (but opposite in sign) to the radiative effects of increased greenhouse gas emissions (Wigley, 1991; Charlson et al., 1992; Penner et al., 1992). Because there is so much concern regarding greenhouse gas-induced climate change, the study of this potential opposite effect of industrial emissions is expected to be quite intense in the near future (Penner et al., 1994).

To appreciate what is at issue here, it is necessary to understand the concept of radiative forcing. Averaged globally and annually, about 240 watts per meter squared ($W\ m^{-2}$) of solar energy is absorbed by the earth-atmosphere system (Hartmann, 1994). This must be balanced by an equal emission of thermal energy back to space for equilibrium. A *change* in average net radiation at the tropopause, because of a change in either solar or terrestrial radiation, perturbs the system and this perturbation is defined as the *radiative forcing*. In response to this perturbation, the climate system will try and reach a new equilibrium state. For example, the increase in longwave opacity of the atmosphere resulting from enhanced concentrations of greenhouse gases such as carbon dioxide (CO_2) and methane (CH_4) is a positive radiative forcing because it leads to a reduction in outgoing thermal

radiation. For equilibrium, given that there is no change in solar input, the temperature of the surface-troposphere system must increase. The individual contributions to this positive forcing, since pre-industrial times, is shown in Figure 8-15 (Houghton et al., 1990). Carbon dioxide is the single most important contributor with a radiative forcing of 1.50 W m^{-2} for the period 1765 to 1990. The total for all greenhouse gases attributable to anthropogenic sources is 2.45 W m^{-2}.

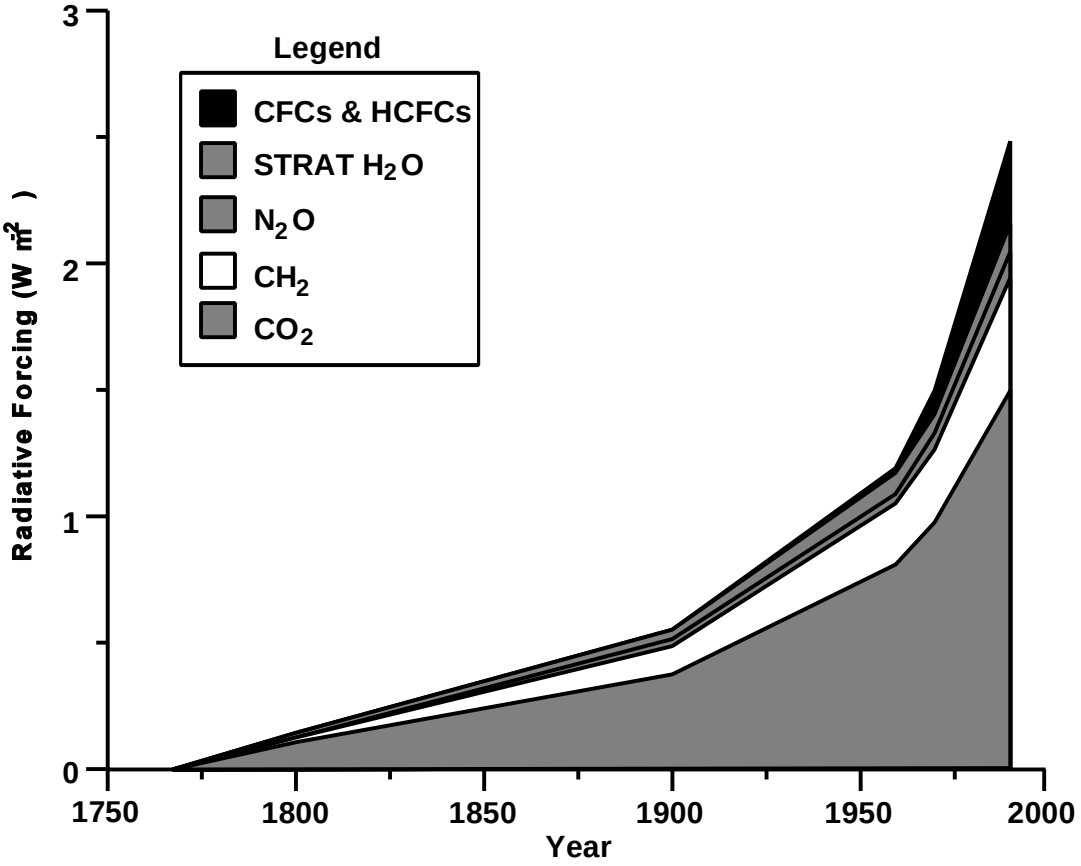

Figure 8-15. Changes in radiative forcing (W m^{-2}) due to increases in greenhouse gas concentrations between 1765 and 1990. Values are changes in forcing from 1765 concentrations.

Source: Houghton et al. (1990).

Human activity has also led to an increase in the abundance of tropospheric aerosols, primarily as a result of enhanced SO_2 emission, but also from biomass burning. This aerosol

layer produces a radiative forcing by perturbing the amount of solar energy that is absorbed by the earth-atmosphere system. By increasing the amount of solar energy reflected by the planet, aerosols produce a direct radiative forcing. They can also force the climate system indirectly by modifying the microphysical properties of clouds, primarily by reducing the effective drop size of water clouds. Both the direct and indirect radiative forcing of aerosols are negative (i.e., in response to this perturbation, the planet will cool).

Aerosols in the stratosphere have been implicated in the loss of O_3 through heterogeneous chemistry involving chlorine compounds (Hoffman and Solomon, 1989; Schoeberl et al., 1993; Hoffman et al., 1994). Although the chlorine is primarily of anthropogenic origin, the enhanced concentrations of aerosols are a result of volcanic eruptions. Anthropogenic SO_2 does not change the stratospheric aerosol burden appreciably. Therefore, this effect of aerosols is not relevant to this discussion.

The succeeding sections of this chapter are devoted to the estimation of aerosol radiative forcing. Translating this forcing into a climate response requires the incorporation of the forcing into a climate model. The model simulations, of course, are only as reliable as the models, which typically incorporate numerous feedbacks in the climate system that are only represented to some degree of approximation. There are certainly many feedbacks missing from current climate models, and it is quite possible that some feedbacks have been modeled quite incorrectly. Moreover, the radiative forcing due to anthropogenic aerosols needs to be estimated separately from that due to naturally occurring aerosols in order to evaluate the impact of human activity. The relationship between these aspects of the problem is shown in Figure 8-16.

As has been mentioned, the radiative forcing due to aerosols is opposite in sign to that due to greenhouse gases, but the degree of offset in forcing may not translate into offsetting climatic consequences. We can only judge these by studying model simulations. Also, it must be kept in mind that climate variations occur in the absence of radiative forcing as a result of interactions between the atmosphere, oceans, and the various elements of the land surface such as snow cover and vegetation.

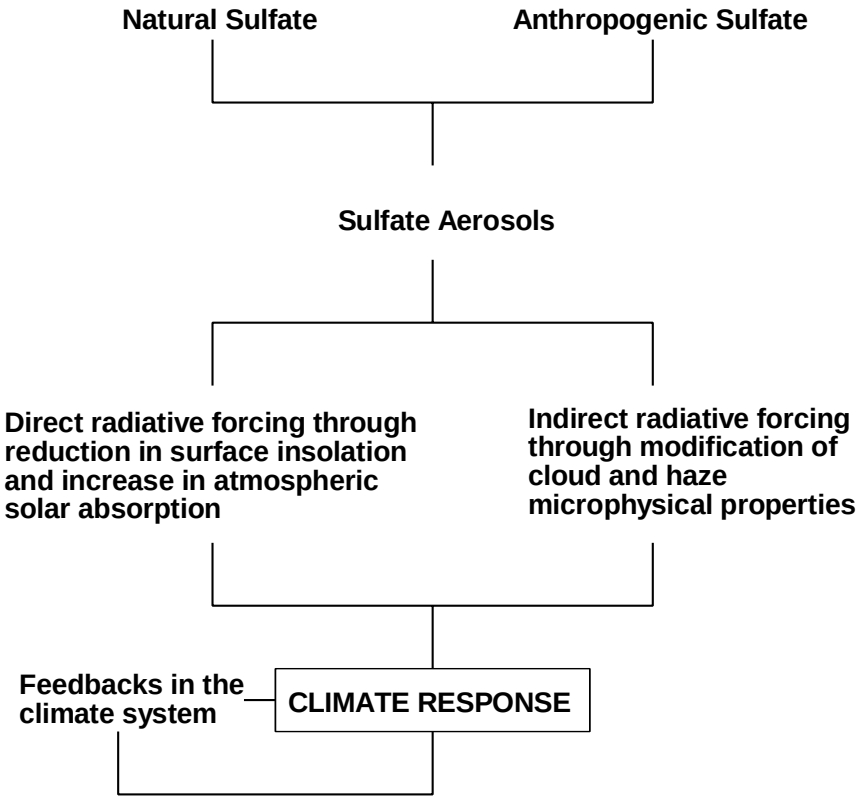

Figure 8-16. A schematic diagram showing the relationship between the radiative forcing of sulfate aerosols and climate response.

Source: Harshvardhan (1993).

8.8.3 Solar Radiative Forcing by Aerosols

Aerosol radiative forcing results from enhanced reflection of solar energy which enters the top of the Earth's atmosphere as a collimated beam of infinite width, but is subsequently scattered and absorbed to some degree even on the clearest day. Figure 8-17 shows this process schematically. Throughout the troposphere molecules, constituting the atmosphere, scatter sunlight by Rayleigh scattering (see the discussion of visibility for the definition of Raleigh scattering), which is highly wavelength dependent. In the lower troposphere, sunlight is scattered by aerosols or haze and absorbed by aerosols and water vapor. Because the aerosol loading is quite variable, this component of aerosol scattered solar radiation is also variable.

The degree to which a layer of particles scatters solar radiation is primarily determined by the nondimensional parameter referred to as the scattering optical depth of the layer, τ_s,

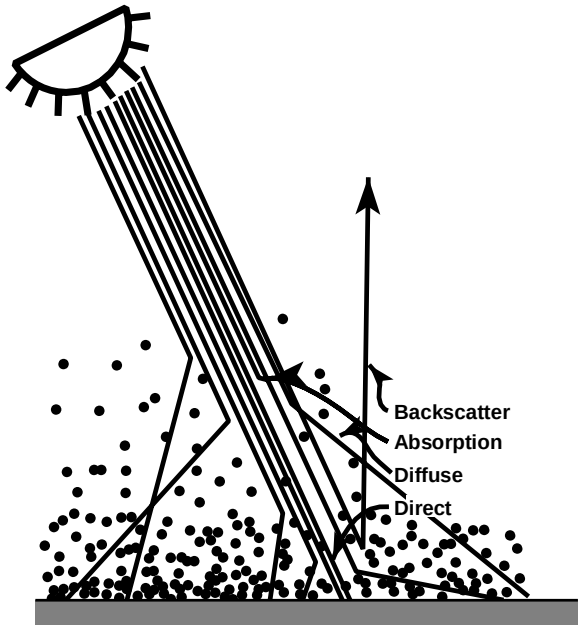

Figure 8-17. Extinction of direct solar radiation by aerosols showing the diffusely transmitted and reflected components, as well as the absorbed components.

which in turn is the column integrated volume scattering coefficient for particles, σ_{sp} (units are km^{-1}, see sections on visibility for details). Because the scattering coefficient for particles depends on wavelength, the attenuation of the direct beam of sunlight is also wavelength dependent. This spectral behavior is usually expressed by the proportionality

$$\sigma_{sp} \propto \lambda^{-\alpha} \tag{8-37}$$

where λ is the wavelength in micrometers (μm). The exponent, α, is the turbidity parameter introduced by Ångström (1964) and varies between 0.5 and 1.5 for aerosols (Twomey, 1977). For particles that are very small compared to the wavelength (Rayleigh scattering), $\alpha = 4$, and for relatively larger particles, such as cloud drops, $\alpha = 0$. The downwelling portion of the radiation scattered by molecules and aerosols forms diffuse skylight whereas the unattenuated beam of solar radiation is said to be the directly transmitted or beam radiation. The upwelling portion of scattered radiation, together with energy reflected by the surface, is the diffuse reflection of the earth-atmosphere system. It is the perturbation in this

component of radiant energy by enhanced aerosol loadings that constitutes the radiative forcing to the system by aerosols. The sum of directly and diffusely transmitted solar energy is the global solar radiation incident on a surface.

Figure 8-18, from Iqbal (1983), shows computations of the spectral distribution of a solar energy incident on a horizontal surface for a solar zenith angle of 60° (air mass = 2) and standard clear conditions. The atmosphere contains 350 Dobson units of ozone (O_3), 2 ppt/cm of water vapor, and a nonabsorbing aerosol layer corresponding to a surface visibility of 28 km. The ground reflectance is 0.2. Some features of Figure 8-18 are worth noting. Virtually all solar radiation at wavelengths less than 0.29 μm is removed by O_3 absorption. Rayleigh scattering by molecules is the predominant source of the diffuse radiation at shorter wavelengths, but the contribution falls off very dramatically with increasing wavelength because of the inverse fourth power dependence. Aerosol scattering contributes to the diffuse component at visible and near-infrared wavelengths. Absorption by the strong water vapor bands is quite evident in the near-infrared.

An increase in the optical depth of aerosols results in a decrease in the direct beam radiation, which could be substantial, but the downwelling portion of the enhanced scattered radiation compensates for this to a large extent. This is illustrated in Figure 8-19, which shows surface measurements of direct, diffuse, and global solar radiation, made using a multifilter rotating shadowband radiometer (Harrison and Michalsky, 1994; Harrison et al., 1994) at Albany, NY, on two clear days in August of 1992 and 1993. The total atmospheric optical depth in 1992 was influenced by the eruption of Mt. Pinatubo in June 1991. Although the volcanic aerosols were in the stratosphere, their effect on direct and diffuse transmitted radiation is similar to that due to tropospheric aerosols. The quantity plotted is the spectral irradiance convolved with the average human eye response that peaks at 550 nm and falls to zero at 400 and 700 nm. The main feature of the plot is the substantial difference in direct and diffuse radiation, but quite similar global irradiances. Close inspection shows that on the hazier day (in 1992), the global transmitted radiation was somewhat less (i.e., the volcanic aerosol caused a negative radiative forcing to the earth-atmosphere system by increasing the planetary albedo). Locally, tropospheric aerosol optical

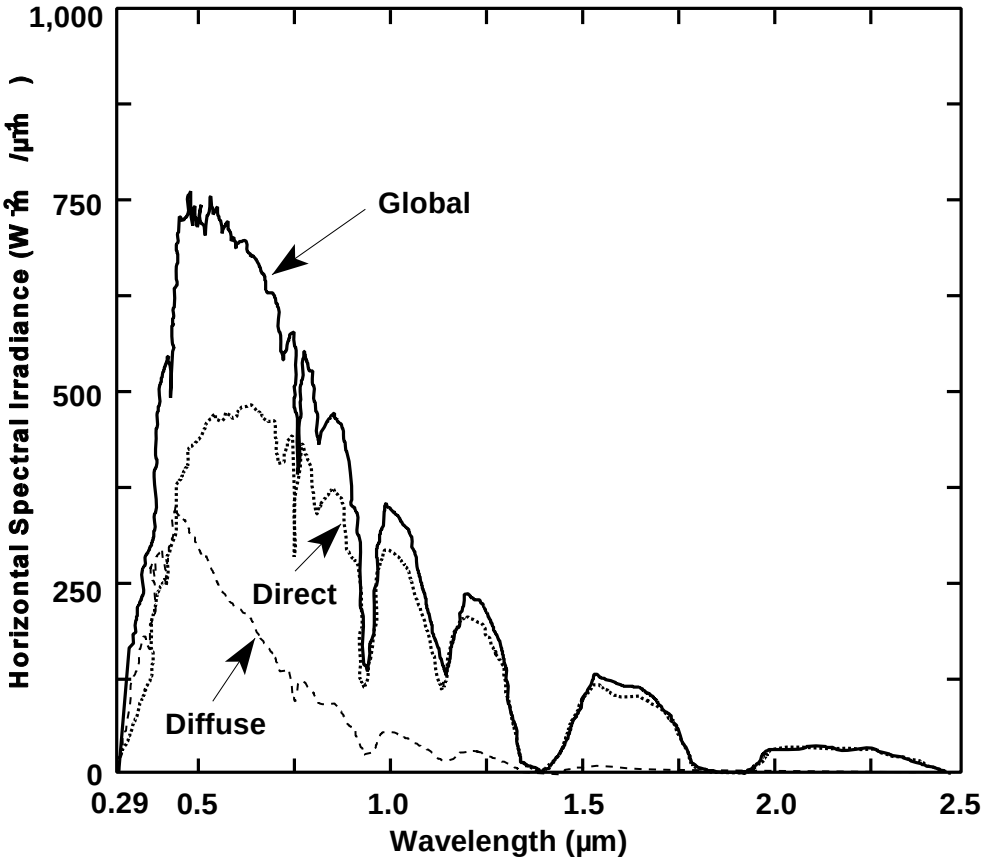

Figure 8-18. Global, direct, and diffuse spectral solar irradiance on a horizontal surface for a solar zenith angle of 60° and ground reflectance of 0.2. Atmospheric conditions are visibility, 28 km; water vapor, 2 ppt/cm.; ozone, 350 Dobson units.

Source: Iqbal (1983).

depths are much larger than the stratospheric optical depth and one would expect a more obvious diminution of global transmitted radiation than is shown here.

Figure 8-19 is for the spectrally integrated irradiance. Within the solar spectrum, wavelengths are affected to different degrees by the presence of aerosols. In particular there have been some studies on the effect of aerosols on transmitted UV to the surface. This an important consideration, especially for UV-B (280 nm $<\lambda <$ 320 nm). Many theoretical studies have been made of the effect of stratospheric aerosols on transmitted UV (Michelangeli et al., 1989, 1992; Davies, 1993; Box, 1995). They have shown that global transmitted UV can increase with the addition of a thin aerosol layer when the sun is low in

the sky and the layer is above the absorption region. The process responsible for this is single scattering which changes the direction of the incident radiation such that there is a shorter path through the absorbing layer and more is transmitted to the ground. However, when the sun is high in the sky or the scattering layer is below the absorbers this effect does not occur.

For tropospheric aerosols, the net effect is a reduction in global irradiance at all wavelengths similar to the total energy shown in Figure 8-19. Frederick et al. (1989) have calculated the expected change in Robertson-Berger meter readings from 1969 to 1986 for 34.5°N based on changes in column ozone as reported by Watson et al. (1988). They compared ratios with and without an aerosol layer of optical depth 0.1 independent of wavelength in the lowest 2 km for 1986 only. For clear atmospheres, the ratio changed from 1.02 without the aerosol to 0.92 with the aerosol indicating that the effect on UV-B transmission of the depletion in column ozone from 1969 to 1986 could be compensated by a concomitant increase in particulate matter. Measurements made at Barcelona, Spain, by Lorente et al. (1994) show that the UV-B at the surface is reduced by 37% during the most polluted days and UV-A is reduced by 30% compared to the clearest days. By reflecting some UV back to space, tropospheric aerosols actually decrease the irradiance of this flux to the surface.

8.8.3.1 Modeling Aerosol Direct Solar Radiative Forcing

Some basic aspects of scattering and absorption by small particles typically present in aerosol layers govern the sign and magnitude of the direct radiative forcing by aerosols. These properties are discussed in Section 8.2 of this chapter. The reflectance of an aerosol layer is chiefly determined by the optical depth, single scattering albedo, ω_{0}, and some measure of the scattering phase function. The single scattering albedo, the ratio of the light-scattering coefficient and the light-extinction coefficient, is a measure of the absorptance of the aerosol layer. Related quantities are the specific extinction and specific scattering coefficients, ψ_{ext} and ψ_{scat}, which are defined as the coefficients per unit mass in units of m^2g^{-1}. The phase function determines the probability that incident radiation will scatter into a particular direction given by the scattering angle measured from the forward direction of the incident radiation.

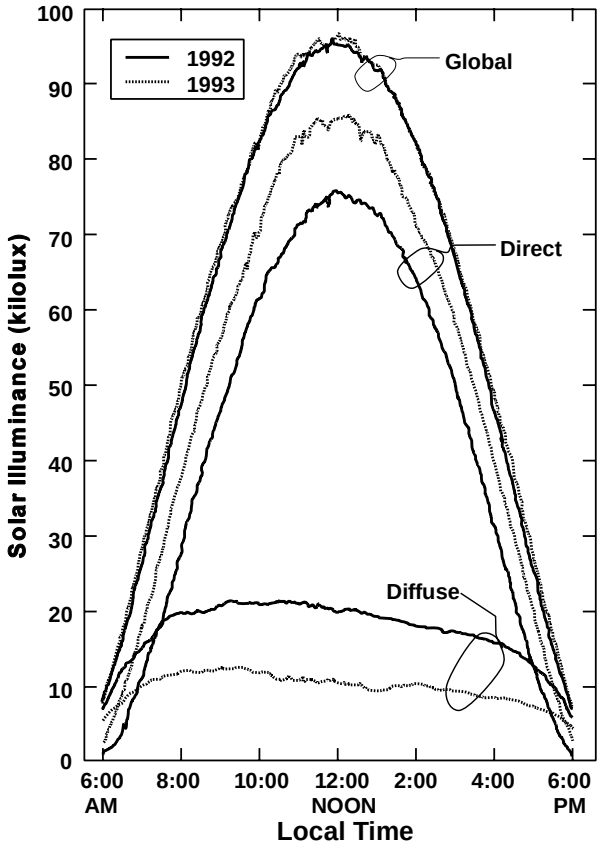

Figure 8-19. Surface measurements of direct, diffuse, and global solar radiation expressed as illuminance, at Albany, NY, on August 23, 1992, and August 26, 1993.

Source: Harrison and Michalsky (1994).

At visible wavelengths, the optical depth of tropospheric aerosols ranges from less than 0.05 in remote, pristine environments to about 1.0 near the source of copious emissions (Weller and Leiterer, 1988). The optical depth decreases quite rapidly with increasing wavelength if the layer is composed of fine particles as can be seen from Equation 8-37. Aerosol layers, therefore, tend to be fairly transparent at thermal wavelengths and their radiative forcing is confined to solar wavelengths. Because there are strong water vapor absorption bands in the solar near-infrared (see Figure 8-20), the dominant effect of tropospheric aerosols is in the visible wavelengths. Harshvardhan (1993) has shown that, to the first order, the change in the albedo with the addition of a thin aerosol layer over a surface of reflectance, R_s, is

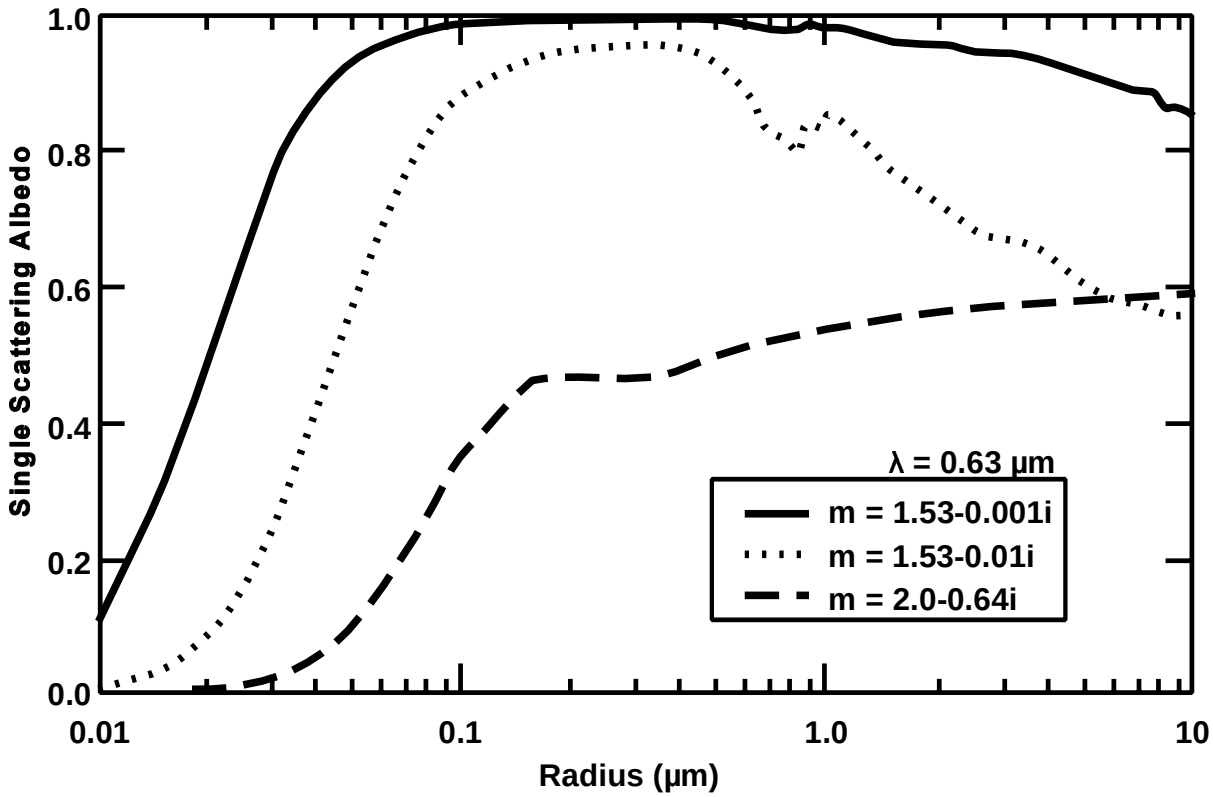

Figure 8-20. Single scattering albedo of monodispersed spherical aerosols of varying radius and three different refractive indices at a wavelength of 0.63 μm.

Source: Harshvardhan (1993).

$$\Delta R \approx R_a(1 - R_s)^2 - 2A_aR_s \tag{8-38}$$

where R_a and A_a are the reflectance and absorptance, respectively, of the aerosol layer. The perturbation, ΔR, will be positive when

$$(1 - \omega_0)/\omega_0\beta < (1 - R_s)^2/2R_s \tag{8-39}$$

where β is the average backscatter fraction and can be computed from the scattering phase function. A positive value for the change in albedo implies a negative solar radiative forcing because the planetary albedo increases and less solar energy is absorbed by the earth-atmosphere system.

From Equation 8-39, it is obvious that the sign of the forcing will be determined to a large extent by the single scattering albedo. At visible wavelengths, most constituents of tropospheric aerosols, with the exception of elemental carbon, are nonabsorbing and $\omega_{oo} = 1.0$ (Bohren and Huffman, 1983) so that the change in albedo will be positive. Aerosols with absorbing components can be modeled as equivalent scatterers of refractive index, $m = n - ik$, with the imaginary index being a measure of particle absorption. Figure 8-20, shows the computed values of single scattering albedo at a wavelength of 0.63 μm for single particles of varying radius. The three separate curves are for aerosols composed of carbon ($m = 2.0 - 0.64i$) and two models of sulfate aerosols containing absorptive components. Given the properties of an aerosol layer, the change in albedo can be computed from Equation 8-38. To calculate the radiative forcing, one must also include the effects of other atmospheric constituents such as molecular scattering, stratospheric O_3, water vapor absorption, and, most importantly, cloud cover.

8.8.3.2 Global Annual Mean Radiative Forcing

Charlson et al. (1991) calculated the global mean radiative forcing due to anthropogenic aerosols by making the following assumptions. They assumed that the perturbation would be exceedingly small over cloudy areas because cloud optical depths are one to two orders of magnitude greater than aerosol optical depths (Rossow and Schiffer, 1991). For nonabsorbing aerosols, they found that the change in planetary albedo could be expressed as

$$\Delta R_p \approx T^2 (1 - N_c) (1 - R_s^2) (2\beta\tau) \tag{8-40}$$

where T is the transmittance of the atmosphere above the aerosol layer and N_c is the global mean cloud fraction. The planetary mean radiative forcing is then

$$\Delta F_R = \Delta R_p S_o / 4 \tag{8-41}$$

where $S_o/4$ is the annual global mean insolation of the earth-atmosphere system (Hartmann, 1994) with S_o being the solar constant, which equals to 1,370 W m^{-2}. For the generally accepted values of T = 0.71, N_c = 0.6, R_s = 0.15 and β = 0.3, Charlson et al. (1991)

$$\Delta F_R = 30.0\tau \tag{8-42}$$

obtained such that for τ, the optical depth at visible wavelengths ranging from 0.05 to 0.10, the direct solar radiative forcing is 1.5 to 3.0 W m^{-2}, a value comparable to the long-wave radiative forcing of all the anthropogenic greenhouse gases (Section 8.8.2).

The above estimate was refined by Charlson et al. (1992) in which the anthropogenic sulfate aerosol burden was actually related to the source strength of anthropogenic SO_2, the fractional yield of emitted SO_2 that reacts to produce sulfate aerosol and the sulfate lifetime in the atmosphere. The scattering properties of the sulfate aerosol were also modeled in terms of a relative humidity factor that accounts for the increase in particle size associated with deliquescent or hygroscopic accretion of water with increasing RH. The relationship between optical depth and the areal mean column burden of anthropogenic sulfate aerosol, $B_{sulfate}$, is

$$\tau = \chi_{sulfate}\, f(RH)\, B_{sulfate} \tag{8-43}$$

where $\chi_{sulfate}$ is the molar scattering cross section of sulfate at a reference low RH (30%) and f(RH) is the relative humidity factor. The sulfate burden, is related to SO_2 emissions and sulfate lifetime. For an emission rate of 90×10^{12} g of sulfur per year, a yield fraction of 0.4, a sulfate lifetime of 0.02 years (7 days) and the molar scattering cross section of sulfate of 500 $m^2 mol^{-1}$ (corresponding to specific extinction coefficient of 5 $m^2 g^{-1}$), Charlson et al. (1992) estimated that ΔF_R = 1.0 W m^{-2}, with an uncertainty factor of 2, which perhaps should be more considering that the uncertainty in the specific extinction coefficient alone is higher (Hegg et al., 1993, 1994; Anderson et al., 1994).

The above is an estimate for the forcing due to industrial emissions. Another anthropogenic source of aerosols is biomass burning. Penner et al. (1992) have estimated

that the radiative forcing due to this activity could be as much as 0.9 W m^{-2}, which is comparable to the sulfate forcing. One difference is that the smoke produced is somewhat absorbing and the atmosphere would experience a positive forcing of 0.5 W m^{-2}. Estimates of the global forcing due to biomass burning are even more uncertain than those for sulfate because of the sparsity of data on the relevant radiative properties of biomass aerosols.

8.8.4 Climate Response

8.8.4.1 Early Studies

Global Background Aerosols

The role of aerosols in modifying the Earth's climate through solar radiative forcing has been a topic of discussion for many decades. Modeling studies assumed a climatological background distribution of aerosols such as that of Toon and Pollack (1976). Two simple types of climate models were used to calculate the effects of aerosols on climate: (1) the radiative-convective model, which resolves radiative perturbations in an atmospheric column, and (2) the energy balance model, which allows for latitudinal dependence, but parameterizes all processes in terms of the surface temperature. A typical study was that of Charlock and Sellers (1980) who used an enhanced one-dimensional radiative-convective model that included the effects of meridional heat transport and heat storage. The model was run with and without a prescribed aerosol layer of visible optical depth equal to 0.125 for conditions representative of 40° and 50° N latitude. The annual mean surface temperature with aerosols was 1.6 °C lower than that for the aerosol-free run.

Coakley et al. (1983) were the first to use an energy balance model to compute the latitudinally dependent radiative forcing for the Toon and Pollack (1976) aerosol distribution, including the effects of absorbing components. Even for moderately absorbing aerosols ($m = 1.5 - 0.01i$), the solar radiative forcing was negative, except in the 80° to 90° N latitude belt, which has a very high surface albedo. Here the criterion given by Equation 8-31 is not satisfied and the change in albedo is negative (i.e., the solar radiative forcing is positive). The model results showed global mean surface temperature decreases ranging from 3.3 °C for nonabsorbing aerosols to 2.0 °C for the absorbing aerosols. The maximum temperature drop was at polar latitudes even for the absorbing layer because advective processes responded to the aerosol-

induced cooling at low- and middle-latitudes. Other two-dimensional model studies have confirmed this basic picture (Jung and Bach, 1987).

Regional and Seasonal Effects

Apart from global studies, there have been several programs devoted to ascertaining the effects of aerosols on regional and seasonal scales. An example is the radiative effect of aerosols in the Arctic (Rosen et al., 1981). A field experiment, the Arctic Gas and Aerosol Sampling Program, was conducted in 1983 (Schnell, 1984). It was determined that aerosols had a substantial absorbing component. The study by MacCracken et al. (1986) used both one- and two-dimensional climate models to evaluate the climatic effects. They found that the initial forcing of the surface-atmosphere system is positive for surface albedos greater than 0.17, and the equilibrium response of the one-dimensional radiative-convective model showed surface temperature increases of 8 °C. Infrared emission from the warmer atmosphere was found to be an important forcing agent of the surface. The two-dimensional model was run through the seasonal cycle and had an interactive cryosphere. Peak warming occurred in May, a month later than the peak radiative forcing, as a result of earlier snow melt.

Massive Aerosol Loads

In the 1980s, there were several studies related to what became known as the "nuclear winter" phenomenon (Turco et al., 1983) (i.e., the climatic consequences of widespread nuclear war). Modeling efforts ranged from radiative-convective models (Cess et al., 1985) to three-dimensional general circulation models (GCM) (Thompson et al., 1987; Ghan et al., 1988), and mesoscale models (Giorgi and Visconti, 1989) with interactive smoke generation and removal processes and fairly detailed smoke optics. A review of modeling efforts has been made by Schneider and Thompson (1988) and Turco et al. (1990). The latter study summarized the best estimates of possible reduction in surface temperature from the smoke lofted into the atmosphere during the initial acute phase.

General Circulation Model studies (Thompson et al., 1987; Ghan et al., 1988) indicate that for a July smoke injection, the average land temperatures over the latitude zone from 30° to 70° N, over a 5-day period, would decrease by 5 °C for smoke of optical depth equal to 0.3, but could decrease by 22 °C for large loadings of optical depth equal to

3.0. However, the temperature in the interior of land masses could drop by as much as 30 °C. The temperature perturbations for smoke injections in other seasons are smaller. At lower latitudes, the cooling is moderated by the delay in smoke transport (assuming initial injection in high northern latitudes), and the more humid climate. Model studies also indicate a dramatic decrease in rainfall over land and a failure of the Asian monsoon (Ghan et al., 1988).

8.8.4.2 Recent Regional Studies

There have been more recent studies of possible climatic effects resulting from severe aerosol loading on regional scales. The Arctic haze problem has been investigated extensively. Blanchet (1989, 1991), using a GCM, studied the effects of increasing aerosol loads north of 60° N. Although the solar heating rate in the troposphere increased quite dramatically, the temperature did not rise substantially. The positive forcing of 0.1 to 0.3 $Kday^{-1}$ resulted in a decrease in the meridional heat flux. Quite importantly, the simulated cloud cover in the experiment was altered sufficiently to produce changes in net radiative fluxes at the top were locally an order of magnitude greater than the initial forcing. This implies that it may be very difficult to identify climate change effects due to aerosols alone. Another effect of aerosols at high latitudes that has the potential for affecting climate is the change in surface albedo due to deposition of soot. This was studied by Vogelmann et al. (1988) with respect to the nuclear winter problem. They found that the cooling due to smoke aerosol could be moderated somewhat by the "dirty" snow at very high latitudes.

Several studies have examined the effect of smoke from forest fires on climate. Since these are natural phenomena, it is important to understand their effects in order to place anthropogenic effects in context. Evidence of substantial climatic effects is present only when the smoke loading is substantial. For example, Robock (1988) examined the situation in northern California where a subsidence inversion trapped smoke in mountain valleys for several days in September 1987. One station recorded an anomaly in the maximum temperature of −20 °C. Veltischev et al. (1988) analyzed data covering the period of major historical fires in Siberia, Europe, and Canada. They estimated that the optical depth of

smoke following fires in Siberia in 1915 was about 3.0 and surface temperature dropped by 5 °C.

Other studies have also shown a relationship between smoke and surface temperature. Robock (1991) studied the smoke from Canadian fires in July 1982. He compared forecasted temperatures with observations and found that regions of negative anomaly were well correlated with the smoke layer. Westphal and Toon (1991) used a mesoscale model with interactive smoke physics and optics to simulate the smoke plume and its meteorological effects. They calculated the albedo of the smoke-covered area to be 35%, and the resulting surface cooling was 5 °C.

Perhaps the most extensive recent investigation of the possible climatic effects of heavy aerosol burdens was the study of the Kuwait oil fires in 1991. Several modeling studies were undertaken. Browning et al. (1991) simulated the smoke plume with a long-range dispersion model and concluded that the smoke would remain in the troposphere and not be lofted into the stratosphere where the residence time would be much longer. They estimated a maximum temperature drop of 10 °C beneath the plume, within about 200 km (i.e., only a regional, not global climatic effect). Bakan et al. (1991) used a GCM with an interactive tracer model to simulate the plume dispersion and climatic effects. The maximum temperature drop was estimated to be about 4 °C near the source. The local and regional nature of the effect was confirmed during a field experiment undertaken in May/June, 1991. The smoke from the oil fires had insignificant global effects because (1) particle emissions were less than expected, (2) the smoke was not as black as expected, (3) the smoke was not carried high in the atmosphere, and (4) the smoke had a short atmospheric residence time (Hobbs and Radke, 1992).

The study of severe events such as those described above is useful for investigating model response since such strong forcings usually provide unambiguous climate response signals. The simulated climate response to the more modest radiative forcing due to the distribution of natural and usual anthropogenic sulfate or smoke aerosols is well within the internal model variability. However, an estimate of the magnitude of possible effects can be obtained by model simulations that integrate the chemistry, optics, and meteorology of anthropogenic aerosols.

8.8.4.3 Integrated Global Studies

Ideally, one should study the problem in an integrated manner, in which the emissions of sulfate precursors are tracked globally and the radiative forcing of the resulting aerosols computed locally in space and time. A further step would be to let the radiative response impact climate interactively. This latter step could be carried out by a GCM coupled to an oceanic model. Recent studies have accomplished various elements in this scenario.

Global three-dimensional models of the tropospheric sulfur cycle consider emission, transport, chemistry, and removal processes for both natural and anthropogenic sources. The primary natural source is dimethylsulfide (DMS), which is released by oceanic phytoplankton (Nguyen et al., 1983; Shaw, 1983; Charlson et al., 1987). The DMS reacts in air to form sulfate aerosols. Anthropogenic emissions are over land, especially in the heavily industrialized areas of the Northern Hemisphere. Examples of such sulfur cycle models are the Lagrangian model of Walton et al. (1988) and Erickson et al. (1991), known as the GRANTOUR model, and the Eulerian transport model of Langner and Rodhe (1991) and Langner et al. (1992), known as the MOGUNTIA model. Both models use prescribed mean winds, typically obtained from GCM simulations, to provide monthly mean concentrations of sulfate aerosols.

With such detailed input, it is possible to construct global maps of the radiative forcing due to sulfate and compare the magnitude with that due to greenhouse gases. Kiehl and Briegleb (1993) carried out such a study using the monthly mean sulfate abundances from the MOGUNTIA model. For meteorological parameters, they used 1989 monthly mean temperature and moisture fields data from the European Center for Medium Range Weather Forecasting. Vertical distributions of clouds were taken from a GCM simulation using the National Center for Atmospheric Research Community Climate Model (CCM2) since such detailed observations are lacking. However, attempts were made to adjust the total cloud cover to correspond to observations.

The radiative forcing was calculated by Kiehl and Briegleb using an 18-band δ-Eddington model in the shortwave and a 100 cm^{-1} resolution band model in the longwave, which includes the contributions due to trace gases such as CH_4, NO_2, and chlorofluorocarbons. The optical properties of sulfate aerosol were calculated spectrally using the refractive indices for 75% sulfuric acid (H_2SO_4) and 25% water (H_2O) and an

assumed log-normal size distribution that has a geometric mean diameter by volume of 0.42 μm. The specific extinction coefficient of the dry particles was found to be a very strong function of wavelength, decreasing from 10 m^2g^{-1} at 0.3 μm to less than 2.0 m^2g^{-1} at 1.0 μm. This is significant in interpreting the computed forcing when comparisons are made with earlier studies that used a constant value for the specific extinction coefficient.

The value of the specific extinction coefficient depends on the size distribution of the aerosols but that also affects the phase function such that changes in the coarse particle or fine particle mode do not greatly affect the total radiative forcing (Kiehl and Briegleb, 1993). This is because the extinction cross section has a sharp maximum for particles that are of the same dimension as the wavelength and falls off rapidly for smaller and larger particles (Covert et al., 1980).

The direct radiative forcing is calculated by adding the sulfate burden to the model and computing the change in absorbed solar radiation. Figures 8-21a and 8-21b, from Kiehl and Briegleb (1993) show the annual mean direct solar radiative forcing resulting from anthropogenic sulfate aerosols (global mean = -0.28 W m^{-2}) and anthropogenic plus natural sulfate (global mean = -0.54 W m^{-2}). The patterns are similar to those obtained earlier by Charlson et al. (1991), but the magnitude is roughly half. Most of the difference is due to the assumption of a constant value of 5.0 m^2g^{-1} for the specific extinction coefficient in the earlier study, but there was also a difference in the phase function used. Therefore, assumptions regarding radiative properties were able to account for all the differences. Points to note in the figure are the local concentrations of anthropogenic forcing and particularly the hemispheric asymmetry in the forcing, even when natural sulfate is included. Although the southern hemisphere is largely ocean, the direct forcing due to natural sulfate is substantial only in the clear oceanic areas since, in the presence of clouds, the additional sulfate effect is minimal.

To place the role of anthropogenic sulfate in perspective, Kiehl and Briegleb (1993) compared the direct radiative forcing with that of increasing greenhouse gases from preindustrial times to the present. The greenhouse gas forcing is calculated by computing the spatial distribution of the change in the net longwave flux at the tropopause for the trace gas increases from the preindustrial period to the present. The annual averaged results for

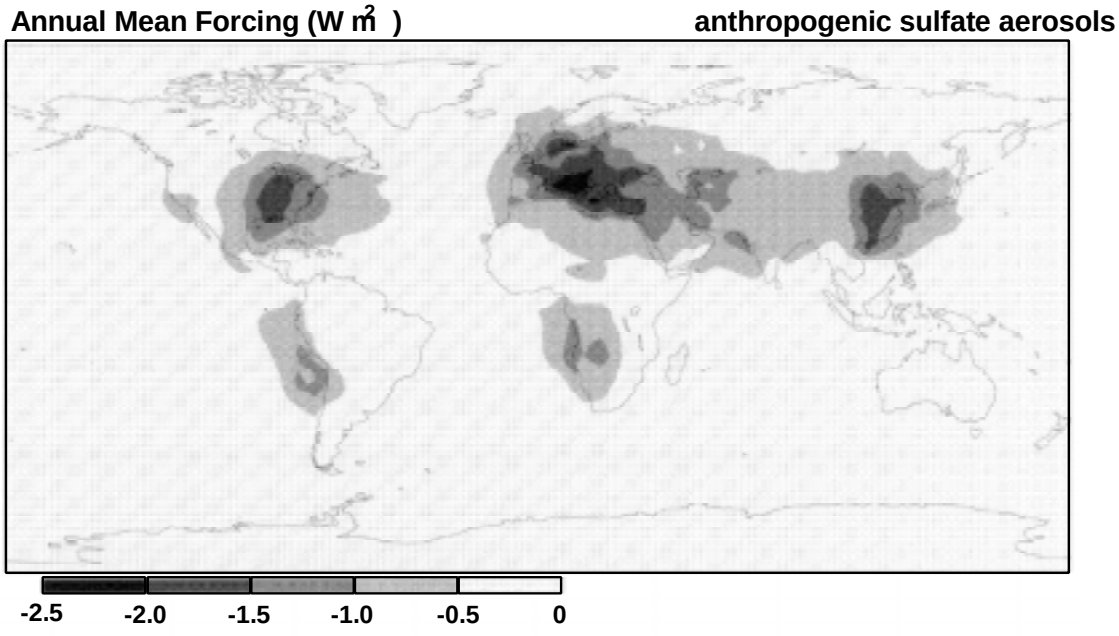

Figure 8-21a. Annual mean direct radiative forcing (W m^{-2}) resulting from anthropogenic sulfate aerosols.

Source: Kiehl and Briegleb (1993).

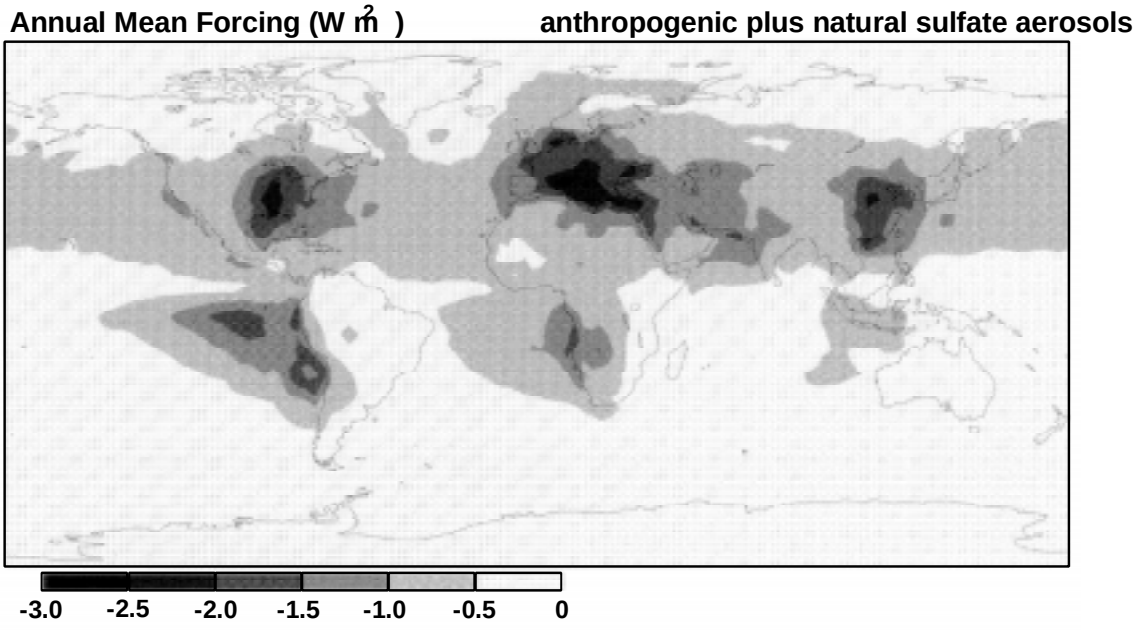

Figure 8-21b. Annual mean direct radiative forcing (W m^{-2}) resulting from anthropogenic and natural sulfate aerosols.

Source: Kiehl and Briegleb (1993).

greenhouse gases alone and in combination with anthropogenic sulfate are shown in Figure 8-22a and 8-22b, respectively. The greenhouse gas forcing is, of course, positive and is the greatest in the clear regions over the land and oceanic deserts. The global annual mean is 2.1 W m^{-2}. When the negative forcing of aerosols is added, the global annual mean direct radiative forcing due to anthropogenic activities is 1.8 W m^{-2}. However, locally, there are regions where the anthropogenic sulfate forcing cancels the greenhouse forcing.

The forcing is simply an initial perturbation. Because the sulfate forcing is in the shortwave and felt primarily at the surface (for nonabsorbing aerosols), a coupled atmospheric-oceanic climate model is required to determine the effect on climate. Taylor and Penner (1994) have used the GRANTOUR model to provide the sulfate input to a GCM (CCM1), which was coupled to a 50 m mixed-layer ocean model with sea ice and a specified meridional oceanic heat flux.

To assess the anticipated patterns of climate response to anthropogenic emissions of both SO_2 and CO_2, Taylor and Penner performed four 20-simulated-year integrations in which the atmospheric CO_2 concentration was fixed at either the preindustrial level (275 ppm) or the present day concentration (345 ppm). Anthropogenic sulfur emissions, corresponding to 1980, were either included or excluded. Table 8-7 summarizes their annual average results. The global average anthropogenic sulfate forcing was found to be -0.95 W m^{-2}; more than three times larger than calculated by Kiehl and Briegleb (1993). The differences in the annual anthropogenic sulfate forcing value in the two studies is due partially to the sulfate chemistry in the model used by Taylor and Penner, (1994). For example, there is a stronger seasonal cycle with enhanced northern hemisphere concentrations in summer. The remainder may be contributed to the use of a constant specific scattering coefficient (8.5 m^2g^{-1} at 0.55 μm) instead of the RH-dependent model used by Kiehl and Briegleb (1993). As noted earlier, the value of the specific scattering coefficient chosen could be a gross overestimate and, therefore the values of the sulfate forcing shown in Table 8-7 are probably much too high.

Some noteworthy features of Table 8-7 are that the combined CO_2 and sulfate forcing is not linearly additive and there is a pronounced asymmetry in the climate response in the two hemispheres. What is clear is that the anthropogenic sulfate is expected to reduce somewhat the anticipated warming resulting from the increased emission of greenhouse gases, especially

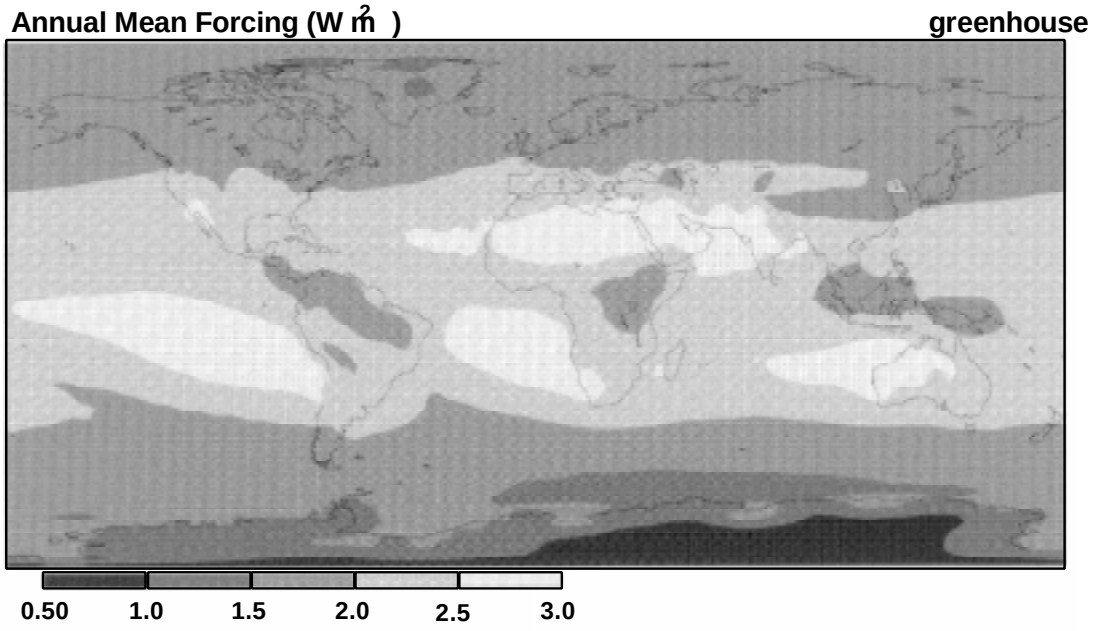

Figure 8-22a. Annual averaged greenhouse gas radiative forcing (W m^{-2}) from increases in CO_2, CH_4, N_2O, CFC-11, and CFC-12 from preindustrial time to the present.

Source: Kiehl and Briegleb (1993).

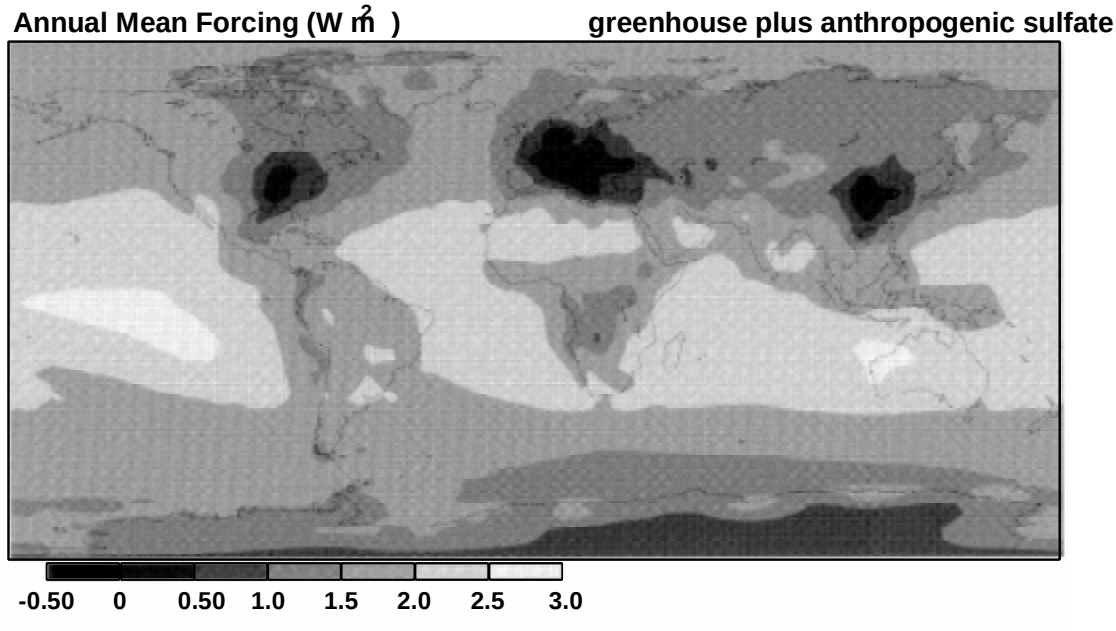

Figure 8-22b. Annual averaged greenhouse gas forcing plus anthropogenic sulfate aerosol forcing (W m^{-2}).

Source: Kiehl and Briegleb (1993).

TABLE 8-7. RADIATIVE FORCING AND CLIMATE STATISTICS

Case	ΔF ($W\ m^{-2}$)	T_s ($^\circ C$)	ΔT_s ($^\circ C$)	P ($mm\ d^{-1}$)	ΔP ($mm\ d^{-1}$)	C (%)	ΔC (%)	SI (%)	ΔSI (%)
Northern Hemisphere									
Preindustrial		12.5		3.40		56.6		4.87	
Present-day CO_2	1.26	14.5	1.9	3.48	0.09	55.0	-1.7	4.13	-0.74
Present-day sulfate	-1.60	11.3	-1.2	3.36	-0.04	56.9	0.3	5.54	0.67
Combined CO_2 and sulfate	-0.34	13.0	0.5	3.43	0.03	55.8	-0.9	4.85	-0.02
Observed climate statistics		14.9		2.6		58.9		4.4	
Southern Hemisphere									
Preindustrial		12.5		3.54		62.4		6.64	
Present-day CO_2	1.25	14.8	2.3	3.61	0.08	61.1	-1.3	4.39	-2.26
Present-day sulfate	-0.30	11.7	-0.8	3.48	-0.06	63.1	0.7	7.24	0.59
Combined CO_2 and sulfate	0.95	13.6	1.1	3.56	0.02	62.1	-0.3	5.40	-1.24
Observed climate statistics		13.5		2.7		65.6		4.5	
Global average									
Preindustrial		12.5		3.47		59.5		5.76	
Present-day CO_2	1.26	14.6	2.1	3.55	0.08	58.0	-1.5	4.26	-1.50
Present-day sulfate	-0.95	11.5	-1.0	3.42	-0.05	60.0	0.5	6.39	0.63
Combined CO_2 and sulfate	0.31	13.3	0.8	3.49	0.02	58.9	-0.6	5.13	-0.63
Observed climate statistics		14.2		2.7		62.2		4.5	

ΔF = radiative forcing; T_s = surface temperature; P = precipitation; C = cloud cover; SI = sea ice coverage.

Source: Taylor and Penner (1994).

in the Northern Hemisphere. On a regional scale, Taylor and Penner (1994) found that the strongest response was in the polar regions associated with an increase in sea ice. Note that the change in sea ice coverage, (ΔSI), in the northern hemisphere is essentially zero as the sulfate completely cancels the CO_2 effect. Also, the greatest cooling is found over broad regions of the Northern Hemisphere continents where all the sulfur emission is occurring. However, the maximum cooling is not over Europe where the maximum radiative forcing occurs, but further north, and associated with changes in sea ice.

Comparative Lifetimes of the Forcing

One extremely important aspect in comparing the effects of CO_2 and sulfur emissions is the disparate lifetimes of the forcing mechanisms. The residence times of trace gases that result in a positive longwave forcing of the climate system is from decades to a century or more (Houghton et al., 1990). On the other hand, the cycling time for sulfate in the troposphere is only about a week (Langner and Rodhe, 1991), which is dependent on the frequency of precipitation removal (Charlson et al., 1992). Therefore, any changes in industrial emission patterns will be reflected immediately in the sulfate forcing, but the concentration of CO_2 and the accompanying forcing will continue to rise for more than a century even if emissions were kept constant at present levels. See Figure 8-23.

One could infer from the above discussion that sulfate emissions are providing some amelioration of greenhouse warming, and that a curtailment of such emissions might result in enhanced global warming. However, given the uncertainties in present estimates of the effects of aerosols, especially the fact that many feedbacks are not fully included, it would be premature to base any decisions on these current discussions of the possible effects of aerosols on climate.

8.8.5 Aerosol Effects on Clouds and Precipitation

8.8.5.1 Indirect Solar Radiative Forcing

Cloud Microphysical Properties

A substantial portion of the solar energy reflected back to space by the earth system is due to clouds. The albedo (i.e., reflectivity) of clouds, in turn, depends to a large extent on the optical thickness, which is the column integrated light-extinction coefficient (see

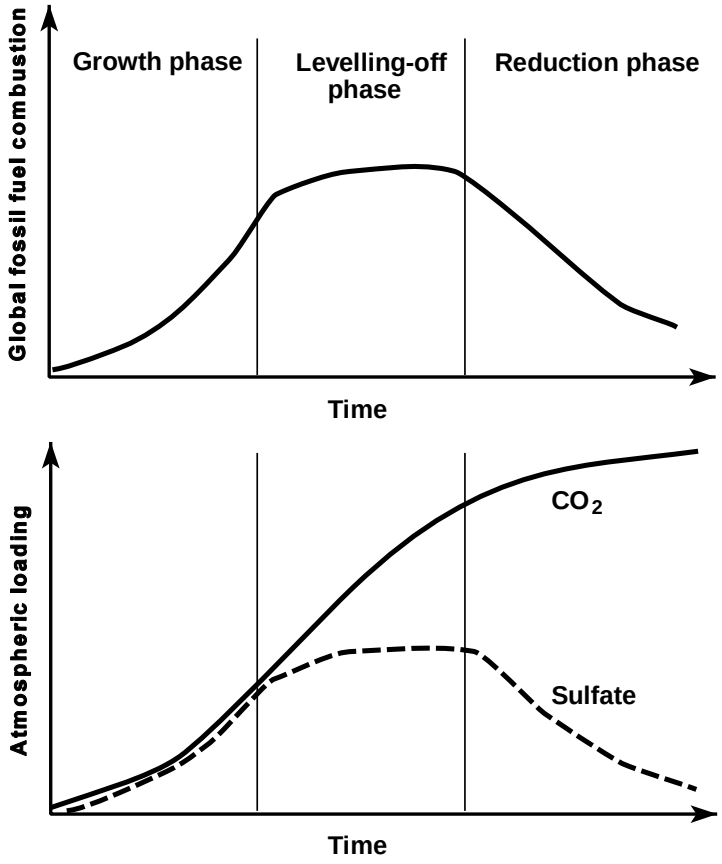

Figure 8-23. Schematic illustration of the difference between response times of climate forcing due to CO_2 (heating) and sulfate (cooling) during different patterns of global fossil fuel consumption.

Source: Charlson et al. (1991)

Section 8.8.3). The light-extinction coefficient is related to the size distribution and number concentration of cloud droplets. Because these cloud droplets nucleate on aerosols, it is to be expected that changes in aerosol loading could affect cloud albedo, particularly that marine stratiform clouds. Because of their effect on the Earth's radiative energy budget, marine status and stratocumulus cloud systems are likely to influence climate and climate change. Their high albedo compared with ocean background provide a large negative shortwave forcing which is not compensated in thermal wavelengths because of their low altitude (Randall et al., 1984). Recent studies by Ramanathan et al. (1995) and Cess et al. (1995) indicate that more solar radiation is being absorbed by clouds in cloudy atmospheres than originally believed. This finding has, however, not been confirmed.

Stephens (1994) gave the volume light-extinction coefficient of a cloud of spherical polydispersed drops ranging in size as:

$$\sigma_{ext} = \pi \int_{r_{min}}^{r_{max}} n(r) Q_{ext}(r) r^2 dr \tag{8-44}$$

where n(r) represents the size distribution and is the number concentration per unit volume per unit radius increment and Q_{ext} is the extinction efficiency factor (see Section 8.3.1) which approaches the value of 2.0 for drops that are large relative to the wavelength. At visible wavelengths, this limit for the extinction efficiency factor is satisfied by cloud drops that are typically 10 μm in radius. Therefore,

$$\sigma_{ext} \propto \int_{r_{min}}^{r_{max}} n(r) r^2 dr. \tag{8-45}$$

The mass concentration of water in clouds, called the liquid water content, M (in kg^{-3}), is proportional to the total volume of liquid water in a unit volume of air. This may be written as

$$M \propto \int_{r_{min}}^{r_{max}} n(r) r^3 dr \tag{8-46}$$

because the volume of each cloud drop is (4/3) π r^3. Comparing Equations 8-45 and 8-46, one can see that

$$\sigma_{ext} \propto M/r_e \tag{8-47}$$

where r_e is the effective radius, defined as the ratio

$$r_e = \frac{\int_{r_{min}}^{r_{max}} n(r) r^3 dr}{\int_{r_{min}}^{r_{max}} n(r) r^2 dr}. \qquad (8\text{-}48)$$

For identical meteorological conditions, the liquid water content will be the same in two cloud layers that are composed of droplets of different effective radius. If other paramaters remain the same, the light-extinction coefficient will increase as the effective radius decreases (Equation 8-47). Therefore, if the geometric depth of two cloud layers is the same and the column amount of liquid water is the same, the cloud with more numerous, but smaller drops, will have a larger optical depth and a higher albedo. This sets the stage for a potentially important indirect effect of anthropogenic aerosols on the Earth's radiation balance. As suggested by Twomey (1974), the addition of cloud nuclei by pollution can lead to an increase in the solar radiation reflected by clouds, a negative radiative forcing that is in addition to the direct radiative forcing discussed in Section 8.8.3.

Another radiative consequence of pollution is the emission of elemental carbon, which can be incorporated into clouds and increase the absorptance at visible wavelengths at which pure water is nonabsorbing. This mechanism decreases the single scattering albedo of the cloud material (see Figure 8-20), causing a decrease in the reflectance of the layer. There are, therefore, two competing mechanisms, but Twomey et al. (1984) assessed the relative magnitudes of the two effects based on observations of clean and polluted air in Arizona, and concluded that increases in albedo from increases in cloud droplet concentration would dominate over the absorption effect.

Cloud Lifetimes

Another possible indirect effect of aerosols on clouds and precipitation is that of increased cloud condensation nuclei (CCN), the inhibition of precipitation (Albrecht, 1989; Twomey, 1991). Cloud condensation nuclei can be either hygroscopic or deliquescent, having large light scattering efficiency due to hygroscopic growth. With more droplets, coagulative growth, which is the mechanism of water removal in liquid water clouds, will be hindered. This will result in

longer residence times for clouds and a higher mean albedo time, which, again, is indirect negative solar radiative forcing.

There is some observational evidence that cloud amounts have increased during the recent decades. Henderson-Sellers (1986, 1989) has analyzed surface based meterological observations from several stations in the United States and Canada. There is coherent increase in cloud amount in all seasons between 1900 and 1982 with most of the increase occuring between 1930 and 1950. Attribution of this increase to anthropogenic causes is very difficult. The possibility of jet contrails playing a role has been mentioned by Changnon (1981) but this would not explain the increase in the 1930-1950 time frame. Warren et al. (1988) have also noted a positive trend in the total cloud amount and also for all classes of clouds globally over the oceans. An increase in aerosol concentration is compatible with an increase in cloud lifetimes for low level clouds so there is a plausible link between these observations and anthropogenic activities but nothing definitive can be said at the moment.

Cloud Chemistry

Novakov and Penner (1993) pointed out that anthropogenic activity could modify the nucleating properties of anthropogenic sulfate. It has already been mentioned that carbon black influences the direct radiative forcing. The presence of carbon black and other organics can also alter the hygroscopic properties of sulfate aerosols. For instance, the condensation of hydrophobic organics onto preexisting sulfate particles may render these inactive as CCN. On the other hand, the condensation of sulfuric acid vapor on a hydrophobic organic aerosol may convert it to a hydrophilic particle. Because the indirect radiative forcing depends on the ability of sulfate to nucleate, organics may enhance or diminish the potential indirect radiative forcing.

8.8.5.2 Observational Evidence

The relationship between the availability of CCN and cloud droplet size distribution has been a subject of research in cloud physics for decades. It has been known, for instance, that continental clouds are composed of far more numerous, but smaller drops than maritime clouds (Wallace and Hobbs, 1977). The more difficult question is whether the additional

contribution to CCN by anthropogenic activities has increased the reflectance of clouds over large areas of the Earth. If so, this would be an additional indirect radiative forcing attributable to sulfate emissions.

The most dramatic evidence of such an indirect effect (albeit on a small scale) is the observation of "ship tracks" in marine stratocumulus (Conover, 1966; Coakley et al., 1987). These are visible in satellite images as white lines against a gray background and follow the path of ships that have been emitting effluents. King et al. (1993) reported the first radiation and microphysics measurements on ship tracks obtained from a research aircraft as it flew within marine stratocumulus clouds off California. Comparing the flight track with satellite images, they were able to locate two distinct ship tracks in which they measured enhanced droplet concentration, and liquid water contents, greater than in the surrounding clouds. They also derived the effective radius of the cloud drops and found that there was a significant decrease within the ship tracks. The radiation measurements were consistent with increased optical depths in the ship tracks. The increased liquid water content is compatible with the suppression of drizzle as a result of slower coagulative growth (Albrecht, 1989), an indirect aerosol effect.

Twomey (1991) estimated that the visible reflectance of clouds, R, is affected by cloud droplet concentration, N, according to the following relationship for a fixed liquid water content, M.

$$\left(\frac{dR}{dN}\right)_M = \frac{R(1-R)}{3N} \tag{8-42}$$

The parameter, dR/dN, the susceptibility, is a measure of the sensitivity of cloud reflectance to changes in microphysics (Platnick and Twomey, 1994). It has a maximum value at $R = 0.5$ and is inversely proportional to the cloud droplet concentration such that when the cloud droplet concentration is low as in marine clouds, the susceptibility is high. It is, therefore, not surprising that emissions from ships can influence cloud albedo.

To determine whether the indirect effect of aerosols on clouds is detectable on a global scale, Schwartz (1988) compared cloud albedos in the two hemispheres and also historic changes in surface temperature from preindustrial times. The sulfate signal is expected in

both: cloud albedos in the Northern Hemisphere should be higher, and the rate of greenhouse warming should be slower. The results of his study were inconclusive in that no inter-hemispheric differences were found. However, more recent studies suggest some influence of sulfate emissions.

Falkowski et al. (1992) showed that cloud albedos in the central North Atlantic Ocean, far from continental emission sources, were well correlated with chlorophyll in surface waters. These correspond to higher ocean productivity and DMS emissions, indicating that natural sources of sulfate emission can influence cloud albedo. More substantial evidence of the effect of sulfate aerosol has been presented by Han et al. (1994) who made a near-global survey of the effective droplet radii in liquid water clouds by inverting satellite visible radiances obtained from advanced very-high-resolution radiometer (AVHRR) measurements. Han et al. (1994) found systematic differences between the effective radius of continental clouds (global mean effective radius = 8.5 μm) and maritime clouds (global mean effective radius = 11.8 μm), which is the expected result based on differences in CCN concentrations. In addition, they found inter-hemispheric differences in the effective radius over both land and ocean. Northern Hemisphere clouds had smaller effective radii, the difference being 0.4 μm for ocean and 0.8 μm for land. However, Southern Hemisphere clouds tended to be optically thicker, which explains why Schwartz (1988) was unable to detect inter-hemispheric albedo differences.

8.8.5.3 Modeling Indirect Aerosol Forcing

If the appropriate radiative properties of aerosols are known, it is fairly straightforward to model the direct solar radiative forcing of aerosols (Section 8.8.3) and estimate possible climatic responses (Section 8.8.4). Calculations of the indirect forcing of aerosols, on the other hand, is much more difficult since several steps are involved and the uncertainty at each level is high. Charlson et al. (1992) proposed that enhancements in albedo would occur only for marine stratocumulus clouds and for a uniform global increase of droplet concentration of 15% in only these clouds, the global mean solar radiative forcing would be -1.0 W m^{-2}, which is comparable to the direct forcing (Section 8.8.4) and of the same sign. The greatest uncertainty in this estimate is the degree that cloud droplet number concentration is enhanced by increasing emissions. The uncertainty has been estimated by Kaufman et al.

(1991) to be at least a factor of 2. Leaitch and Isaac (1994) have addressed this issue based on their observations of the relationship between cloud droplet concentrations and cloud water sulfate concentrations. They find that the assumptions in Kaufman et al. (1991) are within reasonable bounds. The Scientific Steering Committee for the International Global Aerosol Program concluded that the uncertainties involved in determining the indirect effects of aerosols on the Earth's radiation balance are so great that no formal value can be given at this time (Hobbs, 1994).

The indirect forcing has been included in climate model simulations by Kaufman and Chou (1993) who used a zonally averaged multilayer energy balance model and by Jones et al. (1994) who used a GCM. Kaufman and Chou (1993) modeled the competing effects of enhanced anthropogenic emissions of CO_2 and SO_2 since preindustrial times. They concluded that SO_2 has the potential of offsetting CO_2-induced warming by 60% for present conditions and 25% by the year 2060 given the Intergovernmental Panel on Climate Change BAU (business as usual) scenario of industrial growth (Intergovernmental Panel on Climate Change, 1994). They also found a small inter-hemispheric difference in climate response, with the Northern Hemisphere cooler than Southern Hemisphere by about $-0.2\ ^{\circ}C$.

Jones et al. (1994) used a GCM with a prognostic cloud scheme and a parameterization of the effective radius of cloud water droplets that links effective radius to cloud type, aerosol concentration and liquid water content. The parameterization is based on extensive aircraft measurements. The distribution of column sulfate mass loading was obtained from the model of Langner and Rodhe (1991) separately for natural and anthropogenic sources. Simulated effective radius distributions of low-level clouds showed land-ocean contrasts and also inter-hemispheric differences as observed by Han et al. (1994). The indirect forcing due to anthropogenic sulfate was estimated by performing a series of single-timestep calculations with the GCM. For present conditions, the mean northern hemisphere forcing was calculated to be $-1.54\ W\ m^{-2}$ and the southern hemisphere forcing was $-0.97\ W\ m^{-2}$. This is comparable to the estimates of Charlson et al. (1992) and Kaufman and Chou (1993) and substantially larger than the direct forcing estimates of Kiehl and Briegleb (1993). The combined direct and indirect forcing is more than half the total positive forcing of greenhouse gas emissions. It should be noted that the indirect effect is greatest when the atmosphere is very clean and so, in principle, could saturate with time. The direct effect is

linear with emissions and may dominate in the future. In any case, the negative forcing of sulfate aerosols must be considered in any overall estimate of the total anthropogenic effect on climate.

8.9 SUMMARY

8.9.1 Visibility Effects

This chapter presents (1) an overview of the effects of particulate matter on visibility, and combines information from this chapter and other recent reviews by the National Research Council (NRC), the National Acid Precipitation Assessment Program (NAPAP), and Environmental Protection Agency (U.S. EPA) and (2) a discussion on the effects of particulate matter on climate.

Several definitions of visibility have been noted in this chapter, and they are generally consistent with each other. Section 169A of the 1977 Clean air Act Amendments (42 U.S.C. 7491) and the U.S. EPA 1979 Report to Congress defined visibility impairment as a reduction in visual range and atmospheric discoloration. The National Research Council's Committee on Haze in National and Wilderness Areas said, "Visibility is the degree to which the atmosphere is transparent to visible light." These definitions indicate that visibility is determined by the clarity (or transparency) and color fidelity of the atmosphere. Visibility can be numerically quantified by equating it with the contrast transmittance of the atmosphere. This quantification is consistent with both (1) the use of visual range to quantify visibility, and (2) the definition recommended by the NRC.

All evaluations of visibility have focused on daytime visibility as perceived by a human observer looking through one or more sight paths in the Earth's atmosphere. Weber's Law indicates that if an object is just perceptible, the brightness of the object differs from the brightness of its surroundings by a constant fraction, i.e., a constant percentage of the surrounding brightness. A perception threshold of 2% brightness change is most commonly used, but 5% is sometimes used in visibility analyses. Either contrast or modulation can be used to quantify changes in brightness. Weber's law is not exact, so perception thresholds depend on the viewing conditions. The eye is the most sensitive to objects that subtend an angle of

approximately 1/3 degree, is somewhat less sensitive to objects that subtend larger angles, and becomes rapidly less sensitive as the size of the object is decreased below a subtended angle of 0.1 degree. Many factors, such as the brightness level and the pattern of brightness surrounding the object being viewed can affect the perception threshold. The contrast threshold of 2% generally applies to objects that subtend an angle between 0.1 and 1.0 degree and are viewed against uniform backgrounds.

The atmosphere is a very thin layer on the Earth and has strong vertical gradients. Because of these gradients and the curvature of the Earth, the properties of the atmosphere exhibit substantial variations in sight paths longer than roughly 100 km. The visual range is the greatest distance at which a dark target can be perceived against the horizonal sky. Because of the non-uniformities in the atmosphere, the visual range provides a meaningful characterization of the Earth's atmosphere only for haze levels that cause the visual range to be much less than 100 km.

A sight path through the atmosphere is illuminated by direct sunlight, diffused skylight, and light reflected by the Earth's surface. An observer looking through the atmosphere sees light from two sources: (1) the light reflected from the object or terrain feature being viewed that is transmitted through the sight path to the observer, and (2) the light scattered by the atmosphere into the line of sight and then transmitted to the observer. These are known as the transmitted radiance and the path radiance (air light), respectively.

Visibility is determined by the competition between the transmitted radiance and the path radiance. The transmitted radiance carries all of the information about the nature of the object being viewed. When this radiance is dominant, the features of the object can be easily perceived and the visibility is good. The path radiance contains information only about the uniformity of the intervening atmosphere, and no information about the object being viewed. When the path radiance is dominant, it tends to obscure the object. These effects are easily seen by viewing objects at various distances in a dense fog, but can also be seen on a clear day if sight paths of sufficient length are available.

The transmitted radiance is attenuated by light extinction. The strength of that attenuation is quantified by the light-extinction coefficient, which describes the rate of energy loss with distance from a beam of light. The light-extinction coefficient for green light in particle-free air (Raleigh scattering) is 1% per km, or 0.01 km^{-1}. Extinction coefficients are

most often measured in units of inverse megameters (Mn^{-1}), and in these units the extinction coefficient for clean air is 10 Mn^{-1}.

Light extinction is caused by light scattering and light absorption by particles and gases. In visibility analyses it is useful to consider each of these separate contributions to the light-extinction coefficient; the coefficients for light absorption by gases (σ_{ag}), light scattering by gases (σ_{sg}), light absorption by particles (σ_{ap}), and light scattering by particles (σ_{sp}). Because of their different origins and composition, atmospheric particles are frequently divided into coarse and fine particles. The corresponding division of coefficients for light scattering and absorption then becomes, the coefficient for light-scattering and light-absorption by fine particles (σ_{sfp} and σ_{afp}) and the coefficient for light scattering and light-absorption by coarse particles (σ_{scp} and σ_{acp}). The components of the light-extinction coefficient are related as follows:

$$\sigma_{ext} = \sigma_{abs} + \sigma_{scat}$$
$$\sigma_{ab} = \sigma_{ag} + \sigma_{ap}$$
$$\sigma_{scat} = \sigma_{sg} + \sigma_{sp}$$
$$\sigma_{sp} = \sigma_{sfp} + \sigma_{scp}$$
$$\sigma_{ap} = \sigma_{afp} + \sigma_{acp}$$

Light scattering by gases (Raleigh Scattering) is nearly constant, but decreases with increasing altitude. Light absorption by gases is almost entirely due to NO_2, and is typically significant only near NO_2 sources, e.g., in or downwind of urban areas or in plumes. Light absorption by particles is principally caused by elemental carbon. Light scattering by particles is typically the most important component of light extinction in causing visibility degradation. Further discussion of this component of light extinction appears below.

If the average light-extinction coefficient and path length are known, the light transmittance of a sight path can be calculated. Thus, the effect of light extinction on the transmitted radiance is easily quantified.

The calculation of the path radiance is much more difficult. It requires a knowledge if (1) the illumination of the sight path at each point along its length, (2) the light scattering properties of the atmosphere at each point, and (3) the transmittance of the atmosphere

between each point and the observer. The illumination is affected by the clouds in the sky, the haze that contributes to diffuse skylight, and the variations of the reflectance of the Earth's surface under the sight path. Light scattering and light absorption contribute differently, because light absorption does not contribute to the scattering of light into the sight path. Thus, a given amount of light extinction due to light absorption causes less visibility impairment than the same amount of light extinction due to light scattering. Because of the differing effects of scattering and absorption and the highly variable effects of the illumination, the path radiance is not closely linked to light extinction. As a result, the visibility for a specific sight path under specific illumination conditions is not closely linked to the light-extinction coefficient.

All of these effects can be mathematically simulated, and a simple theory for these simulations is present in the text. The theoretical development includes the equations used to generated photographs showing the visual effects with various amounts of haze. For simple situations, e.g., a cloud-free sky and uniform haze, photographic simulation are quite realistic. Examples appear in the National Acid Precipitation Assessment Program study. These photographs, and other comparisons, indicated that the relationship between air pollution and visibility is well understood.

As previously stated, the most important component of light extinction in causing visibility degradation is typically light scattering by particles. Except in dust storms or during fog, snow, or rain, most light scattering by particles is caused by fine particles, i.e. the accumulation mode, ~0.3 to 1.0 μm diameter. Coarse particles typically have a light-scattering efficiency 5 to 10 times less that the efficiency of fine particles. Coarse particles can have important visibility effects in dusty or desert areas, but fine particles dominate the visibility effects in most of the eastern United States.

The light-scattering efficiency of particles is a maximum for particles with a diameter approximately equal to the wavelength of visible light. For a single particle, the maximum in light-scattering efficiency occurs at a diameter approximately equal to

$$D = 0.28/(n-1)\ \mu m$$

where n is the index of refraction of the particulate matter. This formula gives a diameter of 0.85 μm for an index of refraction of 1.33 (e.g. water) and a diameter of 0.56 μm for an index of refraction of 1.5, which is larger than typical for ambient aerosol mixtures. Most fine particles have smaller diameters. Therefore, processes that increase the particle size of fine particles tend to increase the light-scattering efficiency of the particles.

Coagulation of nuclei particles, which can be smaller that 0.1 μm in diameter, in the atmosphere will increase their light-scattering efficiency. Particles in the 0.2 to 0.3 μm in diameter range are small enough that their light-scattering efficiency is roughly half that of particles with the optimum size. Particles in this range coagulate very slowly, so they tend to maintain their size in the atmosphere as long as they are not processed by clouds or fog. Heterogenous processes in clouds and fogs can form particles in any size range, but these processes are the dominant source of particles with a diameter near 0.7 μm, which is near the optimum size for light scattering. Particles in this size range are frequently observed in air samples processed by clouds or fog.

The dominant chemical components of fine particulate matter are sulfates, organic species, nitrates, crustal species, and elemental carbon. Sulfates and organic species dominate visibility impairment in the eastern United States, and nitrates and organic species are dominant in many western urban areas as well as the California Central Valley during winter months. Crustal species are important contributors in dry areas, especially when these areas are farmed. Elemental carbon is most important in urban areas, and in Phoenix, AZ can contribute about one-third of the light extinction during some episodes.

Water uptake, which occurs when hygroscopic aerosol is exposed to elevated humidities, increase light scattering by two mechanisms: (1) the mass concentration of particulate matter is increased, and (2) the increase particle size causes the light scattering efficiency to increase. Thus, the materials present before the water uptake makes a larger contribution to light scattering because they are now a component of larger particles. The overall effect on increasing humidity on light scattering by particles was quantified nearly 20 years ago, but current research is greatly increasing the detailed understanding of the response of aerosol particles to changing humidities and the relationship of this response to the chemical composition of the particles. Humidity effects generally become important at relative humidities between 60 and 70%, and increase the light scattering by a factor of 2 at

approximately 85% relative humidity. The light scattering increase rapidly with relative humidity when the humidity exceeds 90%.

Potential indicators for a visibility and air quality include: (a) fine particle mass and composition, or only fine particle mass; (b) light scattering by dried ambient particles; (c) light scattering by particles under ambient conditions; (d) light extinction calculated from separate measurements of dry scattering and absorption or ambient scattering and absorption; (e) light extinction measured directly; and (f) contrast transmittance of a sight path.

The selection of an indicator should consider such factors as (1) the linkage between the indicator and visibility, (2) the cost and feasibility of monitoring the indicator to determine both compliance with the standard and progress toward achieving the standard, (3) the nature and severity of the interferences inherent in the available monitoring methods, (4) the relationship between the visibility indicator and indicators for other air quality standards, and (5) the usefulness of monitoring data in analyses which have the purpose of determining the optimum control measures to achieve the standard.

In general there is an inverse relationship between an indicator's ability to characterize air quality and its ability to characterize visibility.

There is general agreement in the technical community that contrast transmittance would not be a suitable indicator for regulatory purposes. It is affected by too many factors other than air quality, such as cloud shadows, precipitation, fog, etc. Therefore, only the other indicators merit consideration.

Visibility has value to individual economic agents primarily through its impact upon the activities of consumers. Most economic studies of the effects of air pollution on visibility have focused on the aesthetic effects to the individual, which are, at this time, believed to be the most significant economic impacts of visibility degradation caused by air pollution in the United States. It is well established that people notice those changes in visibility conditions that are significant enough to be perceptible to the human observer, and that visibility conditions affect the well-being of individuals.

One way of defining the impact of visibility degradation on the consumer is to determine the maximum amount the individual would be willing to pay to obtain improvements in visibility or prevent visibility degradation. Two economic valuation techniques have been used to estimate willingness to pay for changes in visibility: (1) the

contingent valuation method, and (2) the hedonic property value method. Both methods have important limitations, and uncertainties exist in the available results. Recognizing these uncertainties is important, but the body of evidence as a whole suggests that economic values for changes in visibility conditions are probably substantial in some cases, and that a sense of the likely magnitude of these values can be derived from available results in some instances. Economic studies have estimated values for two types of visibility effects potentially related to particulate air pollution: (1) use and non-use values for preventing the types of plumes caused by power plant emissions, visible from recreation areas in the southwestern United States; and (2) use values of local residents for reducing or preventing increases in urban hazes in several different locations.

8.9.2 Climate Change

Aerosols of submicron size in the Earth's atmosphere perturb the radiation field. There is no doubt that anthropogenic aerosol emissions, primarily sulfur oxides, have the potential to affect climate; the question is by how much. There are two chief avenues through which aerosols impact the radiation budget of the Earth. The direct effect is that of enhanced solar reflection by the cloud-free atmosphere. Since aerosols, even those containing some absorptive component, are primarily reflective, their impact is felt as a negative radiative forcing (i.e., a cooling) on the climate system. Although there is some uncertainty in the global distribution of such aerosols and in the chemical and radiative properties of the aerosols, the radiative effects can still be modeled within certain bounds. Estimates of this forcing range from -0.3 W m^{-2} to about twice that value for current conditions over pre-industrial times.

The indirect forcing results from the way in which aerosols affect cloud microphysical properties. The most important is the effective radius of cloud droplets, which decrease in the presence of higher concentrations of Cloud Condensation Nuclei (CNN) since more nucleating sites are available for droplets to form. This effect is most pronounced when the concentration, N, is very low, and clouds are moderately reflective. Other effects are the enhancement of cloud lifetimes and also changes in the nucleating ability of CCN through chemical changes. Although estimates of the indirect effect are uncertain by at least a factor of 2, but perhaps much more, it appears to be potentially more important than the direct

effect. Taken together, on a global mean basis, anthropogenic emissions of aerosols could have offset substantially the positive radiative forcing due to greenhouse gas emissions. High priority should be given to acquiring the measurements needed to quantifying these effects with greater accuracy.

The one crucial difference between aerosol forcing and greenhouse (gas) forcing is the atmospheric lifetime of aerosols and gases and hence, forcing. The aerosol forcing is fairly localized, whereas the greenhouse forcing is global. One should, therefore, expect inter-hemispheric differences in the forcing and perhaps climate response. However, climate models are not currently at the level of sophistication needed to determine climate response unambiguously. With few exceptions, global observations of surface temperature can not separate natural and anthropogenic causal mechanisms.

REFERENCES

Adams, K. M.; Kavis, L. I., Jr.; Japar, S. M.; Pierson, W. R. (1989) Real-time, *in situ* measurements of atmospheric optical absorption in the visible via photoacoustic spectroscopy - II. validation for atmospheric elemental carbon aerosol. Atmos. Environ. 23: 693-700.

Ahlquist, N. C.; Charlson, R. J. (1967) A new instrument for evaluating the visual quality of air. J. Air Pollut. Control Assoc. 17: 467-469.

Air & Waste Management Association. (1993) Southern California air quality study data analysis: proceedings of an international specialty conference; July 1992; Los Angeles, CA. Pittsburgh, PA: Air & Waste Management Association.

Albrecht, B. A. (1989) Aerosols, cloud microphysics, and fractional cloudiness. Science (Washington, DC) 245: 1227-1230.

Altshuller, A. P. (1982) Relationships involving particle mass and sulfur content at sites in and around St. Louis, Missouri. Atmos. Environ. 16: 837-843.

Altshuller, A. P. (1985) Relationships involving fine particle mass, fine particle sulfur and ozone during episodic periods at sites in and around St. Louis, MO. Atmos. Environ. 19: 265-276.

Alvarez, L. W.; Alvarez, W.; Asaro, F.; Michel, H. V. (1980) Extraterrestrial cause for the Cretaceous-Tertiary extinction. Science (Washington, DC) 208: 1095-1108.

Anderson, T. L.; Charlson, R. J.; White, W. H.; McMurry, P. H. (1994) Comment on "Light scattering and cloud condensation nucleus activity of sulfate aerosol measured over the northeast Atlantic Ocean" by D. A. Hegg et al. J. Geophys. Res. [Atmos.] 99: 25,947-25,949.

Ångstrőm, A. (1964) The parameters of atmospheric turbidity. Tellus 16: 64-75.

Appel, B. R.; Tokiwa, Y.; Hsu, J.; Kothny, E. L.; Hahn, E.; Wesolowski, J. J. (1983) Visibility reduction as related to aerosol constituents. Sacramento, CA: State of California, Air Resources Board; report no. CA/DOH/AIHL/SP-29. Available from: NTIS, Springfield, VA; PB84-243617.

Appel, B. R.; Tokiwa, Y.; Hsu, J.; Kothny, E. L.; Hahn, E. (1985) Visibility as related to atmospheric aerosol constituents. Atmos. Environ. 19: 1525-1534.

Bakan, S.; Chlond, A.; Cubasch, U.; Feichter, J.; Graf, H.; Grassl, H.; Hasselmann, K.; Kirchner, I.; Latif, M.; Roeckner, E.; Sausen, R.; Schlese, U.; Schriever, D.; Schult, I.; Schumann, U.; Sielmann, F.; Welke, W. (1991) Climate response to smoke from the burning oil wells in Kuwait. Nature (London) 351: 367-371.

Bergstrom, R. W.; Seigneur, C.; Babson, B. L.; Holman, H.-Y.; Wojcik, M. A. (1981) Comparison of the observed and predicted visual effects caused by power plant plumes. Atmos. Environ. 15: 2135-2150.

Blackwell, H. R. (1946) Contrast thresholds of the human eye. J. Opt. Soc. Am. 36: 624-643.

Blanchet, J.-P. (1989) Toward estimation of climatic effects due to Arctic aerosols. Atmos. Environ. 23: 2609-2625.

Blanchet, J.-P. (1991) Potential climate change from Arctic aerosol pollution. In: Sturges, W. T., ed. Pollution of the Arctic atmosphere. New York, NY: Elsevier Science Publishers; pp. 289-322. (Cairns, J.; Harrison, R. M., eds. Environmental management series).

Blandford, J. C. (1994) Transmissometer data reduction and validation (IMPROVE protocol). Fort Collins, CO: Air Resource Specialists, Inc.; technical instruction no. 4400-5000.

Blumenthal, D. L.; Richards, L. W.; Macias, E. S.; Bergstrom, R. W.; Wilson, W. E.; Bhardwaja, P. S. (1981) Effects of a coal-fired power plant and other sources on southwestern visibility (interim summary of EPA's project VISTTA). In: White, W. H.; Moore, D. J.; Lodge, J. P., Jr., eds. Plumes and visibility: measurements and model components, proceedings of the symposium; November 1980; Grand Canyon National Park, AZ. Atmos. Environ. 15: 1955-1969.

Blumenthal, D.; Trijonis, J.; Kelso, R.; Pitchford, M.; McGown, M.; Dodson, T.; Flocchini, R.; Pitchford, A.; Waggoner, A.; Ouimette, J. (1987) Design and initial findings of the RESOLVE (research on operations-limiting visual extinction) desert visibility study. In: Bhardwaja, P. S., ed. Visibility protection: research and policy aspects, an APCA international specialty conference; September 1986; Grand Teton National Park, WY. Pittsburgh, PA: Air Pollution Control Association; pp. 87-98. (APCA transactions series no. TR-10).

Bodhaine, B. A. (1979) Measurement of the Rayleigh scattering properties of some gases with a nephelometer. Appl. Opt. 18: 121-125.

Bohren, C. F.; Huffman, D. R. (1983) Absorption and scattering of light by small particles. New York, NY: John Wiley & Sons.

Box, M. A. (1995) Changes in surface radiation caused by a scattering layer as calculated using radiative perturbation theory. J. Geophys. Res. [Atmos.] 100: 11,581-11,584.

Brookshire, D. S.; Ives, B. C.; Schulze, W. D. (1976) The valuation of aesthetic preferences. J. Environ. Econ. Manage. 3: 325-346.

Brookshire, D. S.; Thayer, M. A.; Schulze, W. D.; d'Arge, R. C. (1982) Valuing public goods: a comparison of survey and hedonic approaches. Am. Econ. Rev. 72: 165-177.

Browning, K. A.; Allam, R. J.; Ballard, S. P.; Barnes, R. T. H.; Bennetts, D. A.; Maryon, R. H.; Mason, P. J.; McKenna, D.; Mitchell, J. F. B.; Senior, C. A.; Slingo, A.; Smith, F. B. (1991) Environmental effects from burning oil wells in Kuwait. Nature (London) 351: 363-371.

Carhart, R. A.; Policastro, A. J.; Wastag, M.; Coke, L. (1989) Evaluation of eight short-term long-range transport models using field data. Atmos. Environ. 23: 85-105.

Carson, R. T.; Mitchell, R. C.; Ruud, P. A. (1990) Valuing air quality improvements: simulating a hedonic equation in the context of a contingent valuation scenario. In: Mathai, C. V., ed. Visibility and fine particles: an A&WMA/EPA international specialty conference; October 1989; Estes Park, CO. Pittsburgh, PA: Air & Waste Management Association; pp. 639-646. (A&WMA transactions series no. TR-17).

Cess, R. D.; Potter, G. L.; Ghan, S. J.; Gates, W. L. (1985) The climatic effects of large injections of atmospheric smoke and dust: a study of climate feedback mechanisms with one- and three-dimensional climate models. J. Geophys. Res. [Atmos.] 90: 12,937-12,950.

Cess, R. D.; Zhang, M. H.; Minnis, P.; Corsetti, L.; Dutton, E. G.; Forgan, B. W.; Garber, D. P.; Gates, W. L.; Hack, J. J.; Harrison, E. F.; Jing, X.; Kiehl, J. T.; Long, C. N.; Morcrette, J.-J.; Potter, G. L.; Ramanathan, V.; Subasilar, B.; Whitlock, C. H.; Young, D. F.; Zhou, Y. (1995) Absorption of solar radiation by clouds: observations versus models. Science (Washington, DC) 267: 496-499.

Changnon, S. A. (1981) Midwestern cloud, sunshine and temperature trends since 1901: possible evidence of jet contrail effects. J. Appl. Meteorol. 20: 496-508.

Charlock, T. P.; Sellers, W. D. (1980) Aerosol effects on climate: calculations with time-dependent and steady-state radiative-convective models. J. Atmos. Sci. 37: 1327-1341.

Charlson, R. J.; Covert, D. S.; Tokiwa, Y.; Mueller, P. K. (1972) Multiwavelength nephelometer measurements in Los Angeles smog aerosol: III. comparison to light extinction by NO_2. In: Hidy, G. M., ed. Aerosols and atmospheric chemistry: the Kendall award symposium at the proceedings of the American Chemical Society; March-April 1971; Los Angeles, CA. New York, NY: Academic Press, Inc.; pp. 333-338.

Charlson, R. J.; Covert, D. S.; Larson, T. V.; Waggoner, A. P. (1978) Chemical properties of tropospheric sulfur aerosols. In: Husar, R. B.; Lodge, J. P., Jr.; Moore, D. J., eds. Sulfur in the atmosphere: proceedings of the international symposium; September 1977; Dubrovnik, Yugoslavia. Atmos. Environ. 12: 39-53.

Charlson, R. J.; Lovelock, J. E.; Andreae, M. O.; Warren, S. G. (1987) Oceanic phytoplankton, atmospheric sulfphur, cloud albedo and climate. Nature (London) 326: 655-661.

Charlson, R. J.; Langner, J.; Rodhe, H.; Leovy, C. B.; Warren, S. G. (1991) Perturbation of the northern hemisphere radiative balance by backscattering from anthropogenic sulfate aerosols. Tellus 43AB: 152-163.

Charlson, R. J.; Schwartz, S. E.; Hales, J. M.; Cess, R. D.; Coakley, J. A., Jr.; Hansen, J. E.; Hofmann, D. J. (1992) Climate forcing by anthropogenic aerosols. Science (Washington, DC) 255: 423-430.

Chestnut, L. G.; Rowe, R. D. (1990a) Methods for valuing acidic deposition and air pollution effects. Section B5. Economic valuation of changes in visibility: a state of the science assessment for NAPAP. In: Irving, P. M., ed. Acidic deposition: state of science and technology, volume IV, control technologies, future emissions, and effects valuation. Washington, DC: The U.S. National Acid Precipitation Assessment Program; pp. 27-153 - 27-175. (State of science and technology report no. 27).

Chestnut, L. G.; Rowe, R. D. (1990b) Preservation values for visibility in the national parks. Washington, DC: U.S. Environmental Protection Agency.

Cismoski, D. S. (1994) nephelometer data reduction and validation (IMPROVE protocol). Fort Collins, CO: Air Resource Specialists, Inc.; August.

Claeys, P.; Casier, J.-G.; Margolis, S. V. (1992) Microtektites and mass extinctions: evidence for a Late Devonian asteroid impact. Science (Washington, DC) 257: 1102-1104.

Coakley, J. A., Jr.; Cess, R. D.; Yurevich, F. B. (1983) The effect of tropospheric aerosols on the earth's radiation budget: a parameterization for climate models. J. Atmos. Sci. 40: 116-138.

Coakley, J. A., Jr.; Bernstein, R. L.; Durkee, P. A. (1987) Effect of ship-stack effluents on cloud reflectivity. Science (Washington, DC) 237: 1020-1022.

Conover, J. H. (1966) Anomalous cloud lines. J. Atmos. Sci. 23: 778-785.

Cooper, J. A.; Watson, J. G. (1979) Portland aerosol characterization study (PACS). Final report for Portland Air Quality Maintenance Area Advisory Committee and Oregon Department of Environmental Quality.

Core, J. E.; Maykut, N.; Weaver, D.; Boylan, J.; Hooper, M. (1987) PANORAMAS: a summary of major findings from the Pacific northwest regional aerosol mass apportionment study. In: Bhardwaja, P. S., ed. Visibility protection: research and policy aspects, an APCA international specialty conference; September 1986; Grand Teton National Park, WY. Pittsburgh, PA: Air Pollution Control Association; pp. 99-112. (APCA transactions series no. TR-10).

Cornsweet, T. N. (1970) Factors other than wavelength that influence hue. In: Visual perception. New York, NY: Academic Press, Inc.; pp. 236-240.

Countess, R. J.; Wolff, G. T.; Cadle, S. H. (1980) The Denver winter aerosol: a comprehensive chemical characterization. J. Air Pollut. Control Assoc. 30: 1194-1200.

Countess, R. J.; Cadle, S. H.; Groblicki, P. J.; Wolff, G. T. (1981) Chemical analysis of size-segregated samples of Denver's ambient particulate. J. Air Pollut. Control Assoc. 31: 247-252.

Covert, D. S.; Waggoner, A. P.; Weiss, R. E.; Ahlquist, N. C.; Charlson, R. J. (1980) Atmospheric aerosols, humidity, and visibility. In: Hidy, G. M.; Mueller, P. K.; Grosjean, D.; Appel, B. R.; Wesolowski, J. J., eds. The character and origins of smog aerosols: a digest of results from the California Aerosol Characterization Experiment (ACHEX). New York, NY: John Wiley & Sons, Inc.; pp. 559-581. (Advances in environmental science and technology: v. 9).

Cummings, R. G.; Brookshire, D. S.; Schulze, W. D., eds. (1986) Valuing environmental goods: an assessment of the contingent valuation method. Totowa, NJ: Rowman and Allanheld.

Daniel, T. C.; Hill, A. C. (1987) Measuring visibility values: comparison of perceptual assessment methods. In: Bhardwaja, P. S., ed. Visibility protection: research and policy aspects, an APCA international specialty conference; September 1986; Grand Teton National Park, WY. Pittsburgh, PA: Air Pollution Control Association; pp. 287-303. (APCA transactions series no. TR-10).

Davidson, J. A.; Cantrell, C. A.; McDaniel, A. H.; Shetter, R. E.; Madronich, S.; Calvert, J. G. (1988) Visible-ultraviolet absorption cross sections for NO2 as a function of temperature. J. Geophys. Res. [Atmos.] 93: 7105-7112.

Davies, R. (1993) Increased transmission of ultraviolet radiation to the surface due to stratospheric scattering. J. Geophys. Res. [Atmos.] 98: 7251-7253.

Dessens, H. (1944) Relation entre l'absorption par l'atmosphere et la visibilite [Relationship between atmospheric absorption and visibility]. Comptes Rendus 218: 685-687.

Drivas, P. J.; Bass, A.; Heinold, D. W. (1981) A plume blight visibility model for regulatory use. In: White, W. H.; Moore, D. J.; Lodge, J. P., Jr. Plumes and visibility: measurements and model components: proceedings of the symposium; November 1980; Grand Canyon National Park, AZ. Atmos. Environ. 15: 2179-2184.

Duffie, J. A.; Beckman, W. A. (1991) Solar engineering of thermal processes. 2nd ed. New York, NY: John Wiley & Sons, Inc.

Duntley, S. Q.; Boileau, A. R.; Preisendorfer, R. W. (1957) Image transmission by the troposphere I. J. Opt. Soc. Am. 47: 499-506.

Dzubay, T. G.; Clubb, K. W. (1981) Comparison of telephotometer measurements of extinction coefficients with scattering and absorption coefficients. In: White, W. H.; Moore, D. J.; Lodge, J. P., Jr., eds. Plumes and visibility: measurements and model components, proceedings of the symposium; November 1980; Grand Canyon National Park, AZ. Atmos. Environ. 15: 2617-2624.

Dzubay, T. G.; Stevens, R. K.; Lewis, C. W.; Hern, D. H.; Courtney, W. J.; Tesch, J. W.; Mason, M. A. (1982) Visibility and aerosol composition in Houston, Texas. Environ. Sci. Technol. 16: 514-525.

Edlén, B. (1953) The dispersion of standard air. J. Opt. Soc. Am. 43: 339-344.

Eldering, A.; Larson, S. M.; Hall, J. R.; Hussey, K. J.; Cass, G. R. (1993) Development of an improved image processing based visibility model. Environ. Sci. Technol. 27: 626-635.

Eldred, R. A.; Cahill, T. A. (1994) Trends in elemental concentrations of fine particles at remote sites in the United States of America. Atmos. Environ. 28: 1009-1019.

Eltgroth, M. W.; Hobbs, P. V. (1979) Evolution of particles in the plumes of coal-fired power plants— II. A numerical model and comparisons with field measurements. Atmos. Environ. 13: 953-975.

Ensor, D. S.; Waggoner, A. P. (1970) Angular truncation error in the integrating nephelometer. Atmos. Environ. 4: 481-487.

Erickson, D. J., III; Walton, J. J.; Ghan, S. J.; Penner, J. E. (1991) Three-dimensional modeling of the global atmospheric sulfur cycle: a first step. Atmos. Environ. Part A 25: 2513-2520.

Falkowski, P. G.; Kim, Y.; Kolber, Z.; Wilson, C.; Wirick, C.; Cess, R. D. (1992) Natural versus anthropogenic factors affecting low-level cloud albedo over the north Atlantic. Science (Washington, DC) 256: 1311-1313.

Ferman, M. A.; Wolff, G. T.; Kelly, N. A. (1981) The nature and sources of haze in the Shenandoah Valley/Blue Ridge Mountains area. J. Air Pollut. Control Assoc. 31: 1074-1082.

Fischhoff, B.; Furby, L. (1988) Measuring values: a conceptual framework for interpreting transactions with special reference to contingent valuation of visibility. J. Risk Uncertainty 1: 147-184.

Frederick, J. E.; Snell, H. E.; Haywood, E. K. (1989) Solar ultraviolet radiation at the earth's surface. Photochem. Photobiol. 50: 443-450.

Ghan, S. J.; MacCracken, M. C.; Walton, J. J. (1988) Climate response to large atmospheric smoke injections: sensitivity studies with a tropospheric general circulation model. J. Geophys. Res. [Atmos.] 93: 8315-8337.

Giorgi, F.; Visconti, G. (1989) Two-dimensional simulations of possible mesoscale effects of nuclear war fires: 2. model results. J. Geophys. Res. [Atmos.] 94: 1145-1163.

Gordon, J. I. (1964) Visibility III: optical properties of objects and backgrounds. Appl. Opt. 3: 556-562.

Graves, P.; Murdoch, J. C.; Thayer, M. A.; Waldman, D. (1988) The robustness of hedonic price estimation: urban air quality. Land Econ. 64: 220-233.

Groblicki, P. J.; Wolff, G. T.; Countess, R. J. (1981) Visibility-reducing species in the Denver "brown cloud" - I. relationships between extinction and chemical composition. In: White, W. H.; Moore, D. J.; Lodge, J. P., Jr., eds. Plumes and visibility: measurements and model components, proceedings of the symposium; November 1980; Grand Canyon National Park, AZ. Atmos. Environ. 15: 2473-2484.

Haecker, G. (1905) Untersuchungen uber Nebeltransparenz [Fog transparency investigations]. Meteorol. Zeit. 22: 343-353.

Han, Q.; Rossow, W. B.; Lacis, A. A. (1994) Near-global survey of effective droplet radii in liquid water clouds using ISCCP data. J. Clim. 7: 465-497.

Handler, A. (1989) Annual report on the establishment and operation of the eastern pine particle visibility network. search Triangle Park, NC: U.S. Environmental Protection Agency; EPA report no. 600/3-89/026. Available from: NTIS, Springfield, VA; PB89-165948.

Hansen, J. E.; Lacis, A. A. (1990) Sun and dust versus greenhouse gases: an assessment of their relative roles in global climate change. Nature (London) 346: 713-719.

Harrison, L.; Michalsky, J. (1994) Objective algorithms for the retrieval of optical depths from ground-based measurements. Appl. Opt. 33: 5126-5132.

Harrison, L.; Michalsky, J.; Berndt, J. (1994) Automated multifilter rotating shadow-band radiometer: an instrument for optical depth and radiation measurements. Appl. Opt. 33: 5118-5125.

Harshvardhan. (1993) Aerosol—climate interactions. In: Hobbs, P. V., ed. Aerosol-cloud-climate interactions. New York, NY: Academic Press; pp. 75-95.

Hartmann, D. L. (1994) Emission temperature of a planet. In: Global physical climatology. New York, NY: Academic Press; p. 25.

Hasan, H.; Dzubay, T. G. (1987) Size distributions of species in fine particles in Denver using a microorifice impactor. Aerosol Sci. Technol. 6: 29-39.

Hasan, H.; Lewis, C. W. (1983) Integrating nephelometer response corrections for bimodal size distributions. Aerosol Sci. Technol. 2: 443-453.

Hegg, D. A.; Ferek, R. J.; Hobbs, P. V. (1993) Light scattering and cloud condensation nucleus activity of sulfate aerosol measured over the northeast Atlantic Ocean. J. Geophys. Res. [Atmos.] 98: 14,887-14,894.

Hegg, D. A.; Ferek, R. J.; Hobbs, P. V. (1994) Reply. J. Geophys. Res. [Atmos.] 99: 25,951-25,954.

Heintzenberg, J. (1978) The angular calibration of the total scatter/backscatter nephelometer: consequences and applications. Staub Reinhalt. Luft 38: 62-63.

Heintzenberg, J.; Quenzel, H. (1973) On the effect of the loss of large particles on the determination of scattering coefficients with integrating nephelometers. Atmos. Environ. 7: 503-507.

Heisler, S. L.; Baskett, R. (1981) Particle sampling and analysis in the California San Joaquin Valley. Westlake Village, CA: Environmental Research & Technology, Inc.; ERT document no. P-5381-701.

Heisler, S. L.; Henry, R. C.; Watson, J. G.; Hidy, G. M. (1980a) The 1978 Denver winter haze study. Westlake Village, CA: Environmental Research & Technology, Inc.; document no. P-5417-1.

Heisler, S. L.; Henry, R. C.; Watson, J. G. (1980b) The sources of the Denver haze in November and December of 1978. Presented at: 73rd annual meeting of the Air Pollution Control Association; June; Montreal, PQ, Canada. Pittsburgh, PA: Air Pollution Control Association; paper no. 80-58.6.

Henderson-Sellers, A. (1986) Increasing cloud in a warming world. Clim. Change 9: 267-309.

Henderson-Sellers, A. (1989) North American total cloud amount variations this century. Paleogeog. Paleoclim. Paleoecol. 75: 175-194.

Hering, S. V.; McMurry, P. H. (1991) Optical counter response to monodisperse atmospheric aerosols. Atmos. Environ. Part A 25: 463-468.

Hidy, G. M.; Appel, B. R.; Charlson, R. J.; Clark, W. E.; Friedlander, S. K.; Hutchison, D. H.; Smith, T. B.; Suder, J.; Wesolowski, J. J.; Whitby, K. T. (1975) Summary of the California Aerosol Characterization Experiment. J. Air Pollut. Control Assoc. 25: 1106-1114.

Hidy, G. M.; Mueller, P. K.; Grosjean, D.; Appel, B. R.; Wesolowski, J. J., eds. (1980) The character and origins of smog aerosols: a digest of results from the California Aerosol Characterization Experiment (ACHEX). New York, NY: John Wiley & Sons.

Hildemann, L. M.; Mazurek, M. A.; Cass, G. R.; Simoneit, B. R. T. (1994) Seasonal trends in Los Angeles ambient organic aerosol observed by high-resolution gas chromatography. Aerosol Sci. Technol. 20: 303-317.

Hobbs, P. V., ed. (1994) A plan for an international global aerosol program (IGAP). Seattle, WA: University of Washington; p. 3.

Hobbs, P. V.; Radke, L. F. (1992) Airborne studies of the smoke from the Kuwait oil fires. Science (Washington, DC) 256: 987-991.

Hoffman, D. J.; Solomon, S. (1989) Ozone destruction through heterogeneous chemistry following the eruption of El Chichón. J. Geophys. Res. [Atmos.] 94: 5029-5041.

Hoffman, D. J.; Oltmans, S. J.; Komhyr, W. D.; Harris, J. M.; Lathrop, J. A.; Langford, A. O.; Deshler, T.; Johnson, B. J.; Torres, A.; Matthews, W. A. (1994) Ozone loss in the lower atmosphere over the United States in 1992-1993: evidence for heterogeneous chemistry on the Pinatubo aerosol. Geophys. Res. Letters 21: 65-68.

Hofmann, D. J. (1993) Twenty years of balloon-borne tropospheric aerosol measurements at Laramie, Wyoming. J. Geophys. Res. [Atmos.] 98: 12,753-12,766.

Holland, A. C.; Gagne, G. (1970) The scattering of polarized light by polydisperse systems of irregular particles. Appl. Opt. 9: 1113-1121.

Houghton, J. T.; Jenkins, G. J.; Ephraums, J. J., eds. (1990) Climate change: the IPCC scientific assessment. Cambridge, MA: Cambridge University Press; p. 55.

Hugon, M. (1930) Variation de la brillance des lointains avec la distance. Sci. Ind. Phot. 1: 161-168, 201-212.

Husar, R. B.; Patterson, D. E. (1984) Haze climate of United States. Research Triangle Park, NC: U.S. Environmental Protection Agency, Atmospheric Sciences Research Laboratory; EPA report no. EPA-600/3-86/07. Available from: NTIS, Springfield, VA; PB87-141057.

Husar, R. B.; Poirot, R. (1992) Exploration of the AIRS database: weekly cycle of ozone and PM 10 aerosols. Presented at: 85th annual meeting of the Air & Waste Management Association; June; Kansas City, MO. Pittsburgh, PA: Air & Waste Management Association; paper no. 92-77.06.

Husar, R. B.; Wilson, W. E. (1993) Haze and sulfur emission trends in the eastern United States. Environ. Sci. Technol. 27: 12-16.

Husar, R. B.; White, W. H.; Blumenthal, D. L. (1976) Direct evidence of heterogeneous aerosol formation in Los Angeles smog. Environ. Sci. Technol. 10: 490-491.

Husar, R. B.; Holloway, J. M.; Patterson, D. E.; Wilson, W. E. (1981) Spatial and temporal pattern of eastern U.S. haziness: a summary. Atmos. Environ. 15: 1919-1928.

Intergovernmental Panel on Climate Change. (1994) Climate change 1994: radiative forcing of climate and an evaluation of the IPCC 1S92 emission scenarios. Cambridge, United Kingdom: Cambridge University Press.

Iqbal, M. (1983) An introduction to solar radiation. New York, NY: Academic Press; p. 162.

Irwin, J.; Schenk, D.; McClelland, G. H.; Schulze, W. D.; Stewart, T.; Thayer, M. (1990) Urban visibility: some experiments on the contingent valuation method. In: Mathai, C. V., ed. Visibility and fine particles: an

A&WMA/EPA international specialty conference; October 1989; Estes Park, CO. Pittsburgh, PA: Air & Waste Management Association; pp. 647-658. (A&WMA transactions series no. TR-17).

Jaklevic, J. M.; Gattis, R. C.; Goulding, F. S.; Loo, B. W.; Thompson, A. C.. (1981) Aerosol analysis for the regional air pollution study. Research Triangle Park, NC: U.S. Environmental Protection Agency; EPA report no. 600/4-81-006. Available from: NTIS, Springfield, VA; PB81-157141.

Japar, S. M.; Szkarlat, A. C.; Pierson, W. R. (1984) The determination of the optical properties of airborne particle emissions from diesel vehicles. Sci. Total Environ. 36: 121-130.

Japar, S. M.; Brachaczek, W. W.; Gorse, R. A., Jr.; Norbeck, J. M.; Pierson, W. R. (1986) The contribution of elemental carbon to the optical properties of rural atmospheric aerosols. Atmos. Environ. 20: 1281-1289.

John, W.; Wall, S. M.; Ondo, J. L.; Winklmayr, W. (1990) Modes in the size distributions of atmospheric inorganic aerosol. Atmos. Environ. Part A 24: 2349-2359.

Johnson, C. D.; Latimer, D. A.; Bergstrom, R. W.; Hogo, H. (1980) User's manual for the plume visibility model (PLUVUE). Research Triangle Park, NC: U.S. Environmental Protection Agency; EPA report no. EPA-450/4-80-032. Available from: NTIS, Springfield, VA; PB81-163297.

Johnson, C. E.; Malm, W. C.; Persha, G.; Molenar, J. V.; Hein, J. R. (1985) Statistical comparisons between teleradiometer-derived and slide-derived visibility parameters. J. Air Pollut. Control Assoc. 35: 1261-1265.

Jones, A.; Roberts, D. L.; Slingo, A. (1994) A climate model study of indirect radiative forcing by anthropogenic sulfate aerosols. Nature (London) 370: 450-453.

Joseph, D. B.; Metsa, J.; Malm, W. C.; Pitchford, M. (1987) Plans for IMPROVE: a federal program to monitor visibility in class I areas. In: Bhardwaja, P. S., ed. Visibility protection: research and policy aspects, an APCA international specialty conference; September 1986; Grand Teton National Park, WY. Pittsburgh, PA: Air Pollution Control Association; pp. 113-125. (APCA transactions series no. TR-10).

Judd, D. B.; Wyszecki, G (1975) Color in business, science and industry. 3rd ed. New York, NY: John Wiley & Sons.

Jung, H. J.; Bach, W. (1987) The effects of aerosols on the response of a two-dimensional zonally-averaged climate model. Theor. Appl. Climatol. 38: 222-233.

Kahneman, D.; Knetsch, J. L. (1992) Valuing public goods: the purchase of moral satisfaction. J. Environ. Econ. Manage. 22: 57-70.

Kaufman, Y. J.; Chou, M.-D. (1993) Model simulations of the competing climatic effects of SO_2 and CO_2. J. Clim. 6: 1241-1252.

Kaufman, Y. J.; Fraser, R. S.; Mahoney, R. L. (1991) Fossil fuel and biomass burning effect on climate—heating or cooling? J. Clim. 4: 578-588.

Kerker, M. (1969) The scattering of light and other electromagnetic radiation. New York, NY: Academic Press, Inc. (Loebl, E. M., ed. Physical chemistry: a series of monographs, no. 16).

Kerker, M; Aden, A. L (1991) Scattering of electromagnetic waves from two concentric spheres. J. Appl. Physiol. 22: 1242-1246.

Kiehl, J. T.; Briegleb, B. P. (1993) The relative roles of sulfate aerosols and greenhouse gases in climate forcing. Science (Washington, DC) 260: 311-314.

King, M. D.; Radke, L. F.; Hobbs, P. V. (1993) Optical properties of marine stratocumulus clouds modified by ships. J. Geophys. Res. [Atmos.] 98: 2729-2739.

Koenig, J. Q.; Larson, T. V.; Hanley, Q. S.; Rebolledo, V.; Dumler, K.; Checkoway, H.; Wang, S.-Z.; Lin, D.; Pierson, W. E. (1993) Pulmonary function changes in children associated with fine particulate matter. Environ. Res. 63: 26-38.

Koschmieder, H. (1924) Theorie der horizontalen Sichtweite II: Kontrast und Sichtweite [Theory of horizontal visibility]. Beitr. Phys. Atmos. 12: 171-181.

Langner, J.; Rodhe, H. (1991) A global three-dimensional model of the tropospheric sulfur cycle. J. Atmos. Chem. 13: 225-263.

Langner, J.; Rodhe, H.; Crutzen, P. J.; Zimmermann, P. (1992) Anthropogenic influence on the distribution of tropospheric sulphate aerosol. Nature (London) 359: 712-716.

Larson, S. M.; Cass, G. R.; Hussey, K. J.; Luce, F. (1988) Verification of image processing based visibility models. Environ. Sci. Technol. 22: 629-637.

Latimer, D. A. (1988) Plume perceptibility thresholds. Presented at: 81st annual meeting of the Air Pollution Control Association; June; Dallas, TX. Pittsburgh, PA: Air Pollution Control Association; paper no. 88-56.6.

Latimer, D. A.; Bergstrom, R. W.; Hayes, S. R.; Liu, M.-K.; Seinfeld, J. H.; Whitten, G. Z.; Wojcik, M. A.; Hillyer, M. J. (1978) The development of mathematical models for the prediction of anthropogenic visibility impairment: volumes I-III. Research Triangle Park, NC: U.S. Environmental Protection Agency, Office of Air Quality Planning and Standards; EPA report no. EPA-450/3-78-110a-c. Available from: NTIS, Springfield, VA; PB-293118-SET.

Latimer, D. A.; Hogo, H.; Daniel, T. C. (1981) The effects of atmospheric optical conditions on perceived scenic beauty. Atmos. Environ. 15: 1865-1874.

Lawson, D. R. (1990) The Southern California Air Quality Study. J. Air Waste Manage. Assoc. 40: 156-165.

Leaitch, W. R.; Isaac, G. A. (1994) On the relationship between sulfate and cloud droplet number concentrations. J. Clim. 7: 206-212.

Lewis, C. W.; Stevens, R. K. (1983) Comparison of factors influencing visual air quality during the winter in Denver, derived from measurements made by General Motors and Motor Vehicle Manufacturers Association in 1978 and Environmental Protection Agency in 1982. Research Triangle Park, NC: U.S. Environmental Protection Agency; EPA preliminary report.

Lioy, P. J.; Daisey, J. M.; Reiss, N. M.; Harkov, R. (1983) Characterization of inhalable particulate matter, volatile organic compounds and other chemical species measured in urban areas in New Jersey— I. summertime episodes. Atmos. Environ. 17: 2321-2330.

Lioy, P. J.; Daisey, J. M.; Greenberg, A.; Harkov, R. (1985) A major wintertime (1983) pollution episode in northern New Jersey: analyses of the accumulation and spatial distribution of inhalable particulate matter, extractable organic matter and other species. Atmos. Environ. 19: 429-436.

Loehman, E.; Boldt, D.; Chaikin, K. (1981) Measuring the benefits of air quality improvements in the San Francisco Bay area. Washington, DC: U.S. Environmental Protection Agency.

Lorente, J.; Redaño, A.; de Cabo, X. (1994) Influence of urban aerosol on spectral solar irradiance. J. Appl. Meteorol. 33: 406-415.

Lowenthal, D. H.; Rogers, C. F.; Saxena, P.; Watson, J. G.; Chow, J. C. (1995) Sensitivity of estimated light extinction coefficients to model assumptions and measurement errors. Atmos. Environ. 29: 751-766.

Lyons, C.; Tombach, I. (1979) Willamette Valley field and slash burning impact air surveillance network data evaluation, v. 2. Pasadena, CA: Aerovironment Inc.

MacAdam, D. L. (1981) Perceptual significance of colorimetric data for colors of plumes and haze. Atmos. Environ. 15: 1797-1803.

MacCracken, M. C.; Cess, R. D.; Potter, G. L. (1986) Climatic effects of anthropogenic Arctic aerosols: an illustration of climate feedback mechanisms with one- and two-dimensional climate models. J. Geophys. Res. [Atmos.] 91: 14,445-14,450.

MacFarland, K. K.; Malm, W.; Molenar, J. (1983) An examination of methodologies for assessing the value of visibility. In: Rowe, R. D.; Chestnut, L. G., eds. Managing air quality and scenic resources at national parks and wilderness areas. Boulder, CO: Westview Press; pp. 151-172.

Macias, E. S.; Vossler, T. L.; White, W. H. (1987) Carbon and sulfate particles in the western U.S. In: Bhardwaja, P. S., ed. Visibility protection: research and policy aspects, an APCA international specialty conference; September 1986; Grand Teton National Park, WY. Pittsburgh, PA: Air Pollution Control Association; pp. 361-372. (APCA transactions series no. TR-10).

Malm, W. (1979) Considerations in the measurement of visibility. J. Air Pollut. Control Assoc. 29: 1042-1052.

Malm, W.; Pitchford, M.; Pitchford, A. (1982) Site specific factors influencing the visual range calculated from teleradiometer measurements. Atmos. Environ. 16: 2323-2333.

Malm, W. C.; Sisler, J. F.; Huffman, D.; Eldred, R. A.; Cahill, T. A. (1994) Spatial and seasonal trends in particle concentration and optical extinction in the United States. J. Geophys. Res. [Atmos.] 99: 1347-1370.

Marians, M.; Trijonis, J. (1979) Empirical studies of the relationship between emissions and visibility in the Southwest. Research Triangle Park, NC: U.S. Environmental Protection Agency, Office of Air Quality Planning and Standards; EPA report no. EPA-450/5-79-009. Available from: NTIS, Springfield, VA; PB80-156136.

McClelland, G.; Schulze, W.; Waldman, D.; Irwin, J.; Schenk, D.; Stewart, T.; Deck, L.; Thayer, M. (1991) Valuing eastern visibility: a field test of the contingent valuation method. Washington, DC: draft report to the U.S. Environmental Protection Agency; cooperative agreement no. CR-815183-01-3.

McDade, C. E.; Tombach, I. H. (1987) Goals and initial findings from SCENES. In: Bhardwaja, P. S., ed. Visibility protection: research and policy aspects, an APCA international specialty conference; September 1986; Grand Teton National Park, WY. Pittsburgh, PA: Air Pollution Control Association; pp. 76-86. (APCA transactions series no. TR-10).

McMurry, P. H.; Stolzenburg, M. R. (1989) On the sensitivity of particle size to relative humidity for Los Angeles aerosols. Atmos. Environ. 23: 497-507.

Meng, Z.; Seinfeld, J. H. (1994) On the source of the submicrometer droplet mode of urban and regional aerosols. Aerosol Sci. Technol. 20: 253-265.

Mercer, G. S. (1994) Transmissometer data reporting (IMPROVE protocol). Fort Collins, CO: Air Resource Specialists, Inc.; technical instruction no. 4500-5100.

Michelangeli, D. V.; Allen, M.; Yung, Y. L. (1989) The effect of El Chichon volcanic aerosols: impact of radiative, thermal, and chemical perturbations. J. Geophys. Res. [Atmos.] 94: 18,429-18,443.

Michelangeli, D. V.; Allen, M.; Yung, Y. L.; Shia, R.-L.; Crisp, D.; Eluszkiewicz, J. (1992) Enhancement of atmospheric radiation by an aerosol layer. J. Geophys. Res. [Atmos.] 97: 865-874.

Middleton, W. E. K. (1952) Vision through the atmosphere. Toronto, ON, Canada: University of Toronto Press.

Middleton, P. (1996) DAQM-simulated spatial and temporal differences among visibility, PM and other air quality concerns under realistic emission change scenarios. J. Air Waste Manage. Assoc.: accepted.

Middleton, P.; Stewart, T. R.; Dennis, R. L. (1983) Modeling human judgments of urban visual air quality. Atmos. Environ. 17: 1015-1021.

Mie, G. (1908) Beiträge zur Optik truber Medien, speziell kolloidaler Metallosüngen [Optics of cloudy media, especially colloidal metal solutions]. Ann. Phys. (Leipzig) 25: 377-445.

Minnaert, M. (1954) The nature of light and colour in the open air. New York, NY: Dover Publications, Inc.

Mitchell, R. C.; Carson, R. T. (1989) Using surveys to value public goods: the contingent valuation method. Washington, DC: Resources for the Future.

Molenar, J. V.; Persha, G.; Malm, W. C. (1990) Long path transmissometer for measuring ambient atmospheric extinction. In: Mathai, C. V., ed. Visibility and fine particles: transactions of an Air & Waste Management Association/U.S. Environmental Protection Agency international specialty conference; October 1989; Estes Park, CO. Pittsburgh PA: Air & Waste Management Association; pp. 293-304. (Transactions TR-17).

Molenar, J. V.; Cismoski, D. S.; Tree, R. M. (1992) Intercomparison of ambient optical monitoring techniques. Presented at: 85th annual meeting of the Air & Waste Management Assocation; June; Kansas City, MO.

Molenar, J. V.; Malm, W. C.; Johnson, C. E. (1994) Visual air quality simulation techniques. Atmos. Environ. 28: 1055-1063.

Moran, M. D.; Pielke, R. A. (1994) Delayed shear enhancement in mesoscale atmospheric dispersion. Presented at: 8th joint conference on applications of air pollution meteorology with A&WMA; January; Nashville, TN. Boston, MA: Meteorological Society; pp. 96-103.

Mueller, P. K.; Watson, J. G. (1982) Eastern regional air quality measurements, v. I. Palo Alto, CA: Electric Power Research Institute; report no. EA-1914.

Mueller, P. K.; Hidy, G. M. (1983) The sulfate regional experiment (SURE): report of findings. Palo Alto, CA: Electric Power Research Institute; EPRI report no. EA-1901. 3v.

Mueller, P. K.; Hansen, D. A.; Watson, J. G., Jr. (1986) The subregional cooperative electric utility, Department of Defense, National Park Service, and EPA study (SCENES) on visibility: an overview. Palo Alto, CA: Electric Power Research Institute; report no. EA-4664-SR.

National Oceanic and Atmospheric Administration. (1992) ASOS (automated surface observing system) user's guide. Washington, DC: National Oceanic and Atmospheric Administration.

National Research Council. (1993) Protecting visibility in national parks and wilderness areas. Washington, DC: National Academy Press. 3v.

Nguyen, B. C.; Bonsang, B.; Gaudry, A. (1983) The role of the ocean in the global atmospheric sulfur cycle. J. Geophys. Res. C: Oceans Atmos. 88: 10,903-10,914.

Novakov, T.; Penner, J. E. (1993) Large contribution of organic aerosols to cloud-condensation-nuclei concentrations. Nature (London) 365: 823-826.

Orr, C., Jr.; Hurd, F. K.; Corbett, W. J. (1958) Aerosol size and relative humidity. J. Colloid Sci. 13: 472-482.

Pace, Y. G.; Watson, J. G.; Rodes, C. E. (1981) Preliminary interpretation of Inhalable Particulate Network data. Presented at: 74th annual meeting of the Air Pollution Control Association; June; Philadelphia, PA. Pittsburgh, PA: Air Pollution Control Association; paper no. 81-5.2.

Patterson, E. M. (1977) Atmospheric extinction between 0.55 "mu"m and 10.6 "mu"m due to soil-derived aerosols. Appl. Opt. 16: 2414-2418.

Patterson, D. E.; Holloway, J. M.; Husar, R. B. (1980) Historical visibility over the eastern U.S.: daily and quarterly extinction coefficient contour maps. Research Triangle Park, NC: U.S. Environmental Protection Agency, Environmental Sciences Research Laboratory; EPA report no. EPA-600/3-80-043a. Available from: NTIS, Springfield, VA; PB81-196974.

Penndorf, R. B. (1958) An approximation method to the Mie theory for colloidal spheres. J. Phys. Chem. 62: 1537-1542.

Penndorf, R. (1957) Tables of the refractive index for standard air and the Rayleigh scattering coefficient for the spectral region between 0.2 and 20.0 μ and their application to atmospheric optics. J. Opt. Soc. Am. 47: 176-182.

Penner, J. E.; Dickinson, R. E.; O'Neill, C. A. (1992) Effects of aerosol from biomass burning on the global radiation budget. Science (Washington, DC) 256: 1432-1433.

Penner, J. E.; Charlson, R. J.; Hales, J. M.; Laulainen, N. S.; Leifer, R.; Novakov, T.; Ogren, J.; Radke, L. F.; Schwartz, S. E.; Travis, L. (1994) Quantifying and minimizing uncertainty of climate forcing by anthropogenic aerosols. Bull. Am. Meteorol. Soc. 75: 375-400.

Pierson, W. R.; Brachaczek, W. W.; Korniski, T. J.; Truex, T. J.; Butler, J. W. (1980a) Artifact formation of sulfate, nitrate, and hydrogen ion on backup filters: Allegheny Mountain experiment. J. Air Pollut. Control Assoc. 30: 30-34.

Pierson, W. R.; Brachaczek, W. W.; Truex, T. J.; Butler, J. W.; Korniski, T. J. (1980b) Ambient sulfate measurements on Allegheny Mountain and the question of atmospheric sulfate in the northeastern United States. Ann. N. Y. Acad. Sci. 338: 145-173.

Pinnick, R. G.; Fernandez, G.; Martinez-Andazola, E.; Hinds, B. D.; Hansen, A. D. A.; Fuller, K. (1993) Aerosol in the arid southwestern United States: measurements of mass loading, volatility, size distribution, absorption characteristics, black carbon content, and vertical structure to 7 km above sea level. J. Geophys. Res. [Atmos.] 98: 2651-2666.

Pitchford, M. L.; Malm, W. C. (1994) Development and applications of a standard visual index. Atmos. Environ. 28: 1049-1054.

Platnick, S.; Twomey, S. (1994) Determining the susceptibility of cloud albedo to changes in droplet concentration with the advanced very high resolution radiometer. J. Appl. Meteorol. 33: 334-347.

Rae, D. A. (1984) Benefits of visual air quality in Cincinnati - results of a contingent ranking survey, final report. Palo Alto, CA: Electric Power Research Institute; report no. RP-1742.

Ramanathan, V.; Callis, L.; Cess, R.; Hansen, J.; Isaksen, I.; Kuhn, W.; Lacis, A.; Luther, F.; Mahlman, J.; Reck, R.; Schlesinger, M. (1987) Climate-chemical interactions and effects of changing atmospheric trace gases. Rev. Geophys. 25: 1441-1482.

Ramanathan, V.; Subasilar, B.; Zhang, G. J.; Conant, W.; Cess, R. D.; Kiehl, J. T.; Grassl, H.; Shi, L. (1995) Warm pool heat budget and shortwave cloud forcing: a missing physics? Science (Washington, DC) 267: 499-503.

Randall, D. A.; Coakley, J. A., Jr.; Fairall, C. W.; Kropfli, R. A.; Lenschow, D. H. (1984) Outlook for research on subtropical marine stratiform clouds. Bull. Am. Meteorol. Soc. 65: 1290-1301.

Reisinger, L. M.; Valenti, R. J. (1984) Visibility and air quality impairment in the southeastern United States - 1983. Presented at: 77th annual meeting of the Air Pollution Control Association; paper no. 84-59.3.

Reisinger, L. M.; Valente, R. J. (1985) Visibility and other air quality measurements made at the Great Smoky Mountains National Park. Muscle Shoals, AL: Tennessee Valley Authority; TVA/ON RED AWR -86/6.

Richards, L. W. (1973) Size distribution of pigment particles: measurement and characterization by light-scattering techniques. In: Patton, T. C., ed. Pigment handbook: volume III, characterization and physical relationships. New York NY: John Wiley & Sons; pp. 89-100.

Richards, L. W. (1988) Sight path measurements for visibility monitoring and research. JAPCA 38: 784-791.

Richards, L. W. (1989) Atmospheric light transmittance and path radiance measurements during the southern California air quality study. Presented at: Air & Waste Management Association 82nd annual meeting; June; Anaheim, CA. Pittsburgh, PA: Air & Waste Management Association; paper no. 89-154.6.

Richards, L. W. (1990) Effect of the atmosphere on visibility. In: Mathai, C. V., ed. Visibility and fine particles: an A&WMA/EPA international specialty conference; October 1989; Estes Park, CO. Pittsburgh, PA: Air & Waste Management Association; pp. 261-270. (A&WMA transactions series no. TR-17).

Richards, L. W. (1994) Recommendations for monitoring the effects of air quality on visibility. In: Proceedings of the international specialty conference, aerosols and atmospheric optics: radiative balance and visual air quality, v. A; September; Showbird, UT. Pittsburgh, PA: Air & Waste Management Association; pp. 6-15.

Richards, L. W.; Anderson, J. A.; Blumenthal, D. L.; Brandt, A. A.; McDonald, J. A.; Waters, N.; Macias, E. S.; Bhardwaja, P. S. (1981) The chemistry, aerosol physics, and optical properties of a western coal-fired power plant plume. Atmos. Environ. 15: 2111-2134.

Richards, L. W.; Anderson, J. A.; Blumenthal, D. L.; McDonald, J. A.; Kok, G. L.; Lazrus, A. L. (1983) Hydrogen peroxide and sulfur (IV) in Los Angeles cloud water. Atmos. Environ. 17: 911-914.

Richards, L. W.; Bergstrom, R. W., Jr.; Ackerman, T. P. (1986) The optical effects of fine-particle carbon on urban atmospheres. Atmos. Environ. 20: 387-396.

Richards, L. W.; Blanchard, C. L.; Blumenthal, D. L. (1991) Navajo generating station visibility study, draft #2. Santa Rosa, CA: Sonoma Technology, Inc.; final report STI-90200-1124-FRD2.

Richards, L. W.; Prouty, J. D.; Stoelting, M.; Korc, M. E.; Jones, C. M. (1995) Visual impact analysis of the plume from the Owens Lake Soda Ash Company soda ash mining and processing project on nearby Class I areas. San Mateo, CA: MHA Environmental Consulting, Inc.; final report no. STI-94490-1445-FR.

Robock, A. (1988) Enhancement of surface cooling due to forest fire smoke. Science (Washington, DC) 242: 911-913.

Robock, A. (1991) Surface cooling due to forest fire smoke. J. Geophys. Res. [Atmos.] 96: 20,869-20,878.

Rood, M. J.; Shaw, M. A.; Larson, T. V.; Covert, D. S. (1989) Ubiquitous nature of ambient metastable aerosol. Nature (London) 337: 537-539.

Rosen, H.; Hansen, A. D. A.; Gundel, L.; Novakov, T. (1978) Identification of the optically absorbing component in urban aerosols. Appl. Opt. 17: 3859-3861.

Rosen, H.; Novakov, T.; Bodhaine, B. A. (1981) Soot in the Arctic. Presented at: the second symposium on Arctic air chemistry; May 1980; Kingston, RI. Atmos. Environ. 15: 1371-1374.

Ross, D. M.; Malm, W. C.; Loomis, R. J. (1987) An examination of the relative importance of park attributes at several national parks. In: Bhardwaja, P. S., ed. Visibility protection: research and policy aspects, an APCA international specialty conference; September 1986; Grand Teton National Park, WY. Pittsburgh, PA: Air Pollution Control Association; pp. 304-319. (APCA transactions series no. TR-10).

Rossow, W. B.; Schiffer, R. A. (1991) ISCCP cloud data products. Bull. Am. Meteorol. Soc. 72: 2-20.

Rowe, R. D.; Chestnut, L. G. (1982) The value of visibility: economic theory and applications for air pollution control. Cambridge, MA: Abt Books.

Ruby, M. G.; Waggoner, A. P. (1981) Intercomparison of integrating nephelometer measurements. Environ. Sci. Technol. 15: 109-113.

Saxena, P.; Hildemann, L. M.; McMurry, P. H.; Seinfeld, J. H. (1995) Organics alter hygroscopic behavior of atmospheric particles. J. Geophys. Res. [Atmos.]: in press.

Schneider, S. H.; Thompson, S. L. (1988) Simulating the climatic effects of nuclear war. Nature (London) 333: 221-227.

Schnell, R. C. (1984) Arctic haze: editorial. Geophys. Res. Lett. 11: 359.

Schoeberl, M. R.; Bhartia, P. K.; Hilsenrath, E. (1993) Tropical ozone loss following the eruption of Mt. Pinatubo. Geophys. Res. Letters 20: 29-32.

Schulze, W. D.; Brookshire, D. S.; Walther, E. G.; MacFarland, K. K.; Thayer, M. A.; Whitworth, R. L.; Ben-David, S.; Malm, W.; Molenar, J. (1983) The economic benefits of preserving visibility in the national parklands of the southwest. Nat. Resour. J. 23: 149-173.

Schwartz, S. E. (1988) Are global cloud albedo and climate controlled by marine phytoplankton? Nature (London) 336: 441-445.

Seigneur, C.; Johnson, C. D.; Latimer, D. A.; Bergstrom, R. W.; Hogo, H. (1983) User's manual for the plume visibility model (PLUVUE II). San Rafael, CA: Systems Applications, Inc.; report no. SYSAPP-83/221.

Seigneur, C.; Johnson, C. D.; Latimer, D. A.; Bergstrom, R. W.; Hogo, H. (1984) User's manual for the plume visibility model (PLUVUE II). Research Triangle Park, NC: U.S. Environmental Protection Agency, Environmental Sciences Research Laboratory; EPA report no. EPA-600/8-84-005. Available from: NTIS, Springfield, VA; PB84-158302.

Shah, J. J.; Watson, J. G., Jr.; Cooper, J. A.; Huntzicker, J. J. (1984) Aerosol chemical composition and light scattering in Portland, Oregon: the role of carbon. Atmos. Environ. 18: 235-240.

Shah, J. J.; Johnson, R. L.; Heyerdahl, E. K.; Huntzicker, J. J. (1986) Carbonaceous aerosol at urban and rural sites in the United States. J. Air Pollut. Control Assoc. 36: 254-257.

Shaw, G. E. (1983) Bio-controlled thermostasis involving the sulfur cycle. Clim. Change 5: 297-303.

Shaw, R. W., Jr.; Paur, R. J. (1983) Measurements of sulfur in gases and particles during sixteen months in the Ohio River Valley. Atmos. Environ. 17: 1431-1438.

Sisler, J. F.; Huffman, D.; Lattimer, D. A.; Malm, W. C.; Pitchford, M. L. (1993) Spatial and temporal patterns and the chemical composition of the haze in the United States: an anlysis of data from the IMPROVE network, 1988-1991. Fort Collins, CO: Colorado State University, Cooperative Institute for Research in the Atmosphere (CIRA).

Sloane, C. S. (1982a) Visibility trends—I. methods of analysis. Atmos. Environ. 16: 41-51.

Sloane, C. S. (1982b) Visibility trends—II. mideastern United States 1948-1978. Atmos. Environ. 16: 2309-2321.

Sloane, C. S. (1983) Summertime visibility declines: meteorological influences. Atmos. Environ. 17: 763-774.

Sloane, C. S. (1986) Effect of composition on aerosol light scattering efficiencies. Atmos. Environ. 20: 1025-1037.

Sloane, C. S.; White, W. H. (1986) Visibility: an evolving issue. Environ. Sci. Technol. 20: 760-766.

Sloane, C. S.; Wolff, G. T. (1984) Relating ambient visibilities to aerosol composition. Presented at: 77th annual meeting of the Air Pollution Control Association; June; San Francisco, CA; Pittsburgh, PA: Air Pollution Control Association; paper no. 84-115.1.

Sloane, C. S.; Wolff, G. T. (1985) Prediction of ambient light scattering using a physical model responsive to relative humidity: validation with measurements from Detroit. Atmos. Environ. 19: 669-680.

Spengler, J. D.; Thurston, G. D. (1983) Mass and elemental composition of fine and coarse particles in six U.S. cities. J. Air Pollut. Control Assoc. 33: 1162-1171.

Stephens, G. L. (1994) Remote sensing of the lower atmosphere: an introduction. New York, NY: Oxford University Press; p. 214.

Stevens, R. K.; Dzubay, T. G. ; Russwurm, G.; Rickel, D. (1978) Sampling and analysis of atmospheric sulfates and related species. Atmos. Environ. 12: 55-68.

Stevens, R. K.; Dzubay, T. G.; Shaw, R. W., Jr.; McClenny, W. A.; Lewis, C. W.; Wilson, W. E. (1980) Characterization of the aerosol in the Great Smoky Mountains. Environ. Sci. Technol. 14: 1491-1498.

Stevens, R. K.; Dzubay, T. G.; Lewis, C. W.; Shaw, R. W., Jr. (1984) Source apportionment methods applied to the determination of the origin of ambient aerosols that affect visibility in forested areas. Atmos. Environ. 18: 261-272.

Tang, I. N. (1980) Deliquescence properties and particle size change of hygroscopic aerosols. In: Willeke, K., ed. Generation of aerosols and facilities for exposure experiments. Ann Arbor, MI: Ann Arbor Science; pp. 153-167.

Tang, I. N.; Wong, W. T.; Munkelwitz, H. R. (1981) The relative importance of atmospheric sulfates and nitrates in visibility reduction. Atmos. Environ. 15: 2463-2471.

Taylor, K. E.; Penner, J. E. (1994) Response of the climate system to atmospheric aerosols and greenhouse gases. Nature (London) 369: 734-737.

Thompson, S. L.; Ramaswamy, V.; Covey, C. (1987) Atmospheric effects of nuclear war aerosols in general circulation model simulations: influence of smoke optical properties. J. Geophys. Res. [Atmos.] 92: 10,942-10,960.

Tolley, G. A.; Randall, A.; Blomquist, G.; Fabian, R.; Fishelson, G.; Frankel, A.; Hoehn, J.; Krumm, R.; Mensah, E.; Smith, T. (1986) Establishing and valuing the effects of improved visibility in eastern United States. Washington, DC: U.S. Environmental Protection Agency.

Tombach, I.; Allard, D. (1983) Comparison of visibility measurement techniques: eastern United States. Palo Alto, CA: Electric Power Research Institute; EPRI report no. EA-4903.

Toon, O. B.; Ackerman, T. P. (1981) Algorithms for the calculaton of scattering by stratified spheres. Appl. Opt. 20: 3657-3660.

Toon, O. B.; Pollack, J. B. (1976) A global average model of atmospheric aerosols for radiative transfer calculations. J. Appl. Meteorol. 15: 225-246.

Trijonis, J. (1979) Visibility in the southwest—an exploration of the historical data base. Atmos. Environ. 13: 833-843.

Trijonis, J. (1982a) Existing and natural background levels of visibility and fine particles in the rural East. Atmos. Environ. 16: 2431-2445.

Trijonis, J. (1982b) Visibility in California. J. Air Pollut. Control Assoc. 32: 165-169.

Trijonis, J.; Yuan, K. (1978) Visibility in the southwest: an exploration of the historical data base. Research Triangle Park, NC: U.S. Environmental Protection Agency, Environmental Sciences Research Laboratory; EPA report no. EPA-600/3-78-039. Available from: NTIS, Springfield, VA; PB-282942.

Trijonis, J.; Thayer, M.; Murdoch, J.; Hagemen, R. (1984) Air quality benefits analysis for Los Angeles and San Francisco based on housing values and visibility. Sacramento, CA: California Air Resources Board.

Trijonis, J.; Thayer, M.; Murdoch, J.; Hageman, R. (1985) Air quality benefit analysis for Los Angeles and San Francisco based on housing values and visibility. Final report. Sacramento, CA: California Air Resources Board; report no. ARB/R-85/237. Available from: NTIS, Springfield, VA; PB85-166049.

Trijonis, J. C.; Pitchford, M.; McGown, M. (1987) Preliminary extinction budget results from the RESOLVE program. In: Bhardwaja, P. S., ed. Visibility protection: research and policy aspects, an APCA international specialty conference; September 1986; Grand Teton National Park, WY. Pittsburgh, PA: Air Pollution Control Association; pp. 872-883. (APCA transactions series no. TR-10).

Trijonis, J. C.; Malm, W. C.; Pitchford, M.; White, W. H. (1991) Visibility: existing and historical conditions—causes and effects. In: Irving, P. M., ed. Acidic deposition: state of science and technology, volume III: terrestrial,

materials, health and visibility effects. Washington, DC: The U.S. National Acid Precipitation Assessment Program. (State of science and technology report no. 24).

Turco, R. P.; Toon, O. B.; Ackerman, T. P.; Pollack, J. B.; Sagan, C. (1983) Nuclear winter: global consequences of multiple nuclear explosions. Science (Washington, DC) 222: 1283-1292.

Turco, R. P.; Toon, O. B.; Ackerman, T. P.; Pollack, J. B.; Sagan, C. (1990) Climate and smoke: an appraisal of nuclear winter. Science (Washington, DC) 247: 166-176.

Twomey, S. (1974) Pollution and the planetary albedo. Atmos. Environ. 8: 1251-1256.

Twomey, S. (1977) Atmospheric aerosols. Amsterdam, The Netherlands: Elsevier Scientific Publishing Company; p. 237.

Twomey, S. (1991) Aerosols, clouds and radiation. Atmos. Environ. Part A 25: 2435-2442.

Twomey, S. A.; Piepgrass, M.; Wolfe, T. L. (1984) An assessment of the impact of pollution on global cloud albedo. Tellus Ser. B 36B: 356-366.

U.S. Environmental Protection Agency. (1979) Protecting visibility: an EPA report to Congress. Research Triangle Park, NC: Office of Air Quality Planning and Standards; EPA report no. EPA-450/5-79-008. Available from: NTIS, Springfield, VA; PB80-220320.

U.S. Environmental Protection Agency. (1982) Air quality criteria for particulate matter and sulfur oxides. Research Triangle Park, NC: Office of Health and Environmental Assessment, Environmental Criteria and Assessment Office; EPA report no. EPA-600/8-82-029aF-cF. 3v. Available from: NTIS, Springfield, VA; PB84-156777.

U.S. Environmental Protection Agency. (1985) Developing long-term strategies for regional haze: findings and recommendations of the visibility task force. Research Triangle Park, NC.

U.S. Environmental Protection Agency. (1988) Workbook for plume visual impact screening and analysis. Research Triangle Park, NC: U.S. Environmental Protection Agency; EPA report no. EPA-450/4-88-015. Available from: NTIS, Springfield, VA; PB89-131286.

U.S. Environmental Protection Agency. (1992) Interagency workgroup on air quality modeling (IWAQM): work plan rationale. Research Triangle Park, NC: Office of Air Quality Planning and Standards; EPA report no. EPA-454/R-92-001.

U.S. Environmental Protection Agency. (1993a) Air quality criteria for oxides of nitrogen. Research Triangle Park, NC: Office of Health and Environmental Assessment, Environmental Criteria and Assessment Office; EPA report no. EPA/600/8-91/049aF-cF. 3v. Available from: NTIS, Springfield, VA; PB95-124533, PB95-124525, PB95-124517.

U.S. Environmental Protection Agency. (1993b) Interagency workgroup on air quality modeling (IWAQM): interim recommendation for modeling long range transport and impacts on regional visibility. Research Triangle Park, NC: Office of Air Quality Planning and Standards; EPA report no. EPA-454/R-93-015.

U.S. Environmental Protection Agency. (1994) A revised user's guide to MESOPUFF II (V5.1). Research Triangle Park, NC: Office of Air Quality Planning and Standards; EPA report no. EPA-454/B-94-025.

U.S. Environmental Protection Agency. (1995a) Interagency workgroup on air quality modeling (IWAQM): assessment of phase I recommendations regarding the use of MESOPUFF II. Research Triangle Park, NC: Office of Air Quality Planning and Standards; EPA report no. EPA-454/R-95-006.

U.S. Environmental Protection Agency. (1995b) Testing of meteorological and dispersion models for use in regional air quality modeling. Research Triangle Park, NC: Office of Air Quality Planning and Standards; EPA report no. EPA-454/B-95-005.

U.S. Environmental Protection Agency. (1995c) A user's guide for the CALMET meteorological model. Research Triangle Park, NC: Office of Air Quality Planning and Standards; EPA report no. EPA-454/B-95-002.

U.S. Environmental Protection Agency. (1995d) A user's guide for the CALPUFF dispersion model. Research Triangle Park, NC: Office of Air Quality Planning and Standards; EPA report no. EPA-454/B-95-006.

U.S. Environmental Protection Agency. (1995e) Interim findings on the status of visibility research. Research Triangle Park, NC: Office of Air and Radiation; EPA report no. EPA-600/R-95/021.

U.S. Naval Oceonographic Office. (1966) Signs of land. Section 2623; p. 660; H. O. publication no. 9.

Valente, R. J.; Reisinger, L. M. (1983) Data summary: visibility and ambient air quality in the Great Smoky Mountain Park research project. TVA/ONR/AQB-83/4.

VanCuren, T. (1989a) Instrumental measurement of visibility reducing particles: staff report. Sacramento, Ca: California Air Resources Board, Research Division; January.

VanCuren, T. (1989b) Instrumental measurement of visibility reducing particles: technical support document. Sacramento, CA: California Air Resources Board, Research Division.

Vasconcelos, L. A. de P.; Macias, E. S.; White, W. H. (1994) Aerosol composition as a function of haze and humidity levels in the southwestern U.S. Atmos. Environ. 28: 3679-3691.

Vel'tishchev, N. N.; Ginzburg, A. S.; Golitsyn, G. S. (1988) Climatic effects of massive fires. Izv. Acad. Sci. USSR Atmos. Oceanic Phys. Engl. Transl. 24: 217-223.

Veress, S. A. (1972) Extinction coefficient. Photogramm. Eng. 38: 183-191.

Vogelmann, A. M.; Robock, A.; Ellingson, R. G. (1988) Effects of dirty snow in nuclear winter simulations. J. Geophys. Res. [Atmos.] 93: 5319-5332.

Wagener, R.; Schwartz, S. E. (1994) Comparison of seasonal and zonal patterns of the direct and indirect radiative forcing of climate by aerosols. Presented at: International Aerosol Research Assembly and American Association for Aerosol Research fourth international aerosol conference; August-September; Los Angeles, CA.

Waggoner, A. P.; Weiss, R. E. (1980) Comparison of fine particle mass concentration and light scattering extinction in ambient aerosol. Atmos. Environ. 14: 623-626.

Waggoner, A. P.; Weiss, R. E.; Ahlquist, N. C.; Covert, D. S.; Will, S.; Charlson, R. J. (1981) Optical characteristics of atmospheric aerosols. In: White, W. H.; Moore, D. J.; Lodge, J. P., Jr., eds. Plumes and visibility: measurements and model components: proceedings of the symposium; November 1980; Grand Canyon National Park, AZ. Atmos. Environ. 15: 1891-1909.

Waggoner, A. P.; Weiss, R. E.; Ahlquist, N. C. (1983) The color of Denver haze. Atmos. Environ. 17: 2081-2086.

Wall, S. M.; John, W.; Ondo, J. L. (1988) Measurement of aerosol size distributions for nitrate and major ionic species. Atmos. Environ. 22: 1649-1656.

Wallace, J. M.; Hobbs, P. V. (1977) Atmospheric science: an introductory survey. New York, NY: Academic Press, Inc.

Walton, J. J.; MacCracken, M. C.; Ghan, S. J. (1988) A global-scale Lagrangian trace species model of transport, transformation, and removal processes. J. Geophys. Res. [Atmos.] 93: 8339-8354.

Warren, S. G.; Hahn, C. J.; London, J.; Chervin, R. M.; Jenne, R. L. (1988) Global distribution of total cloud cover and cloud type over the ocean. Boulder, CO: DOE report no. DOE/ER-0406; NCAR/TN-317+STR.

Watson, J. G.; Chow, J. C.; Shah, J. J. (1981) Analysis of inhalable and fine particulate matter measurements. Research Triangle Park, NC: U.S. Environmental Protection Agency, Office of Air Quality Planning and Standards; EPA report no. EPA-450/4-81-035. Available from: NTIS, Springfield, VA; PB83-111336.

Watson, J. G.; Chow, J. C.; Richards, L. W.; Neff, W. D.; Andersen, S. R.; Dietrich, D. L.; Houck, J. E.; Olnez, I. (1988) The 1987-88 metro Denver brown cloud study: v. I, II, III. Reno, NV: Desert Research Institute; final report no. 8810.1F(1-3).

Watson, J. G.; Chow, J. C.; Richards, L. W.; Haase, D. L.; McDade, C.; Dietrich, D. L.; Moon, D.; Sloane, C. (1991) The 1989-90 Phoenix urban haze study, volume II: the apportionment of light extinction to sources [final report]. Reno, NV: University and Community College System of Nevada, Desert Research Institute; DRI document no. 8931.5F1.

Weiss, R. E.; Larson, T. V.; Waggoner, A. P. (1982) In situ rapid-response measurement of $H_2SO_4/(NH_4)_2SO_4$ aerosols in rural Virginia. Environ. Sci. Technol. 16: 525-532.

Weller, M.; Leiterer, U. (1988) Experimental data on spectral aerosol optical thickness and its global distribution. Contrib. Atmos. Phys. 61: 1-9.

Westphal, D. L.; Toon, O. B. (1991) Simulations of microphysical, radiative, and dynamical processes in a continental-scale forest fire smoke plume. J. Geophys. Res. [Atmos.] 96: 22,379-22,400.

Whitby, K. T.; Husar, R. B.; Liu, B. Y. H. (1972) The aerosol size distribution of Los Angeles smog. J. Colloid Interface Sci. 39: 177-204.

White, W. H. (1975) Estimating the size range of smog aerosol particles with a pair of sunglasses. Atmos. Environ. 9: 1036-1037.

White, W. H. (1986) On the theoretical and empirical basis for apportioning extinction by aerosols: a critical review. Atmos. Environ. 20: 1659-1672.

White, W. H. (1990) The components of atmospheric light extinction: a survey of ground-level budgets. Atmos. Environ. Part A 24: 2673-2679.

White, W. H.; Macias, E. S. (1987) On measurements error and the empirical relationship of atmospheric extinction to aerosol composition in the non-urban west. In: Bhardwaja, P. S., ed. Visibility protection: research and policy aspects, an APCA international specialty conference; September 1986; Grand Teton National Park, WY. Pittsburgh, PA: Air Pollution Control Association; pp. 783-794. (APCA transactions series no. TR-10).

White, W. H.; Macias E. S. (1990) Light scattering by haze and dust at Spirit Mountain, Nevada. In: Mathai, C. V., ed. Visibility and fine particles: an A&WMA/EPA international specialty conference; October 1989; Estes Park, CO. Pittsburgh, PA; Air & Waste Management Association; pp. 914-922. (A&WMA transactions series no. TR-17).

White, W. H.; Seigneur, C.; Heinold, D. W.; Eltgroth, M. W.; Richards, L. W.; Roberts, P. T.; Bhardwaja, P. S.; Conner, W. D.; Wilson, W. E., Jr. (1985) Predicting the visibility of chimney plumes: an intercomparison of four models with observations at a well-controlled power plant. Atmos. Environ. 19: 515-528.

White, W. H.; Seigneur, C.; Heinold, D. W.; Richards, L. W.; Wilson, W. E.; Roberts, P. T. (1986) Radiative transfer budgets for scattering and absorbing plumes: measurements and model predictions. Atmos. Environ. 20: 2243-2257.

White, W. H.; Macias, E. S.; Nininger, R. C.; Schorran, D. (1994) Size-resolved measurements of light scattering by ambient particles in the southwestern U.S.A. Atmos. Environ. 28: 909-921.

Wigley, T. M. L. (1991) Could reducing fossil-fuel emissions cause global warming? Nature (London) 349: 503-506.

Williams, M. D.; Treiman, E.; Wecksung, M. (1980) Plume blight visibility modeling with a simulated photograph technique. J. Air Pollut. Control Assoc. 30: 131-134.

Williams, M.; Chan, L. Y.; Lewis, R. (1981) Validation and sensitivity of a simulated-photograph technique for visibility modeling. Atmos. Environ. 15: 2151-2170.

Wiscombe, W. J.; Mugnai, A. (1988) Scattering from nonspherical Chebyshev particles. 2: means of angular scattering patterns. Appl. Opt. 27: 2405-2421.

Wolff, G. T.; Countess, R. J.; Groblicki, P. J.; Ferman, M. A.; Cadle, S. H.; Muhlbaier, J. L. (1981) Visibility-reducing species in the Denver "brown cloud"—II. sources and temporal patterns. Atmos. Environ. 15: 2485-2502.

Wolff, G. T.; Kelly, N. A.; Ferman, M. A. (1982) Source regions of summertime ozone and haze episodes in the eastern United States. Water Air Soil Pollut. 18: 65-81.

Wolff, G. T.; Kelly, N. A.; Ferman, M. A.; Morrissey, M. L. (1983) Rural measurements of the chemical composition of airborne particles in the eastern United States. J. Geophys. Res. C: Oceans Atmos. 88: 10,769-10,775.

Wolff, G. T.; Korsog, P. E.; Kelly, N. A.; Ferman, M. A. (1985a) Relationships between fine particulate species, gaseous pollutants and meteorological parameters in Detroit. Atmos. Environ. 19: 1341-1349.

Wolff, G. T.; Korsog, P. E.; Stroup, D. P.; Ruthkosky, M. S.; Morrissey, M. L. (1985b) The influence of local and regional sources on the concentration of inhalable particulate matter in southeastern Michigan. Atmos. Environ. 19: 305-313.

Wysecki, G.; Stiles, W. S. (1967) Color science: concepts and methods, quantitative data and formulas. New York, NY: John Wiley & Sons.

Zhang, X. Q.; McMurry, P. H.; Hering, S. V.; Casuccio, G. S. (1993) Mixing characteristics and water content of submicron aerosols measured in Los Angeles and at the Grand Canyon. Atmos. Environ. Part A 27: 1593-1607.

Zhang, X.; Turpin, B. J.; McMurry, P. J.; Herring, S. V.; Stolzenburg, M. R. (1994) Mie theory evaluation of species contributions to the 1990 wintertime visibility reduction in the Grand Canyon. J. Air Waste Manage. Assoc. 44: 153-162.